

AD-A108 116

AIR FORCE INST OF TECH WRIGHT-PATTERSON AFB OH
THE INTERRELATIONSHIPS AND VARIATIONS OF THE RESISTIVITY, POROS--ETC(U)
AUG 81 T R ASHMAN
AFIT-CI-81-617

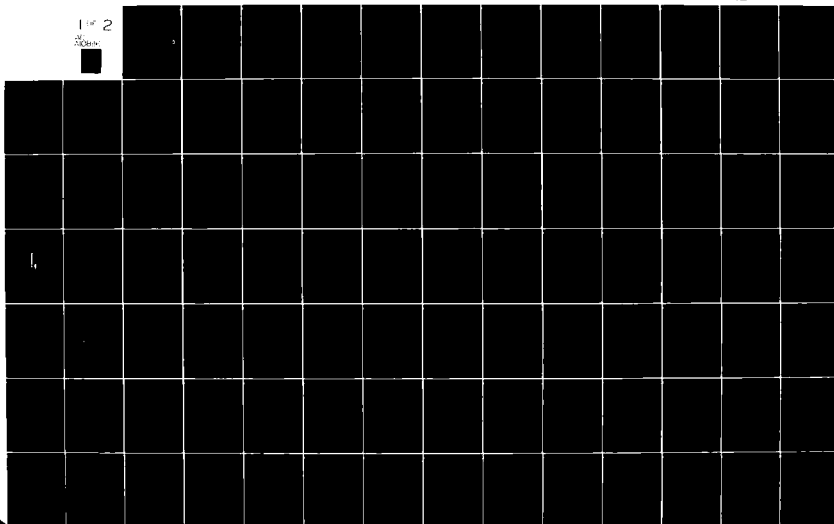
F/G 8/7

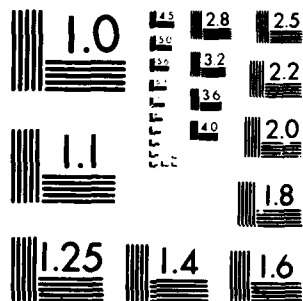
UNCLASSIFIED

NL

1 of 2

AD-A108 116





MICROCOPY RESOLUTION TEST CHART
NATIONAL BUREAU OF STANDARDS 1963 A

AD A108116

DTIC FILE COPY

UNCLASS

SECURITY CLASSIFICATION OF THIS PAGE (When Data Entered)

| REPORT DOCUMENTATION PAGE | | READ INSTRUCTIONS BEFORE COMPLETING FORM |
|---|-----------------------------------|---|
| 1. REPORT NUMBER 81-61T | 2. GOVT ACCESSION NO. 7 D A708 | 3. RECIPIENT'S CATALOG NUMBER 116 |
| 4. TITLE (and Subtitle) The Interrelationships and Variations of the Resistivity, Porosity, and Permeability as Functions of Pressure in a Geopressured Reservoir | | 5. TYPE OF REPORT & PERIOD COVERED THESIS/DISSERTATION |
| 7. AUTHOR(s) Thomas Robert Ashman | | 6. PERFORMING ORG. REPORT NUMBER |
| 9. PERFORMING ORGANIZATION NAME AND ADDRESS AFIT STUDENT AT: University of Texas at Austin | | 8. CONTRACT OR GRANT NUMBER(s) |
| 11. CONTROLLING OFFICE NAME AND ADDRESS AFIT/NR WPAFB OH 45433 | | 10. PROGRAM ELEMENT, PROJECT, TASK AREA & WORK UNIT NUMBERS |
| 14. MONITORING AGENCY NAME & ADDRESS (if different from Controlling Office) LEVEL | | 12. REPORT DATE August 1981 |
| | | 13. NUMBER OF PAGES 133 |
| | | 15. SECURITY CLASS. (of this report) UNCLASS |
| 16. DISTRIBUTION STATEMENT (of this Report) APPROVED FOR PUBLIC RELEASE; DISTRIBUTION UNLIMITED | | 15a. DECLASSIFICATION/DOWNGRADING SCHEDULE |
| 17. DISTRIBUTION STATEMENT (of the abstract entered in Block 20, if different from Report) | | |
| 18. SUPPLEMENTARY NOTES APPROVED FOR PUBLIC RELEASE: IAW AFR 190-17 | | |
| 19. KEY WORDS (Continue on reverse side if necessary and identify by block number) FREDRIC C. LYNCH Director of Public Affairs Air Force Institute of Technology (ATC) Wright-Patterson AFB, OH 45433 | | |
| 20. ABSTRACT (Continue on reverse side if necessary and identify by block number) ATTACHED | | |

DD FORM 1 JAN 73 1473

EDITION OF 1 NOV 65 OBSOLETE

UNCLASS

SECURITY CLASSIFICATION OF THIS PAGE (When Data Entered)

81 11 30 002

THE INTERRELATIONSHIPS AND VARIATIONS OF THE RESISTIVITY,
POROSITY, AND PERMEABILITY AS FUNCTIONS OF PRESSURE
IN A GEOPRESSURED RESERVOIR

APPROVED:

K. P. Gray
William Thayer
Richard W. J. J.

| | |
|--------------------|--|
| Accession For | |
| NTIS GRA&I | <input checked="checked" type="checkbox"/> |
| DTIC TAB | <input type="checkbox"/> |
| Unannounced | <input type="checkbox"/> |
| Justification | |
| By | |
| Distribution/ | |
| Available in Codes | |
| or | |
| Other | |
| A | |

VITA

Thomas Robert Ashman was born in Akron, Ohio on March 2, 1950, the son of Agnes L. and William G. Ashman. He completed studies at the University of Akron, Akron, Ohio, and received the Bachelor of Science Degree in Chemical Engineering in May 1973. He worked as a plant engineer for the Union Carbide Corporation, Linde Division, East Chicago, Indiana until October 1973 when he entered the U. S. Air Force. He served as Base Fuels Officer at several locations and then, as an assignment, entered the Graduate School at the University of Texas at Austin in September 1979.

Permanent Address: 580 Crestview Avenue
Akron, Ohio 44320

This thesis was typed by Rhonda Stumbaugh.

AFIT RESEARCH ASSESSMENT

The purpose of this questionnaire is to ascertain the value and/or contribution of research accomplished by students or faculty of the Air Force Institute of Technology (AFIT). It would be greatly appreciated if you would complete the following questionnaire and return it to:

AFIT/NR
Wright-Patterson AFB OH 45433

RESEARCH TITLE: The Interrelationships and Variations of the Resistivity, Porosity, and Permeability as Functions of Pressure in a Geopressured Reservoir

AUTHOR: Thomas Robert Ashman

RESEARCH ASSESSMENT QUESTIONS:

1. Did this research contribute to a current Air Force project?
☐ a. YES ☐ b. NO
2. Do you believe this research topic is significant enough that it would have been researched (or contracted) by your organization or another agency if AFIT had not?
☐ a. YES ☐ b. NO
3. The benefits of AFIT research can often be expressed by the equivalent value that your agency achieved/received by virtue of AFIT performing the research. Can you estimate what this research would have cost if it had been accomplished under contract or if it had been done in-house in terms of manpower and/or dollars?
☐ a. MAN-YEARS ☐ b. \$
4. Often it is not possible to attach equivalent dollar values to research, although the results of the research may, in fact, be important. Whether or not you were able to establish an equivalent value for this research (3. above), what is your estimate of its significance?
☐ a. HIGHLY SIGNIFICANT ☐ b. SIGNIFICANT ☐ c. SLIGHTLY SIGNIFICANT ☐ d. OF NO SIGNIFICANCE
5. AFIT welcomes any further comments you may have on the above questions, or any additional details concerning the current application, future potential, or other value of this research. Please use the bottom part of this questionnaire for your statement(s).

NAME _____ GRADE _____ POSITION _____

ORGANIZATION _____ LOCATION _____

STATEMENT(s): _____

THE INTERRELATIONSHIPS AND VARIATIONS OF THE RESISTIVITY,
POROSITY, AND PERMEABILITY AS FUNCTIONS OF PRESSURE
IN A GEOPRESSURED RESERVOIR

BY

THOMAS ROBERT ASHMAN, B. S.

THESIS

Presented to the Faculty of the Graduate School of
The University of Texas at Austin
in Partial Fulfillment
of the Requirements
for the Degree of
MASTER OF SCIENCE IN ENGINEERING

THE UNIVERSITY OF TEXAS AT AUSTIN

August 1981

ACKNOWLEDGEMENTS

The author is indebted to Dr. K. E. Gray for his support throughout the project. The author also thanks the other members of his committee, Dr. T. W. Thompson and Dr. P. N. Jogi for their suggestions and recommendations.

The author is especially appreciative of the efforts and help provided him by Dr. P. N. Jogi and Mr. C. Stephenson. Both individuals gave invaluable assistance in the day-to-day work required for completion of this thesis. Appreciation is also extended to all members of the staff at the Center for Earth Sciences and Engineering but especially to the following individuals who provided needed support: Mr. P. Mewhinney, Mr. F. Barth, Mr. T. Bermudez, Dr. S. Kalra, Mr. K. Burkett, Mr. L. Carpenter, and Mr. B. Stadelman. Thanks are also due to Mrs. R. Stumbaugh of the Center for preparing this manuscript and to Ms. J. Canfield for her help in finalizing the data.

Financing of this work by the Center for Earth Sciences and Engineering and the United States Department of Energy is gratefully acknowledged.

T. R. A.

Austin, Texas
June 1981

ABSTRACT

Fluid production from both normally and abnormally pressured reservoirs has long been recognized as a function of the formation fluid properties and the reservoir rock parameters. Fluid production itself, however, changes the stress state of the reservoir resulting in rock deformation which affects total fluid and, therefore, energy recovery.

This study was undertaken as part of a project to determine and predict the effects of fluid production on the Pleasant Bayou geopressured, geothermal reservoir in Brazoria County, Texas. Data was collected from triaxial loading tests conducted on sandstone samples cored from the potential producing horizons of the reservoir. All tests were conducted at overburden and pore pressures which simulated insitu conditions. Empirical relations were developed which reflected changes in the resistivity, porosity, and permeability as functions of the effective stress. Relationships among the parameters were found to be of practical use in predicting formation changes as the reservoir stress state changed due to fluid withdrawal.

Results showed that the resistivity, porosity, and permeability were dependent on the effective stresses in the reservoir. The cementation factor in Archie's equation was also found to be a pressure function. In contrast, using the electrical and hydraulic conductivity analog, the product of the formation factor and the permeability was found to be independent of pressure.

TABLE OF CONTENTS

| | Page |
|---|-------|
| ACKNOWLEDGEMENTS | 111 |
| ABSTRACT | iv |
| LIST OF FIGURES | vii |
| LIST OF TABLES | xviii |
| I. INTRODUCTION AND SCOPE OF INVESTIGATION | 1 |
| I.1 Introduction | 1 |
| I.2 Scope of Investigation | 5 |
| II. REVIEW OF LITERATURE | 7 |
| II.1 Deformation Studies Relating to Porosity and Permeability | 7 |
| II.2 Resistivity Studies | 9 |
| III. THEORETICAL CONSIDERATIONS | 13 |
| III.1 Effective Stress Concepts | 13 |
| III.2 Resistivity and Porosity Relationships | 14 |
| III.3 Resistivity and Permeability Relationships | 16 |
| IV. EQUIPMENT AND EXPERIMENTAL PROCEDURE | 19 |
| IV.1 Simultaneous Property System | 19 |
| IV.2 Pore Fluid System | 22 |
| IV.3 Sample Preparation | 23 |
| IV.4 Test Procedure | 27 |
| V. ANALYSIS OF EXPERIMENTAL RESULTS | 33 |
| V.1 Resistivity Changes with Effective Stress | 33 |
| V.2 Porosity Changes with Effective Stress | 63 |

| | Page |
|--|------|
| V.3 Permeability Changes with Effective Stress | 94 |
| V.4 Discussion of Results | 99 |
| VI. CONCLUSIONS AND RECOMMENDATIONS | 109 |
| VI.1 Conclusions | 109 |
| VI.2 Recommendations | 110 |
| APPENDIX I. RESISTIVITY MEASUREMENT, APPLICATION AND DEPENDENCE | 111 |
| A. Resistivity Measurement Methods | 111 |
| B. Application of Radial Resistivity Measurements | 118 |
| C. Pressure Dependence of Resistivity | 120 |
| APPENDIX II. EQUIPMENT CALIBRATION AND SENSITIVITIES | 126 |
| NOMENCLATURE | 130 |
| BIBLIOGRAPHY | 133 |
| VITA | |

LIST OF FIGURES

| Figure | Page |
|---|------|
| 1. Relative Locations of the Fairways Comprising the Gulf Coast Geothermal Province | 3 |
| 2. Location of the Pleasant Bayou Reservoir in Brazoria County, Texas | 4 |
| 3. The Simultaneous Property System (SPS) | 20 |
| 4. Rock Sample Equipped with Strain Gauges, and Ends Coated with Epoxy | 21 |
| 5. Empty Core Jacket | 24 |
| 6. Passthrough Shoes | 25 |
| 7. Pressure Loading Sequence for Hydrostatic Compression Test at Elevated Pore Pressure | 29 |
| 8. Pressure Loading Sequence for Uniaxial Compaction Test . . | 30 |
| 9. Pressure Loading Sequence for Hydrostatic Compression Test at Atmospheric Pore Pressure | 32 |
| 10. Comparisons of Various Hydrostatic Compression Tests (#14699) | 34 |
| 11. Comparisons of Various Hydrostatic Compression Tests (#15688) | 35 |
| 12. Comparisons of Various Hydrostatic Compression Tests (#14702) | 36 |
| 13. Comparisons of Various Hydrostatic Compression Tests (#14711) | 37 |

| Figure | Page |
|--|------|
| 26. Graph Showing Log F as a Function of Effective Stress (#15665) | |
| a.) Hydrostatic Compression Test ($P_A = P_C = 7.85$ kpsi) | |
| b.) Uniaxial Compaction Test ($P_A = 7.85$ kpsi). | 52 |
| 27. Graph Showing Log F as a Function of Effective Stress (#11755) | |
| a.) Hydrostatic Compression Test ($P_A = P_C = 6.0$ kpsi) | |
| b.) Hydrostatic Compression Test ($P_A = P_C = 12.0$ kpsi) | |
| c.) Uniaxial Compaction Test ($P_A = 6.0$ kpsi) | |
| d.) Uniaxial Compaction Test ($P_A = 12.0$ kpsi). | 53 |
| 28. Graph Showing Log F as a Function of Effective Stress (#14702) | |
| a.) Hydrostatic Compression Test ($P_A = P_C = 7.35$ kpsi) | |
| b.) Hydrostatic Compression Test ($P_A = P_C = 14.7$ kpsi) | |
| c.) Uniaxial Compaction Test ($P_A = 7.35$ kpsi) | |
| d.) Uniaxial Compaction Test ($P_A = 14.7$ kpsi). | 54 |
| 29. Graph Showing Log F as a Function of Effective Stress (#14699) | |
| a.) Hydrostatic Compression Test ($P_A = P_C = 7.35$ kpsi) | |
| b.) Hydrostatic Compression Test ($P_A = P_C = 14.7$ kpsi) | |
| c.) Uniaxial Compaction Test ($P_A = 7.35$ kpsi) | |
| d.) Uniaxial Compaction Test ($P_A = 14.7$ kpsi). | 55 |
| 30. Graph Showing Log F as a Function of Effective Stress (#14696B) | |

| Figure | Page |
|--|------|
| a.) Hydrostatic Compression Test ($P_A = P_C = 7.35$ kpsi) | |
| b.) Uniaxial Compaction Test ($P_A = 14.7$ kpsi) | 56 |
| 31. Graph Showing Log F as a Function of Effective Stress (#15668) | |
| a.) Hydrostatic Compression Test ($P_A = P_C = 7.85$ kpsi) | |
| b.) Hydrostatic Compression Test ($P_A = P_C = 15.7$ kpsi) | |
| c.) Uniaxial Compaction Test ($P_A = 7.85$ kpsi) | |
| d.) Uniaxial Compaction Test ($P_A = 15.7$ kpsi) | 57 |
| 32. Graph Showing Log F as a Function of Effective Stress (#14712) | |
| a.) Hydrostatic Compression Test ($P_A = P_C = 7.35$ kpsi) | |
| b.) Uniaxial Compaction Test ($P_A = 7.35$ kpsi) | |
| c.) Uniaxial Compaction Test ($P_A = 14.7$ kpsi) | 58 |
| 33. Graph Showing Log F as a Function of Effective Stress (#14696A) | |
| a.) Hydrostatic Compression Test ($P_A = P_C = 7.5$ kpsi) | |
| b.) Hydrostatic Compression Test ($P_A = P_C = 15.0$ kpsi) | |
| c.) Uniaxial Compaction Test ($P_A = 7.5$ kpsi) | |
| d.) Uniaxial Compaction Test ($P_A = 15.0$ kpsi) | 59 |
| 34. Graph Showing Log F as a Function of Effective Stress (#14751) | |
| a.) Hydrostatic Compression Test ($P_A = P_C = 7.0$ kpsi) | |
| b.) Uniaxial Compaction Test ($P_A = 7.38$ kpsi) | 60 |
| 35. Graph Showing Log F as a Function of Effective Stress (#14711) | |

| Figure | Page |
|---|------|
| a.) Hydrostatic Compression Test ($P_A = P_C = 7.35$ kpsi) | |
| b.) Hydrostatic Compression Test ($P_A = P_C = 14.7$ kpsi) | |
| c.) Uniaxial Compaction Test ($P_A = 7.35$ kpsi) | |
| d.) Uniaxial Compaction Test ($P_A = 14.7$ kpsi) | 61 |
| 36. Graph Showing Log F as a Function of Effective Stress (#14703) | |
| a.) Hydrostatic Compression Test ($P_A = P_C = 12.0$ kpsi) | |
| b.) Uniaxial Compaction Test ($P_A = 14.7$ kpsi) | 62 |
| 37. Graph Showing Porosities as Functions of Effective Stress (#15665) | |
| a.) Hydrostatic Compression Test ($P_A = P_C = 7.85$ kpsi) | |
| b.) Uniaxial Compaction Test ($P_A = 7.85$ kpsi) | 70 |
| 38. Graph Showing Porosities as Functions of Effective Stress (#11755) | |
| a.) Hydrostatic Compression Test ($P_A = P_C = 6.0$ kpsi) | |
| b.) Hydrostatic Compression Test ($P_A = P_C = 12.0$ kpsi) | |
| c.) Uniaxial Compaction Test ($P_A = 6.0$ kpsi) | |
| d.) Uniaxial Compaction Test ($P_A = 12.0$ kpsi) | 71 |
| 39. Graph Showing Porosities as Functions of Effective Stress (#14702) | |
| a.) Hydrostatic Compression Test ($P_A = P_C = 7.35$ kpsi) | |
| b.) Hydrostatic Compression Test ($P_A = P_C = 14.7$ kpsi) | |
| c.) Uniaxial Compaction Test ($P_A = 7.35$ kpsi) | |
| d.) Uniaxial Compaction Test ($P_A = 14.7$ kpsi) | 72 |

40. Graph Showing Porosities as Functions of Effective Stress
(#14699)
- a.) Hydrostatic Compression Test ($P_A = P_C = 7.35$ kpsi)
 - b.) Hydrostatic Compression Test ($P_A = P_C = 14.7$ kpsi)
 - c.) Uniaxial Compaction Test ($P_A = 7.35$ kpsi)
 - d.) Uniaxial Compaction Test ($P_A = 14.7$ kpsi). 73
41. Graph Showing Porosities as Functions of Effective Stress
(#14696B)
- a.) Hydrostatic Compression Test ($P_A = P_C = 7.35$ kpsi)
 - b.) Uniaxial Compaction Test ($P_A = 14.7$ kpsi). 74
42. Graph Showing Porosities as Functions of Effective Stress(#15668)
- a.) Hydrostatic Compression Test ($P_A = P_C = 7.85$ kpsi)
 - b.) Hydrostatic Compression Test ($P_A = P_C = 15.7$ kpsi)
 - c.) Uniaxial Compaction Test ($P_A = 7.85$ kpsi)
 - d.) Uniaxial Compaction Test ($P_A = 15.7$ kpsi). 75
43. Graph Showing Porosities as Functions of Effective Stress(#14712)
- a.) Hydrostatic Compression Test ($P_A = P_C = 7.35$ kpsi)
 - b.) Uniaxial Compaction Test ($P_A = 7.35$ kpsi)
 - c.) Uniaxial Compaction Test ($P_A = 14.7$ kpsi) 76
44. Graph Showing Porosities as Functions of Effective Stress
(#14696A)
- a.) Hydrostatic Compression Test ($P_A = P_C = 15.0$ kpsi)
 - b.) Uniaxial Compaction Test ($P_A = 7.5$ kpsi)
 - c.) Uniaxial Compaction Test ($P_A = 15.0$ kpsi) 77

| Figure | Page |
|--|------|
| 45. Graph Showing Porosities as Functions of Effective Stress (#14751) | |
| a.) Hydrostatic Compression Test ($P_A = P_C = 7.0$ kpsi) | |
| b.) Uniaxial Compaction Test ($P_A = 7.38$ kpsi) | 78 |
| 46. Graph Showing Porosities as Functions of Effective Stress (#14765) | |
| Uniaxial Compaction Test ($P_A = 14.765$ kpsi). | 79 |
| 47. Graph Showing Porosities as Functions of Effective Stress (#14711) | |
| a.) Hydrostatic Compression Test ($P_A = P_C = 7.35$ kpsi) | |
| b.) Hydrostatic Compression Test ($P_A = P_C = 7.35$ kpsi) | |
| c.) Uniaxial Compaction Test ($P_A = 7.35$ kpsi) | |
| d.) Uniaxial Compaction Test ($P_A = 14.7$ kpsi) | 80 |
| 48. Graph Showing Porosities as Functions of Effective Stress (#14703) | |
| a.) Hydrostatic Compression Test ($P_A = P_C = 12.0$ kpsi) | |
| b.) Uniaxial Compaction Test ($P_A = 14.7$ kpsi) | 81 |
| 49. Graph Showing F as a Function of Porosity and Effective Stress (#15665) | |
| a.) Hydrostatic Compression Test ($P_A = P_C = 7.85$ kpsi) | |
| b.) Uniaxial Compaction Test ($P_A = 7.85$ kpsi) | 82 |
| 50. Graph Showing F as a Function of Porosity and Effective Stress (#11755) | |
| a.) Hydrostatic Compression Test ($P_A = P_C = 6.0$ kpsi) | |

| Figure | Page |
|--|------|
| <ul style="list-style-type: none"> b.) Hydrostatic Compression Test ($P_A = P_C = 12.0$ kpsi) c.) Uniaxial Compaction Test ($P_A = 6.0$ kpsi) d.) Uniaxial Compaction Test ($P_A = 12.0$ kpsi) | 83 |
| 51. Graph Showing F as a Function of Porosity and Effective Stress (#14702) | |
| <ul style="list-style-type: none"> a.) Hydrostatic Compression Test ($P_A = P_C = 7.35$ kpsi) b.) Hydrostatic Compression Test ($P_A = P_C = 14.7$ kpsi) c.) Uniaxial Compaction Test ($P_A = 7.35$ kpsi) d.) Uniaxial Compaction Test ($P_A = 14.7$ kpsi) | 84 |
| 52. Graph Showing F as a Function of Porosity and Effective Stress (#14699) | |
| <ul style="list-style-type: none"> a.) Hydrostatic Compression Test ($P_A = P_C = 7.35$ kpsi) b.) Hydrostatic Compression Test ($P_A = P_C = 14.7$ kpsi) c.) Uniaxial Compaction Test ($P_A = 7.35$ kpsi) d.) Uniaxial Compaction Test ($P_A = 14.7$ kpsi) | 85 |
| 53. Graph Showing F as a Function of Porosity and Effective Stress (#14696B) | |
| <ul style="list-style-type: none"> a.) Hydrostatic Compression Test ($P_A = P_C = 7.35$ kpsi) b.) Uniaxial Compaction Test ($P_A = 14.7$ kpsi) | 86 |
| 54. Graph Showing F as a Function of Porosity and Effective Stress (#15688) | |
| <ul style="list-style-type: none"> a.) Hydrostatic Compression Test ($P_A = P_C = 7.35$ kpsi) b.) Hydrostatic Compression Test ($P_A = P_C = 15.7$ kpsi) c.) Uniaxial Compaction Test ($P_A = 7.85$ kpsi) d.) Uniaxial Compaction Test ($P_A = 15.7$ kpsi) | 87 |

| Figure | Page |
|--|------|
| 55. Graph Showing F as a Function of Porosity and Effective Stress (#14712) | |
| a.) Hydrostatic Compression Test ($P_A = P_C = 7.35$ kpsi) | |
| b.) Uniaxial Compaction Test ($P_A = 7.35$ kpsi) | |
| c.) Uniaxial Compaction Test ($P_A = 14.7$ kpsi) | 88 |
| 56. Graph Showing F as a Function of Porosity and Effective Stress (#14696A) | |
| a.) Hydrostatic Compression Test ($P_A = P_C = 15.0$ kpsi) | |
| b.) Uniaxial Compaction Test ($P_A = 7.5$ kpsi) | |
| c.) Uniaxial Compaction Test ($P_A = 15.0$ kpsi) | 89 |
| 57. Graph Showing F as a Function of Porosity and Effective Stress (#14765 kpsi) | |
| Uniaxial Compaction Test ($P_A = 14.765$ kpsi) | 90 |
| 58. Graph Showing F as a Function of Porosity and Effective Stress (#14751) | |
| a.) Hydrostatic Compression Test ($P_A = P_C = 7.0$ kpsi) | |
| b.) Uniaxial Compaction Test ($P_A = 7.38$ kpsi) | 91 |
| 59. Graph Showing F as a Function of Porosity and Effective Stress (#14711) | |
| a.) Hydrostatic Compression Test ($P_A = P_C = 7.35$ kpsi) | |
| b.) Hydrostatic Compression Test ($P_A = P_C = 14.7$ kpsi) | |
| c.) Uniaxial Compaction Test ($P_A = 7.35$ kpsi) | |
| d.) Uniaxial Compaction Test ($P_A = 14.7$ kpsi) | 92 |

| Figure | Page |
|---|------|
| 60. Graph Showing F as a Function of Porosity and Effective Stress (#14703) | |
| a.) Hydrostatic Compression Test ($P_A = P_C = 12.0$ kpsi) | |
| b.) Uniaxial Compaction Test ($P_A = 14.7$ kpsi) | 93 |
| 61. General Permeability Trend with Effective Stress (#14711) | 97 |
| 62. Regression Line of Normalized $k \times F$ Product as a Function of Effective Stress (All Tests). | 98 |
| 63. Comparisons of Porosities Obtained from Measured Data and From Eqn. 5.12 (#14696B, Uniaxial Compaction Test) . | 106 |
| 64. Comparisons of Permeabilities Obtained From Measured Data and From Eqn. 5.18 (#14699, Uniaxial Compaction Test). | 108 |
| A1-1 Resistivity Circuitry Diagram Showing Voltage Drops Within the System. | 112 |
| A1-2 Frequency Dependence of Resistivity Measurements Made on Two Berea Sandstone Samples | 115 |
| A1-3 Arrangement of Measurement Probes on a Berea Sample used for Two-Electrode and Four-Electrode Resistivity Tests. | 116 |
| A1-4 Comparison of Resistivities Obtained From Two-Electrode and Four-Electrode Methods | 117 |
| A1-5 Cut Samples of Berea Sandstone used for Testing Radial Resistivity Measurements (Eqn. 3.9) | 119 |

| Figure | Page |
|---|------|
| A1-6A Perspex Apparatus used for Measuring Brine & 6B Resistivities (Shown Laid between Heads of the SPS) | 122 |
| A1-7 Graph of 6% NaCl Solution Resistivity as a Function of Pressure | 125 |

LIST OF TABLES

| Table | Page |
|---|------|
| 1. Relative Comparisons of Porosity Reductions with Effective Stress | 66 |
| 2. Coefficients of the Cementation Factor and Formation Factor Expressions | 102 |
| 3. Statistical Parameters for the Coefficients of the Cementation Factor and Formation Factor Expressions | 103 |
| 4. Comparison of Measured and Calculated Porosities for Several Rock Samples | 104 |
| 5. Comparison of Measured and Calculated Porosities for a Typical Rock Sample (#14696B). | 105 |
| 6. Comparisons of Measured and Calculated Permeabilities for Several Rock Samples | 107 |
| A2-1. Equipment Calibrations as Functions of Pressure. . . . | 128 |
| A2-2. Sensitivities for Pressure-Sensing Devices and Rosette Strain Gauges. | 129 |

I. INTRODUCTION AND SCOPE OF THE INVESTIGATION

I.1 Introduction

With alternate forms of energy becoming more and more economically attractive, much interest and research is being focused on geopressured, geothermal reservoirs. These reservoirs contain significant amounts of methane held in solution and are also a viable thermal energy source. However, fluid production over time changes the stress state of the formations which can detrimentally affect the ultimate energy recovery. Therefore, a broad knowledge of the deformation characteristics of the reservoir rocks and of the resulting changes in permeability, porosity, resistivity, and bulk volume is a desirable goal.

Changes in the permeability, porosity, and resistivity which result from changes in the stress state have been approached from several directions. They have been related to deformation of rock under pressure and, therefore, have been extensively studied as direct functions of pressure. Many investigators have approached these parameters from this "rock mechanics" point of view. Most of the studies, however, have been conducted under atmospheric pore pressure conditions which do not fully simulate the insitu state.

Another approach has been to relate the resistivity of rock to its permeability and porosity. This approach is quite practical since the formation resistivity is a measurable parameter via electric logging.

The present work represents both of these viewpoints and was undertaken to study the influence of the effective stress on the re-

sistivity, porosity, and permeability of samples from the Gulf Coast geothermal province. Specifically, an attempt has been made to determine the empirical relationships among these three parameters and between them and the effective stress at elevated, insitu pore pressures. Tests were conducted on samples extracted from wells drilled in the Department of Energy's Pleasant Bayou Geothermal Reservoir in Brazoria County, Texas. Figures 1 and 2 depict the province and reservoir locations.

The Pleasant Bayou prospect is characterized by several geopressured, geothermal zones. Pressures exceed the normal hydrostatic saltwater head by 150% and correspond to a pressure gradient as high as 0.78 psi/ft. Temperatures range from 250°F to 350°F. According to Bebout et al.¹ the reservoir with the best overall quality is a medium to coarse-grained, bedload, fluvial, channel deposit at 14,640 to 14,710 feet. These Frio reservoir sands, however, are also found in other distinct zones from 11,750 to 16,050 feet. Samples were extracted from various depths within this depth range.

This work was undertaken to obtain experimental data to predict the effects of fluid production on the reservoir. As the reservoir is exploited, formation pressures decline resulting in an increase in effective stress and causing possible formation compaction, porosity and permeability reduction, and a fluid recovery decrease.

Empirical equations were developed based on experimental results and previous works^{14,15,17,21,23} which showed the interrelationships among the porosity, permeability, and resistivity. These equations can be practically applied and are useful in estimating the changes in

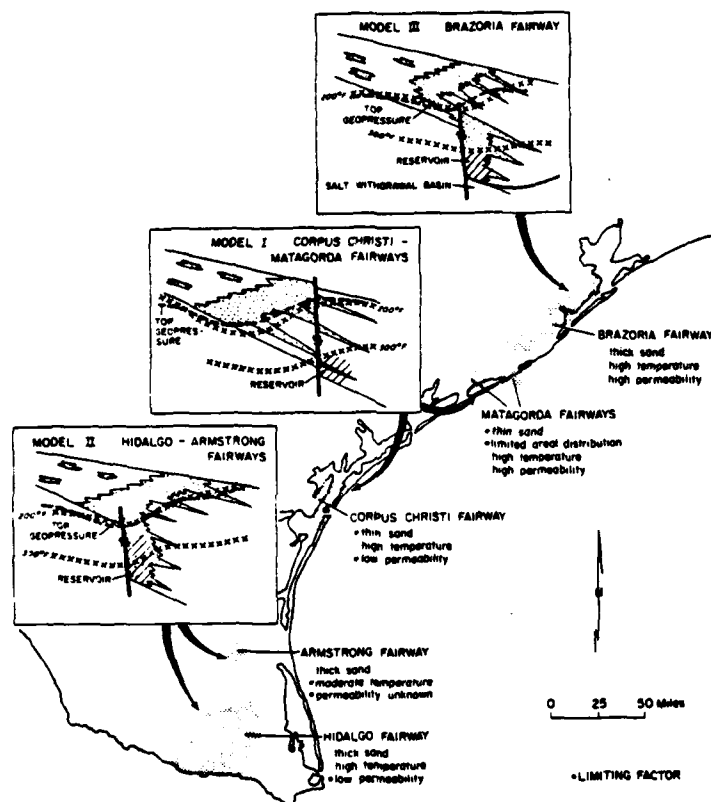


FIGURE 1 RELATIVE LOCATIONS OF THE FAIRWAYS COMPRISING THE GULF COAST GEOTHERMAL PROVINCE (FROM BEBOUT, LOUCKS, AND GREGORY¹)

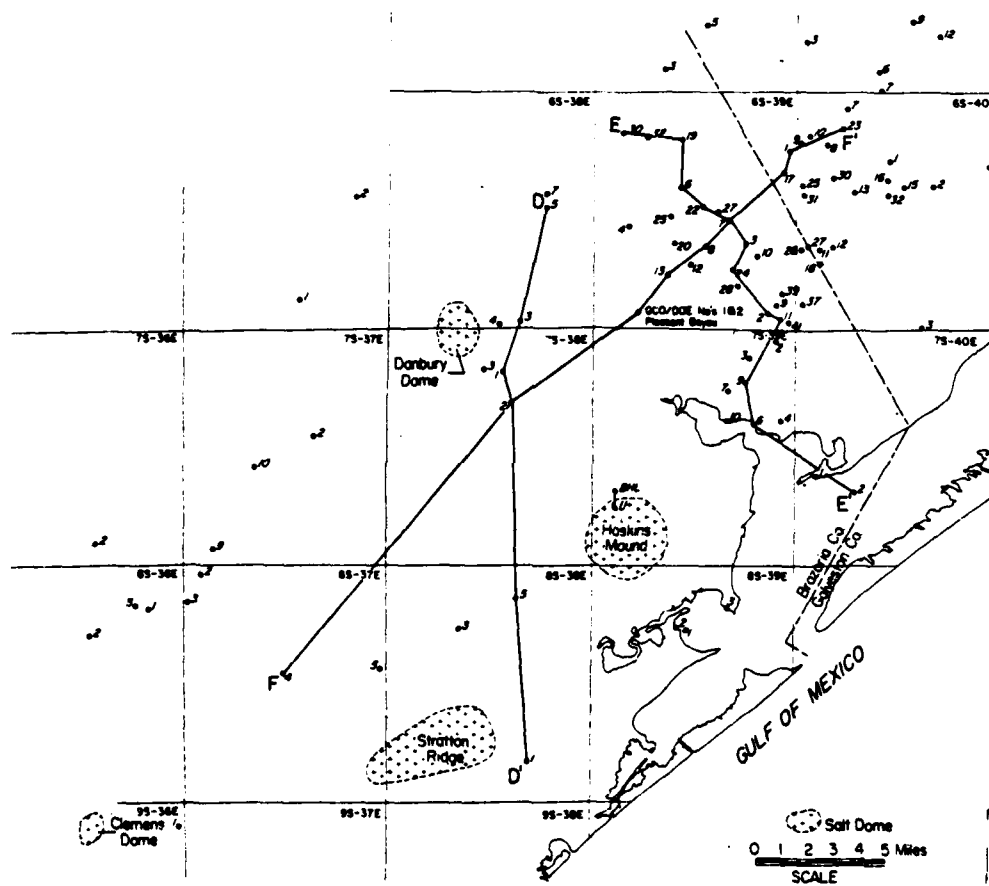


FIGURE 2 LOCATION OF THE PLEASANT BAYOU RESERVOIR IN BRAZORIA COUNTY, TEXAS (FROM BEBOUT, LOUCKS, AND GREGORY¹)

porosity and permeability with effective stress throughout the producing life of the reservoir.

I.2 Scope of Investigation

A review of literature shows that most previous studies on resistivity measurements have been conducted under atmospheric pore pressure conditions, which do not adequately simulate the insitu stress state. In addition, none of these investigations have resulted in practical equations for use in estimating changes in the resistivity, permeability, and porosity with decline of formation pressure.

The objective of this work was to formulate empirical relationships for these parameters as functions of the effective stress. Formation, overburden, and confining pressures were applied to the rock samples which essentially duplicated what were considered to be insitu conditions. Pore pressures were reduced to simulate fluid production, and measurements were taken of the resultant resistivity, permeability, and porosity changes. Results were used to check the validity of the Archie equation and Humble formula under effective stress variations. Relationships were derived in this study which will be helpful in more accurately predicting reservoir fluid and, therefore, energy recovery.

Chapter II provides a review of pertinent literature concerning the interrelationships among and functional properties of resistivity, porosity, and permeability. Chapter III develops the theoretical basis on which this current work rests. Chapter IV presents a description of the equipment utilized and the experimental methods employed. The results obtained from the experiments are analyzed in Chapter V. Also, relationships are developed relating resistivity, porosity and per-

meability to the effective stress state. Finally, in Chapter VI, conclusions from the study are given and some suggestions for future work are discussed.

II. REVIEW OF LITERATURE

II.1 Deformation Studies Relating to Porosity and Permeability

Deformation behavior of rocks and its effects on porosity and permeability have been the subject of many studies. A comprehensive review of literature on the subject has been provided by Scorer and Miller² and Friedman.³ While Scorer and Miller discussed compressibility, porosity and permeability as functions of pressure, Friedman concerned his review mainly with the influence of porosity and permeability on the mechanical behavior of rocks.

Terzaghi⁴ provided the basic concept of effective stress on which most work in soil mechanics and rock mechanics is based. Biot⁵ generalized the concept to the three dimensional case and presented the classical theory of three dimensional consolidation of porous media.

Geertsma⁶ generalized these theories to include viscoelastic deformations in porous rocks. He obtained mathematical relationships for pore and bulk volumetric changes in terms of the effective pressure. He found that three elastic constants and three viscous constants, besides porosity, were needed to describe the volumetric variations in the rock. His experimental results showed that consolidated sandstones deformed essentially elastically.

Nur and Byerlee⁷ derived an exact expression for an effective stress law for elastic deformation of aggregates with pore pressure. Their work demonstrated the exactness and usefulness of the effective stress concept.

Hall⁸ demonstrated experimentally that rock compressibility in undersaturated reservoirs was a strong function of overburden load. He showed that porosity reductions with increasing overburden pressure could significantly effect fluid-in-place calculations.

Fatt⁹ obtained similar results in his studies on porosity and permeability changes in sandstones as functions of overburden pressure. He concluded, however, that porosity changes were negligible, but permeability reductions were large enough to warrant consideration. He used the term "effective permeability" to represent the permeability downhole at high pressure conditions.

Gangi¹⁰ determined theoretical variations of porosity and permeability with applied pressure using phenomenological models based on the Hertz Theory of deformation of spheres. He obtained nonlinear expressions for porosity and permeability as functions of the externally applied pressure which were shown by him to exhibit most of the characteristics of experimental data obtained by others.

Yoelin¹¹ found that variations in bulk compressibility with pressure were usually more significant than changes in porosity. He discovered, however, that some highly compressible sandstones reflected disproportionately greater pore volume variations with increasing overburden pressure.

Gray et al.¹² in their work with rock samples from the geopressured provinces of south Texas, observed small (1-2%) pore volume reductions and significant (10%) permeability declines over a 7,000 psi effective stress range. They found that dynamically determined values of porosity bear very little relation to porosities determined statically.

Even though results from the two methods were closer at high effective stresses, considerable discrepancy still existed. They also found that compaction coefficients were much lower than previously assumed and that in many cases the rocks were considerably inelastic.

II.2 Resistivity Studies

Literature concerning resistivity of formations has long been associated with electric logging. Resistivity and spontaneous potential measurements were the sole purpose of early logging techniques.¹³ The applications of resistivity data since then have grown and have been studied by many investigators.

The classical works of Archie¹⁴ and Winsauer et al.¹⁵ pervade most literature on formation resistivity. Archie developed the concept of formation factor which is defined as the ratio of the resistivity of a 100% saturated rock to the resistivity of the solute. He observed from experimental data that a reasonably accurate relationship existed between the formation factor and the rock porosity at atmospheric pressure. This relationship is expressed as:

$$F = \phi^{-m} \quad 2.1$$

where

F = formation factor

ϕ = porosity (decimal)

m = slope of the log-log linear equation

He found that for loosely or partly consolidated sands of the Gulf Coast, m values varied from 1.3 to 2.0.

Winsauer et al.¹⁵ performed a comprehensive study on the resistivity of brine saturated sands in relation to pore geometry. They developed an expression for the resistivity as a function of the tortuosity of pore channels in a porous rock. Through experiments they derived the following relationship between the formation factor and porosity:

$$F = 0.62 \phi^{-2.15}$$

2.2

Guyod¹⁶ studied the resistance of permeable, brine saturated formations from a more academic point of view. He considered the conductivity of formations dependent on several factors: 1) the amount of conductive solids in the rock; 2) the type and concentration of the solute; 3) the temperature and pressure of the solute; 4) the geometry of the pore space; 5) the shale content. Based upon his observations that the m exponent in Archie's equation (2.1) tended to increase from 1.3 to 2.2 when traversing from noncemented to highly cemented sandstones, he labelled the exponent the "cementation factor," a term which is currently used in literature.

Wyllie and Rose¹⁷ examined the theoretical basis of electric log interpretation and attempted to quantify the cementation factor and porosity parameters. They found the practical range of m varied from 1.3 to 3.0 but emphasized that m was really only of qualitative value. They realized that porosity could be computed only if m was specified, and concluded that tortuosity data obtainable from core analysis was necessary.

Owen¹⁸ agreed with Wyllie and Rose and stated that cementation factors were difficult to determine because of the complexity of the re-

lationship between resistivity and pore geometry. He used a synthetic pore system model to determine m values and found that they corresponded with the observations made by Archie and Guyod. He, like previous investigators, conducted his experiments at atmospheric pressure.

Wyble¹⁹ dealt with resistivity as a function of pressure. In his experimental work, he raised the confining pressure on sandstone samples and measured the resistivity and porosity. He obtained values for the cementation factor and Winsauer coefficient but did not treat them as variables.

Fatt²⁰ also viewed resistivity and porosity as functions of pressure. He showed, however, that the cementation factor was not a constant and that it changed with confining pressure.

Glanville²¹, in his work on formation factors, noted increases in the value of m as the effective stress on the rock samples was increased. He observed these variations at an elevated pore pressure and with changing confining pressure.

Redmond²² also found cementation factor values to increase with pressure. For overburden loads in the range of 10,000 to 15,000 psi, he noted that cementation factors for some sandstones were as high as 8.3. He also observed porosity changes from 7% to 20% over a 16,000 psi overburden pressure range, a variation which was higher than what was observed by other investigators. Finally, Redmond found that resistivity changes with pressure were less pronounced than corresponding changes in permeability.

Friedman,³ in his review, addressed the relationship between resistivity and permeability. He stated that the association between

conductivity, i.e. the reciprocal of resistivity, and the permeability (or hydraulic conductivity) was natural since both were analogously related to the ability of a rock to permit flow. Attempts to show such an analogous relationship, however, have not been successful.

Wyllie and Spangler²³ reported on permeability and resistivity tests made on Pennsylvanian sandstone. They found that for this clean sandstone resistivity decreased with increasing permeability. They concluded, however, that this relationship reflecting the permeability-resistivity analog might not be so apparent for rocks containing shale inclusions, mica flakes, or secondary cementation effects.

Boggus²⁴ found a similar basic relationship between permeability and resistivity for Berea, Pecos, and Banders sandstones. However, he, like Wyllie and Spangler, conducted his tests at atmospheric pressure under zero effective stress conditions.

Tixier²⁵ developed a method for evaluating permeability from electric log resistivity gradients. Although charts stemming from his studies are in use, they are applicable only for hydrocarbon reservoirs and do not attempt to support a universal analog between resistivity and permeability. Field correlations by Lebourg et al.²⁶ are similarly applicable.

Tellinghuisen²⁷ presented a laboratory method for simultaneous determination of rock resistivity and permeability at variable confining pressures. His results merely agreed with the findings of other researchers who studied these two parameters separately.

III. THEORETICAL CONSIDERATIONS

III.1 Effective Stress Concepts

The computations of the deformational characteristics of rocks as reflected in resistivity, porosity, and permeability changes in a producing reservoir were based on the theories developed by Terzaghi⁴ and Biot⁵. A brief explanation of the theory used is presented here.

A change in the pore pressure within the reservoir produces the same effects in the reservoir as an increased loading would. The concept of effective stress says that there is a one to one relationship between external load and pore fluid pressure. Effective stress in general is defined as:

$$P_E = P - P_O \quad 3.1$$

where

P_E = effective stress

P = externally applied stress (compression positive)

P_O = pore pressure

Although the form of the effective stress equation has found widespread acceptance and application, further studies have suggested that the relationship should be as presented by Biot:

$$P_E = P - \eta P_O \quad 3.2$$

where η = constant ≤ 1

The absolute value of η has not been agreed upon. Geertsma,⁶ however, proposed the following form for η :

$$\eta = 1 - \frac{C_R}{C_B} \quad 3.3$$

where

C_R = rock matrix compressibility

C_B = rock bulk compressibility

For most natural aggregates $C_R < C_B$ and $\eta \approx 1$. Therefore, equation 3.2 reduces to 3.1. It is clear from either equation, however, that a decrease in the pore pressure serves to increase the effective compressive stresses, thereby leading to compaction. Compaction of the rock in turn leads to porosity and permeability changes.

In a reservoir, this effective stress concept is useful in representing the rock stresses under insitu conditions. Provided lateral dimensions of the reservoir are large compared to its thickness, reservoirs are assumed to deform predominantly in the vertical plane. Formation compaction is, therefore, characterized by vertical deformation of the reservoir as a result of the effective stress change in the formation.

As a result of fluid withdrawal resulting in formation compaction, the resistivity, porosity, and permeability vary. These rock parameters can be related directly to the effective stress as shown in Sections III.2 and III.3.

III.2 Resistivity and Porosity Relationships

Resistivity as a useful rock parameter was utilized by Archie¹⁴ in his development of the formation factor as

$$F = \frac{R_R}{R_B} \quad 3.4$$

where

F = formation factor

R_R = resistivity of the 100% brine saturated rock
(ohm meters)

R_B = resistivity of the saturating brine (ohm meters)

Archie and later on, several other investigators^{15,16,17} found experimentally that the formation factor could be related to the porosity by

$$F = a \phi^{-m} \quad 3.5$$

where

ϕ = porosity (decimal)

a = constant

m = cementation factor

Equation 3.5 is merely a generalized form of equations 2.1 and 2.2. Values for the coefficient, a , and the exponent, m , vary depending on the rock type. Although in Archie's equation $a = 1$, Winsauer et al.¹⁵ specified $a = 0.62$ for consolidated sandstones. Wyllie and Rose¹⁷ showed that although values of m could range from 1 to infinity, the variations encountered in practice lay well within the limits of 1.3 and 3.0.

Both Archie and Winsauer obtained their results on rock samples under atmospheric pressure conditions. Many investigators^{9,10,19,22,27}, however, have shown that permeability and porosity are functions of pressure. The resistivity and, therefore, the formation factor in turn

have also shown to be pressure dependent.^{20,21,22,27} Two of these same studies^{20,21} have indicated that the cementation factor, m , is sensitive to pressure.

In view of these investigations, Archie's equation can be modified as follows:

$$F(P_E) = a \phi(P_E)^{-m(P_E)} \quad 3.6$$

For the equation to be theoretically correct, boundary conditions must hold. Therefore, since the formation factor should equal 1 for 100% formation porosity, $a = 1$. Equation 3.6, then, can be put into the following form:

$$F(P_E) = \phi(P_E)^{-m(P_E)} \quad 3.7$$

III.3 Resistivity and Permeability Relationships

The flow of current and the flow of fluid through rocks have often been termed analogous. Both resistivity and permeability are essentially dependent upon the same flow paths and subject to the same geometric considerations. Therefore, in rocks composed predominately of nonconductive solids, such as clean sandstones which exist in the producing horizons of a geopressed reservoir, the current flow should follow the same tortuous route as the hydrodynamic brine.

Morita²⁸ showed that in the laboratory radial flow through a cylindrical rock core could be represented by

$$k = \frac{q\mu}{(\Delta P)(L)(R_f)} \left(\frac{K_e}{K_e'} \right) (1000) \quad 3.8$$

where

k = permeability of the rock sample (millidarcies)

q = fluid flow rate (cc/sec)

μ = fluid viscosity (cp)

L = sample axial length (cm)

ΔP = differential pressure across core (atm)

R_f = correction factor for decreased flow rate
(dimensionless); (=0.94 for the work)

$\frac{K_e}{K_{e'}}$ = geometric correction factor (dimensionless);
(=1.00 for this work)

As an analog to Morita's whole core type permeameter, Tellinghuissen²⁷ used the following relationship for computing resistivity:

$$\frac{1}{R_R} = \frac{i}{(\Delta V)(L)(R_f)} \left(\frac{K_e}{K_{e'}} \right) \quad (100) \quad 3.9$$

where

R_R = rock resistivity (ohm-meters)

i = current flow (amperes)

ΔV = voltage drop radially across core (volts)

Appendix I discusses the reliability of resistivity values obtained using this equation.

The interrelationship between permeability and resistivity has also been the focus of several investigations.^{17,23,24,25,26} These studies, however, were not accomplished under varying effective stress conditions and no attempt was made to obtain a relationship between the permeability or resistivity and the pressure.

The interrelationship between permeability and resistivity can be approached using the fluid flow and current analogy discussed above with pressure as an independent variable. Permeability has often been labelled the hydraulic conductivity, a term now adopted by the U. S. Geological Survey. Likewise, resistivity can be called reciprocal electrical conductivity. Since the formation factor is a direct function of the resistivity, F must also be inversely related to the electrical conductivity. Also, since both permeability and formation factor are pressure dependent as discussed in Section III.2, the analogy between the two parameters would imply that a rock experiencing a decrease in permeability with effective stress would also experience a corresponding increase in formation factor. Intuitively then, the $F \times k$ product for a particular clean sandstone should be constant under changing effective stress conditions. This concept can be expressed as

$$F \times k = C \quad 3.10$$

where

C = constant (dependent upon the rock)

Substituting equation 3.7 into 3.10 and solving for k results in

$$k = \frac{C}{\phi(P_E)^{-m(P_E)}} \quad 3.11$$

The applicability of these two equations in relation to experimental results is discussed in Section V.3.

IV. EQUIPMENT AND EXPERIMENTAL PROCEDURE

IV.1 Simultaneous Property System (SPS)

The basic triaxial stress loading vessel and pressure control system, called SPS, which was developed at the Center for Earth Sciences and Engineering and is described in detail by Evans²⁹, was used for all experiments (Figure 3). This system is designed to make measurements on samples under confining pressures up to 30,000 psi and has independent controls for axial loads up to 60,000 psi and pore pressures up to 30,000 psi.

The equipment has the capability for simultaneous determination of static and dynamic moduli, permeability, porosity, and resistivity of rock samples at various stress levels. Static moduli including bulk compressibility, uniaxial compaction coefficient, matrix compressibility, Young's modulus, and Poisson's ratio can be calculated from radial and axial strains measured by two rosette strain gauges cemented onto the rock sample (Figure 4). Stresses are measured by BLH pressure transducers. Dynamic parameters can be calculated from acoustic travel times for p and s waves through the sample. The waves are generated and received by peizo-elastic crystals contained in the transmitting and receiving transducer cells located in the pressure vessel heads (Figure 3).

Permeability and porosity measurements were made using the MTS Intensifier and an HIP screw pump. The intensifier provides constant upstream pressure to cause fluid flow through the rock sample for per-

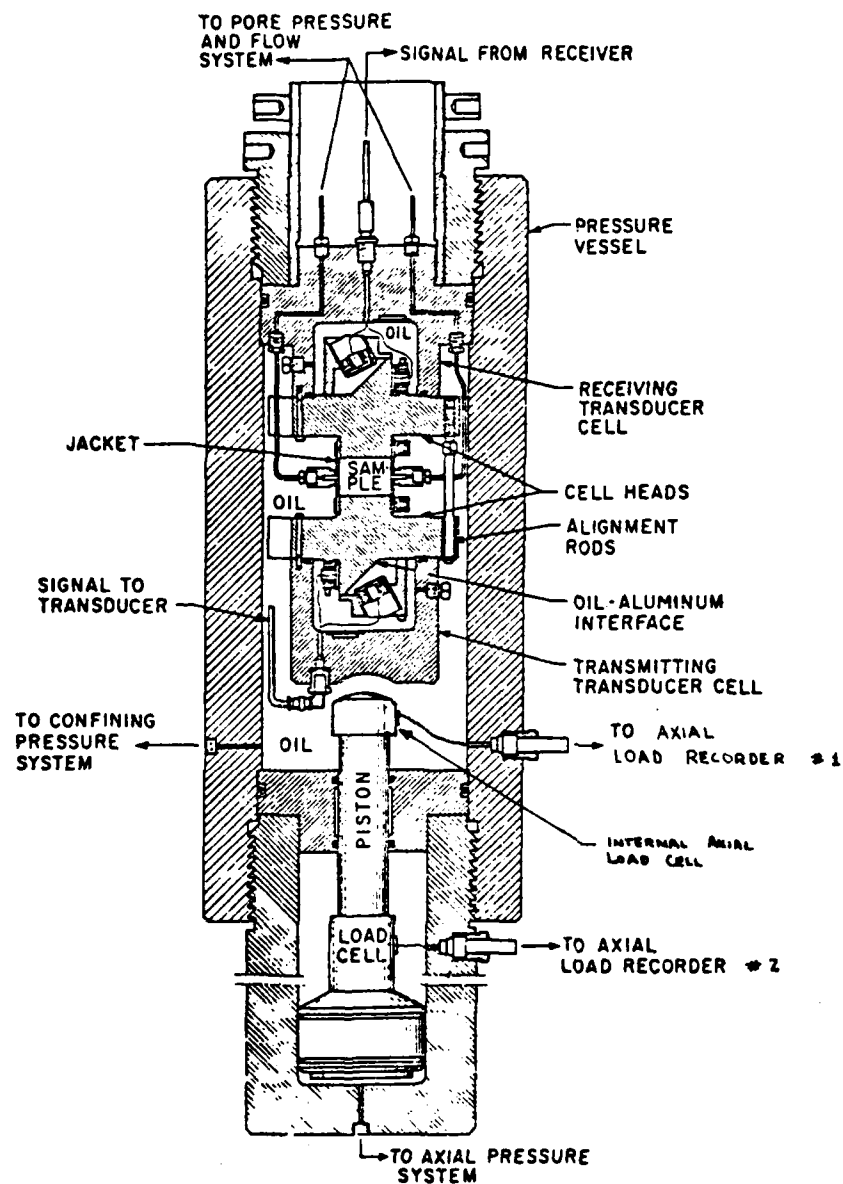


FIGURE 3 THE SIMULTANEOUS PROPERTY SYSTEM (SPS)

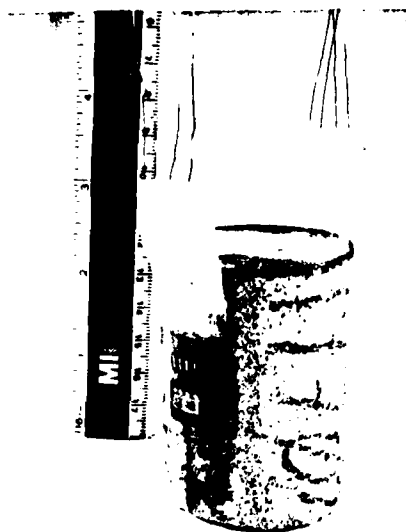


FIGURE 4 ROCK SAMPLE EQUIPPED WITH STRAIN GAUGES,
AND ENDS COATED WITH EPOXY (LEAD WIRES
ARE TAPED TO PREVENT SHORTING)

meability determination at any pore pressure. The screw pump serves to measure pore volume changes for porosity determination under elevated pore pressures. It is rated at 30,000 psi, has a capacity of 11cc, and can detect pore volume changes up to 0.005 cc. At atmospheric pore pressures, volume changes are determined by measurement of expelled fluid into an inverted pipette.

Resistivities were calculated from measured voltage drops across a rock sample incurred by current generated with a General Radio, 1310-B Oscillator. Electrical isolation of the rock sample was achieved by epoxy coatings on the sample ends, by delrin insulation fittings around the 1/8 inch high pressure tubing pore fluid lines, and by a teflon packed and seated high pressure valve installed in the external by-pass line. The actual resistivity measurements were made by closing the by-pass valve and observing the total voltage drop in the resistivity circuit and the voltage drop radially across the cylindrical rock sample. More detail on the methods employed is given in Appendix I.

IV.2 Pore Fluid System

The pore fluid system is an integral part of the SPS. The system can be divided into three components: 1) the pumping and pressure control equipment needed for pore pressure attainment; 2) the core jacket needed for containment of the sample; 3) the pore fluid measuring equipment needed for permeability and porosity determination.

The pressure component is comprised of a Sprague pump, HIP screw pump, MTS intensifier, BHL pressure and Validyne variable reluctance transducers, and associated Autoclave valves and 1/8 inch stainless steel

tubing. The detailed schematic of the system is available in Evans'²⁹ original work. Calibration data for the apparatus is given in Appendix II.

The core jacket is a polyurethane sleeve equipped with two pass-through "shoes." These industrial chromium plated stainless steel "shoes" are molded into the sleeve and serve as pore fluid passthroughs from the upstream fluid line to the core and from the core to the downstream fluid line. The "shoes" also act as current and voltage electrodes for resistivity tests. Figures 5 and 6 depict the core jacket and passthrough arrangement respectively. Tellinghuisen²⁷ provides detail on the basic jacket and "shoe" design.

The pore fluid measurement component is a simple arrangement for determination of flow rates and pore volume changes. A pipette, manual timer, and the MTS intensifier, which maintained a constant upstream pressure, provide necessary data for calculation of permeabilities. A system of pipettes connected to the downstream lines allow the measurement of pore volume changes at atmospheric pore pressure. The calibrated HIP screw pump described above is used to measure pore volume changes at elevated pore pressures.

IV.3 Sample Preparation

Sections of clean sandstone from reservoir depths of 11,700 to 15,700 feet were selected from 4 inch well cores obtained from Pleasant Bayou wells #1 and #2. Most of the sections tested, however, represented various producing zones. These sections were themselves cored perpendicular to the apparent bedding planes with a 2 inch I.D. diamond core barrel. The 2 inch cores were rough cut to a desired length with a

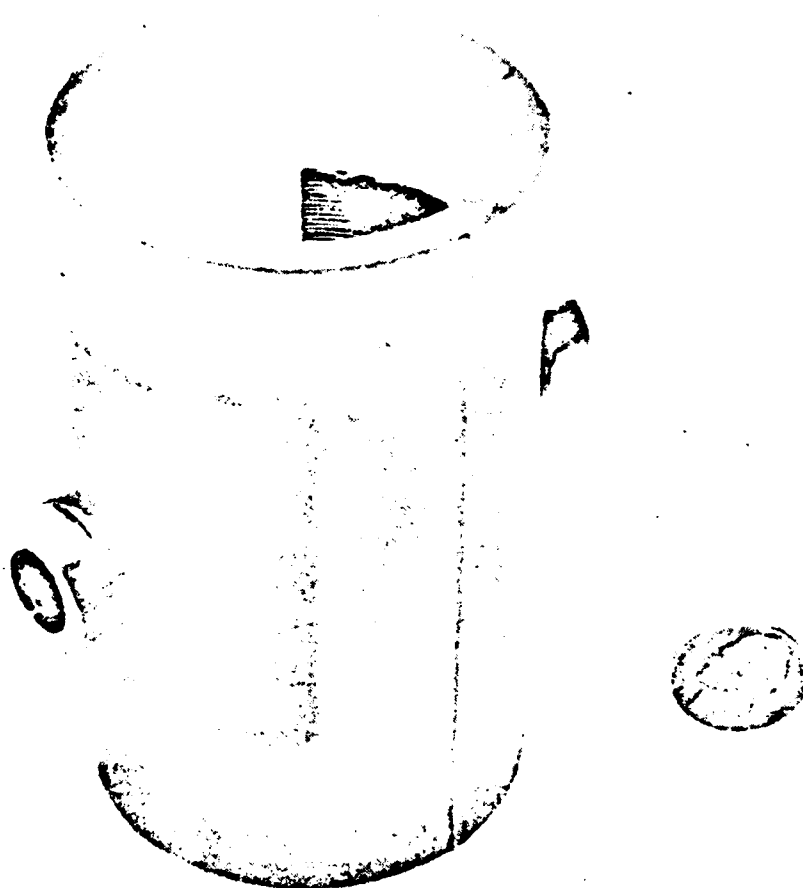


FIGURE 5 EMPTY CORE JACKET (FROM TELLINGHUISSEN²⁷)

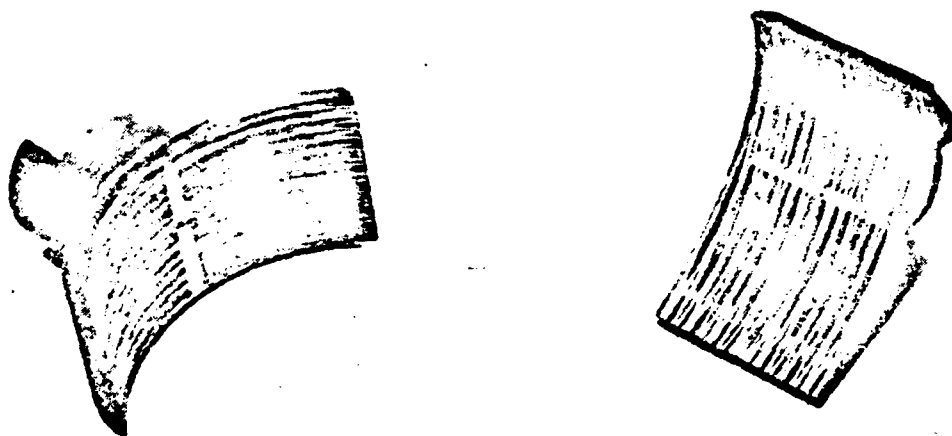


FIGURE 6 PASSTHROUGH SHOES (FROM TELLINGHUISSEN²⁷)

Felker diamond cut-off wheel and finally cut exactly to 2.75 inches on a lathe ensuring that the end faces were square with the sides. This 1.375 length-to-diameter ratio was selected to minimize end effects in the measurements.²⁹

The ends of the samples were epoxied with Armstrong A-12 adhesive and trimmed on a lathe to a 0.004 inch thickness on each end. This procedure isolated the rock sample electrically from the conductive heads of the pressure vessel for proper resistivity measurements. The epoxy did not penetrate significantly (which was checked by cutting coated samples) into the rock to affect any static measurements. However, its effect on dynamic p-wave travel times was corrected for in the final computations of p-wave velocity through the sample.

In order to obtain bulk volumetric changes of the samples with pressure, two 2-element 90° 'tee' rosette strain gauges were cemented diametrically opposite each other on the rock circumference. The rosettes were Micro-Measurement, 1/8 inch, 350 ohm gauges. The varnish insulated lead wires were covered with plastic tape to prevent any possible shorting due to brine penetrating the insulation (Figure 4).

After the gauging process, in order to saturate the rocks, the samples were subjected to a vacuum for two to four hours depending on their individual permeabilities. The vacuum process was followed by flooding the samples with 6% NaCl solution which ensured that the samples were saturated fully and free of air bubbles. The concentration, as stated by Ucock³⁰, is in the range of geothermal brines. It also gave pore fluid resistivities at room temperature which were low enough to allow easy detection of changes in the rock resistivity. The 6% con-

centration also was found to be helpful in preventing clay swelling within samples.

When ready for testing, a prepared sample was measured with dial calipers and inserted into the core jacket. The sample and core jacket were then clamped between the axial heads of the pressure vessel. The strain gauges lead wires were connected to panels leading to the Wheatstone bridge circuitry of two Bell and Howell Mode 8-114 Signal Conditioners. Upstream and downstream pore fluid lines were fitted to the passthrough shoes of the core jacket and leads for radial resistivity measurements were attached to the fittings with alligator clips. Finally, the vessel heads and sample were lowered into the vessel and secured. Pressure loading and rock testing followed.

Initial porosity measurements were made on smaller, 1 inch diameter samples cut adjacent to the respective test samples. These 1 inch samples were oven dried, weighed, vacuumed, saturated, and lastly reweighed to obtain porosity values at atmospheric conditions. The initial porosity was used in calculations as the reference from which variations in this parameter were measured.

IV.4 Test Procedure

Each of the twelve rock samples were subjected to two different pressure loadings: 1) hydrostatic loading in which pore pressure, confining pressure, and axial pressure were equal and increased or decreased simultaneously; 2) triaxial loading in which pore pressure, confining pressure, and axial pressure were not equal. The hydrostatic loading was used basically to put the sample initially at an elevated stress level

from which different effective stress conditions (triaxial loadings) were generated. Three types of triaxial loading were run on the sample: 1) hydrostatic compression test at elevated pore pressure; 2) uniaxial compaction test; 3) hydrostatic compression test at atmospheric pore pressure (not preceded by a hydrostatic loading). These tests are described below.

The procedure for the hydrostatic compression test at elevated pore pressure was to raise the pore, confining, and axial pressures to a value corresponding to the sample depth using a 1 psi/ft overburden gradient. Then, as shown in Figure 7, with the confining and axial pressures kept constant, the pore fluid pressure was reduced in steps to one-half the specimen depth and then increased back to the initial value. In order to check the effective stress concept, a similar variable pore pressure test was also conducted using a pressure level corresponding to $\frac{1}{2}$ psi per foot times the sample depth.

For the uniaxial compaction test (or constant radial strain test), the sample initially was hydrostatically loaded as above. Then as depicted in Figure 8, the pore pressure was reduced in steps while keeping the axial pressure (overburden) constant and while adjusting the confining pressure so that radial (lateral) strain remained constant. As done in the compression test above, the uniaxial compaction test was repeated using a pressure level corresponding to a gradient of $\frac{1}{2}$ psi/ft.

In the hydrostatic compression test at atmospheric pore pressure, no initial hydrostatic loading occurred. As shown in Figure 9, the confining and axial pressures were raised simultaneously in steps to the sample depth using a 1 psi/ft overburden gradient. The pore pressure

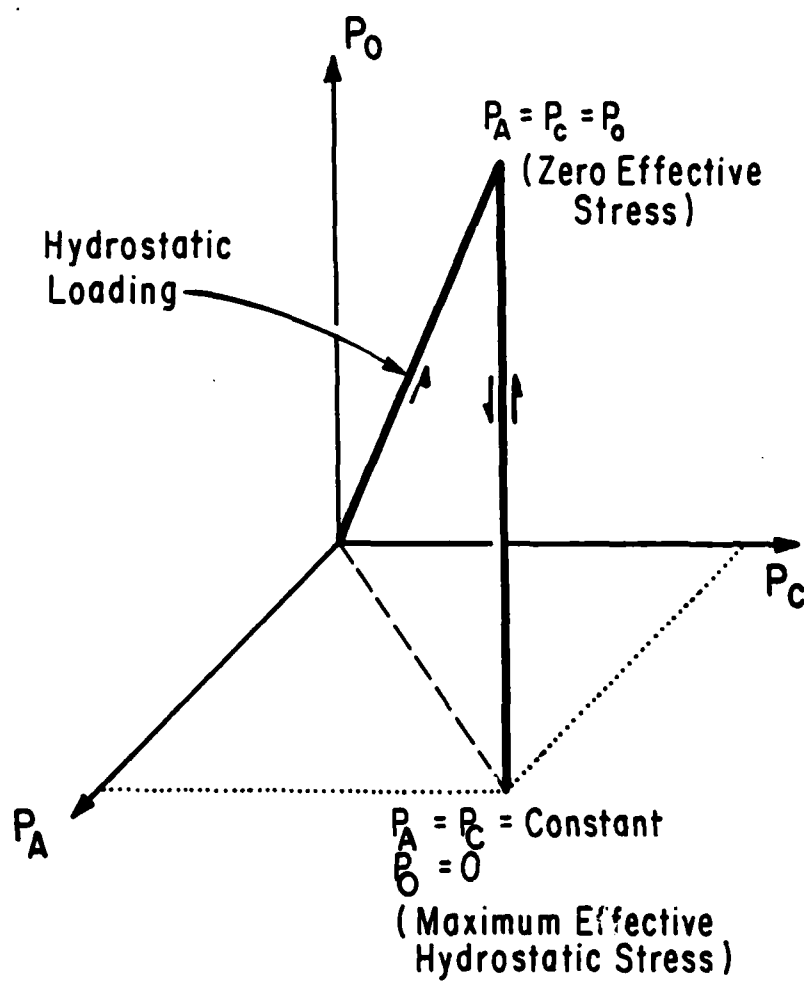


FIGURE 7 PRESSURE LOADING SEQUENCE FOR HYDROSTATIC COMPRESSION
TEST AT ELEVATED PORE PRESSURE

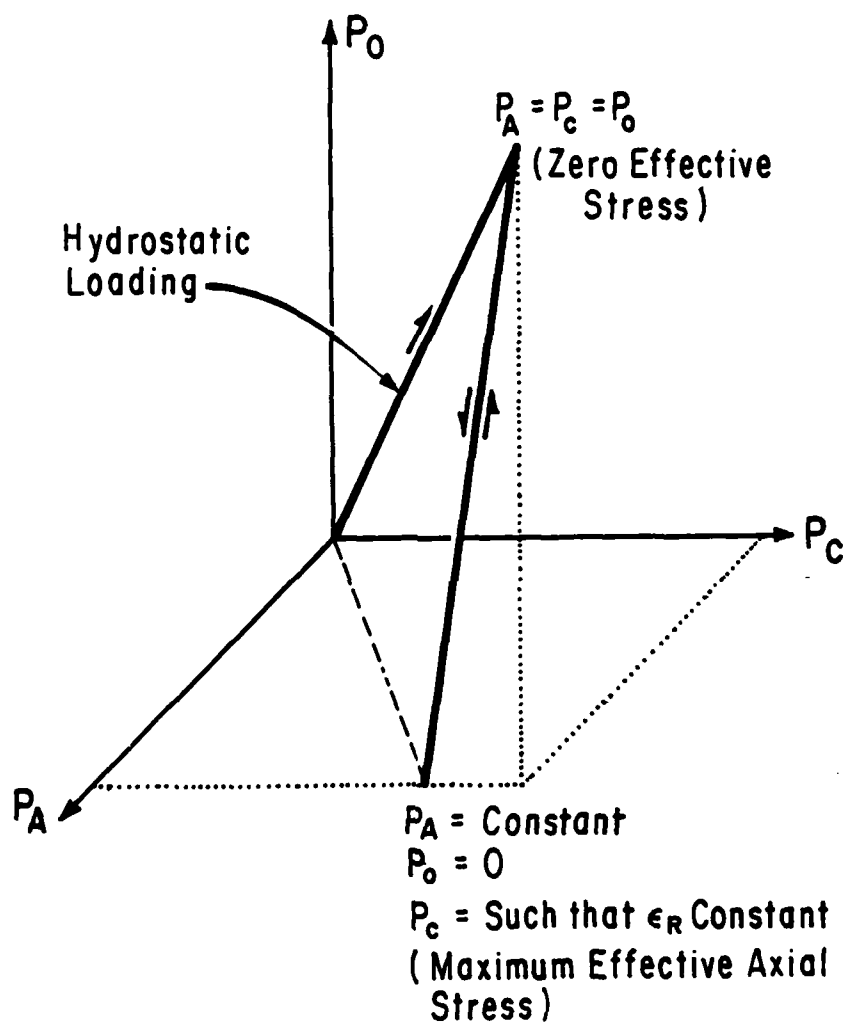


FIGURE 8 PRESSURE LOADING SEQUENCE FOR UNIAXIAL COMPACTION TEST

meanwhile was maintained at an atmospheric level. When a pressure corresponding to the sample depth was achieved, the confining and axial pressures were reduced in steps back to their initial values.

The three triaxial loading tests described above were used to check the validity of the effective stress concept and to determine if significant discrepancies existed among porosity, resistivity, and permeability values when they were obtained under different loading conditions. These parameters were measured at each pressure step which also permitted their dependence on effective stress to be observed.

The porosity was obtained from both static and dynamic measurements. The static methods utilized volumetric strains and pore fluid volume changes for calculation of porosity values. Another static method used resistivity measurements which allowed porosity calculations with the Humble formula (equation 2.2). The dynamic method utilized observed p-wave travel times through the samples which could be used in the Wyllie Time Average Equation (equation 5.7) to compute porosity values.

The resistivity was obtained from voltage drops measured radially across the sample. As discussed in Appendix I, resistivities were converted to formation factors using pore fluid resistivities corrected for pressure. The formation factors, then, were employed in data analysis.

The permeability was calculated using observed flow rates of brine through the sample under a differential pressure driving force. Equation 3.8 for a whole core type permeameter was utilized.²⁸

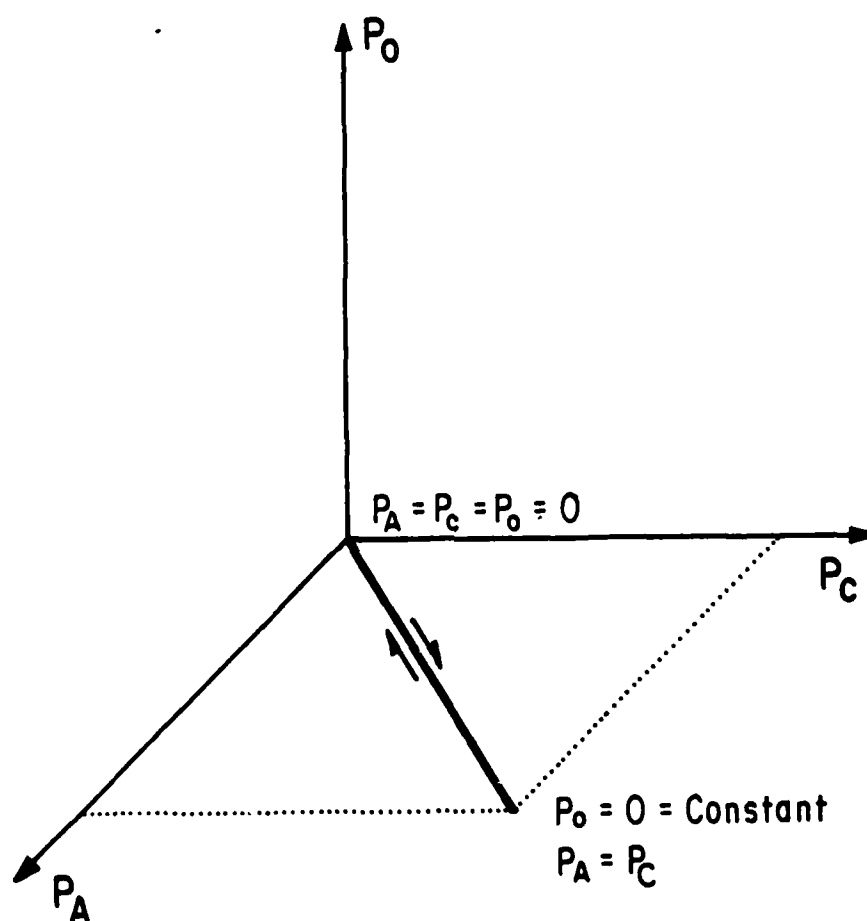


FIGURE 9 PRESSURE LOADING SEQUENCE FOR HYDROSTATIC COMPRESSION TEST
AT ATMOSPHERIC PORE PRESSURE

V. ANALYSIS OF EXPERIMENTAL RESULTS

V.1 Resistivity Changes with Effective Stress

Resistivity changes can best be studied in terms of formation factor variations. The formation factor, F , in contrast to the resistivity, is independent of the electrical properties of the saturating fluid. Therefore, changes in F correspond only to changes in the intrinsic properties of the rock and, as explained in Chapter III, to the pressure.

From resistivity data, formation factors were computed at each pressure step in the triaxial loading tests described in Section IV.4 and were plotted against effective stress. The validity and accuracy of the effective stress concept was checked by comparing the changes in F in each loading test for the same effective stress change.

Figures 10 through 13 show comparisons between variations of F with effective stress for the hydrostatic compression tests. Some difference in curve shapes between tests run at atmospheric pore pressure and tests run at elevated pore pressures can be observed. This difference was probably caused by two phenomena: 1) the opening of microcracks at elevated pore pressures; 2) matrix compressibility. The first factor resulted in a larger and more uniform change in F when the microcracks closed with increasing effective stresses. The second factor, matrix compressibility, was accentuated at elevated pore pressures. With a larger matrix compressibility, η in equation 3.3 decreased, and, therefore, the actual effective stress on the rock sample was reduced. Again

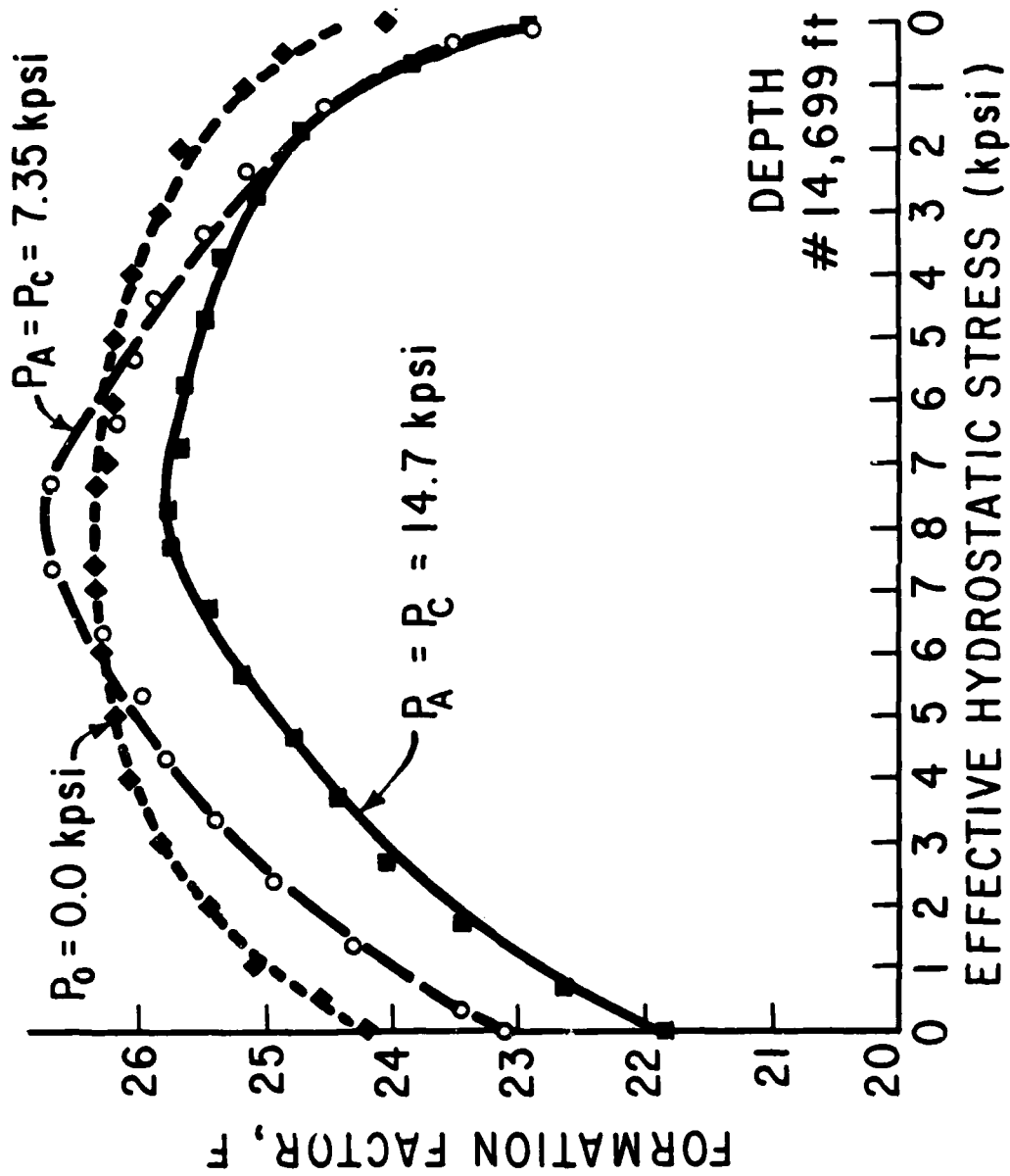


FIGURE 10 COMPARISONS OF VARIOUS HYDROSTATIC COMPRESSION TESTS (#14699)

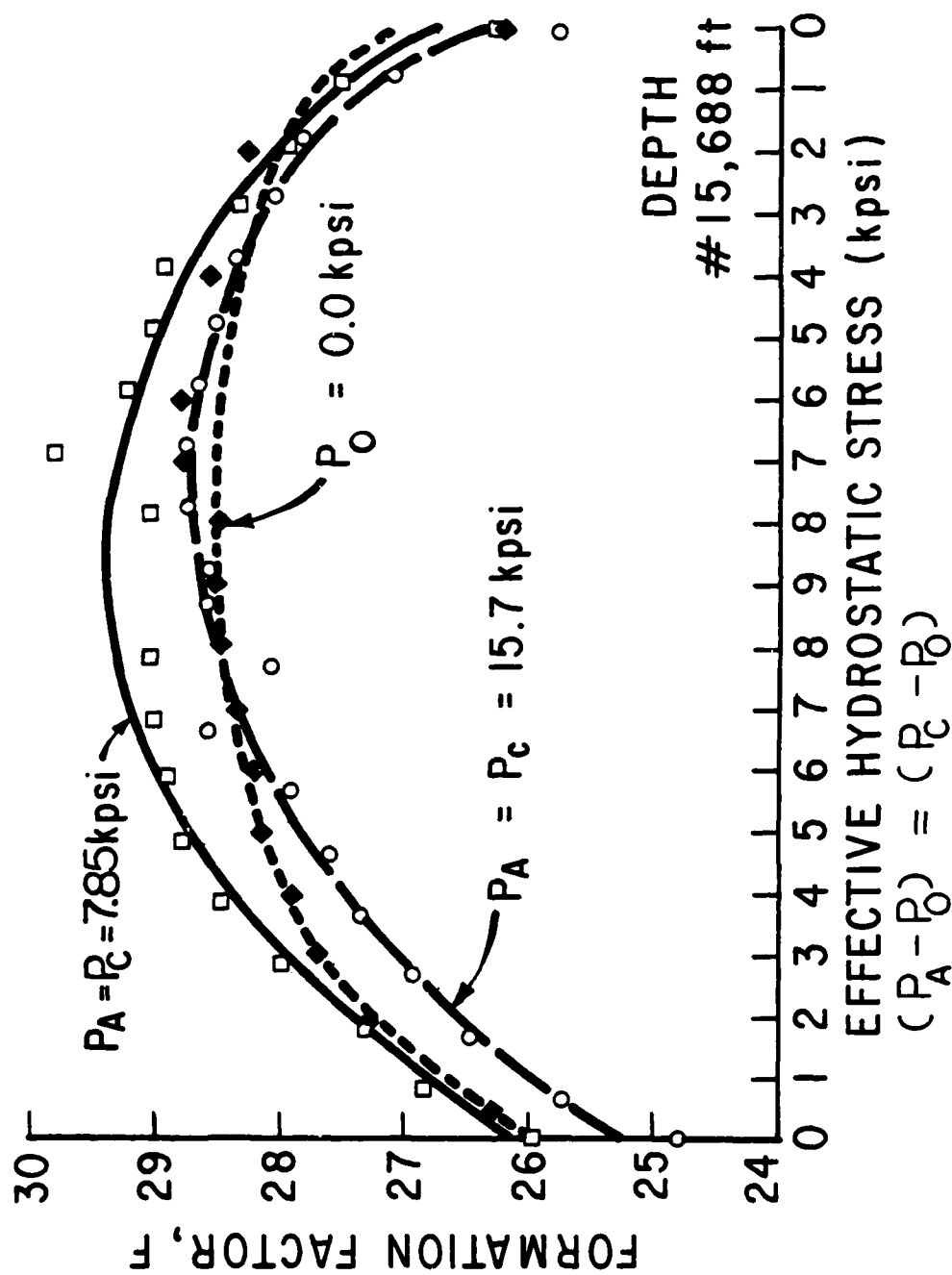


FIGURE 11 COMPARISONS OF VARIOUS HYDROSTATIC COMPRESSION TESTS (#15688)

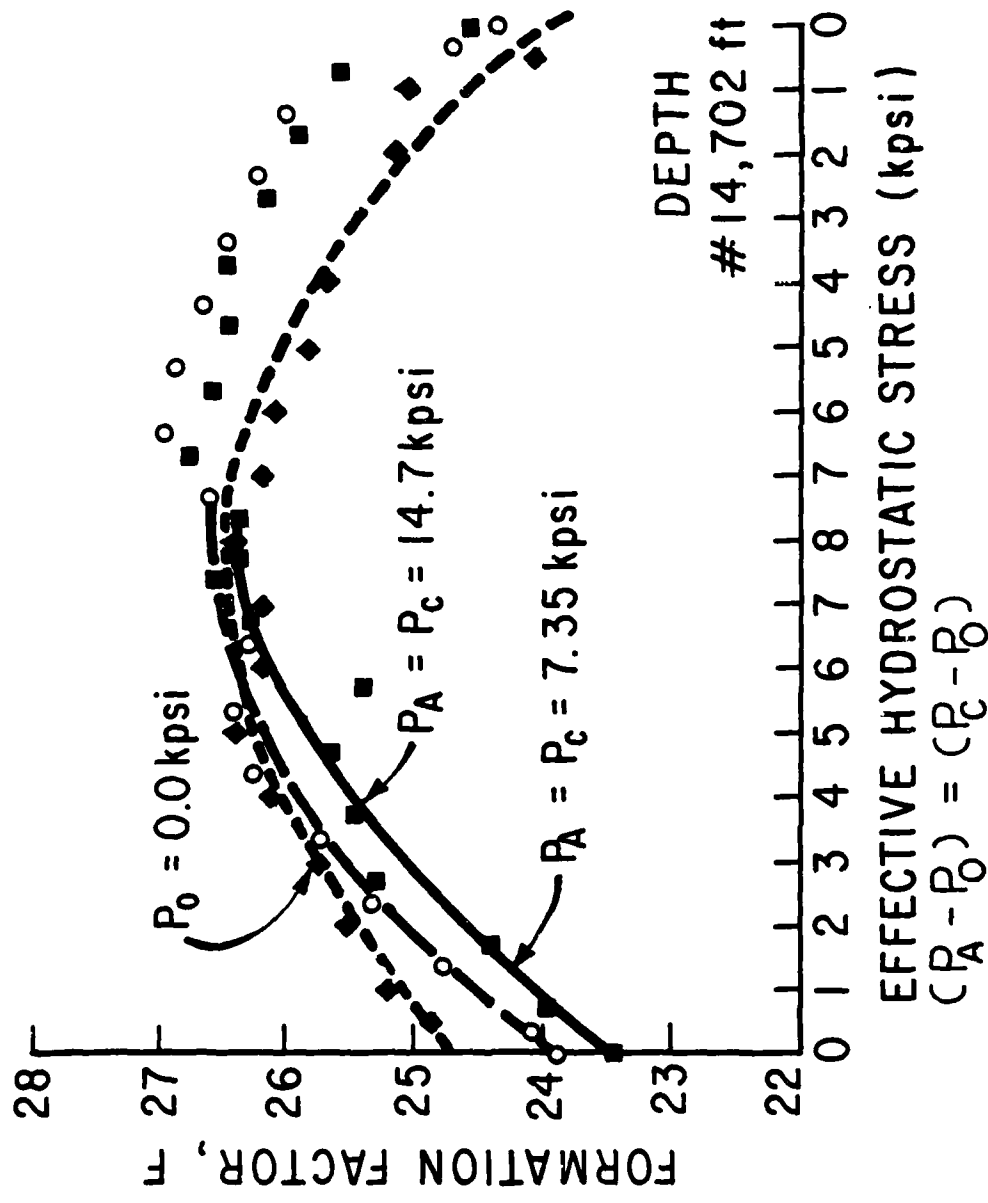


FIGURE 12 COMPARISONS OF VARIOUS HYDROSTATIC COMPRESSION TESTS (#14702)

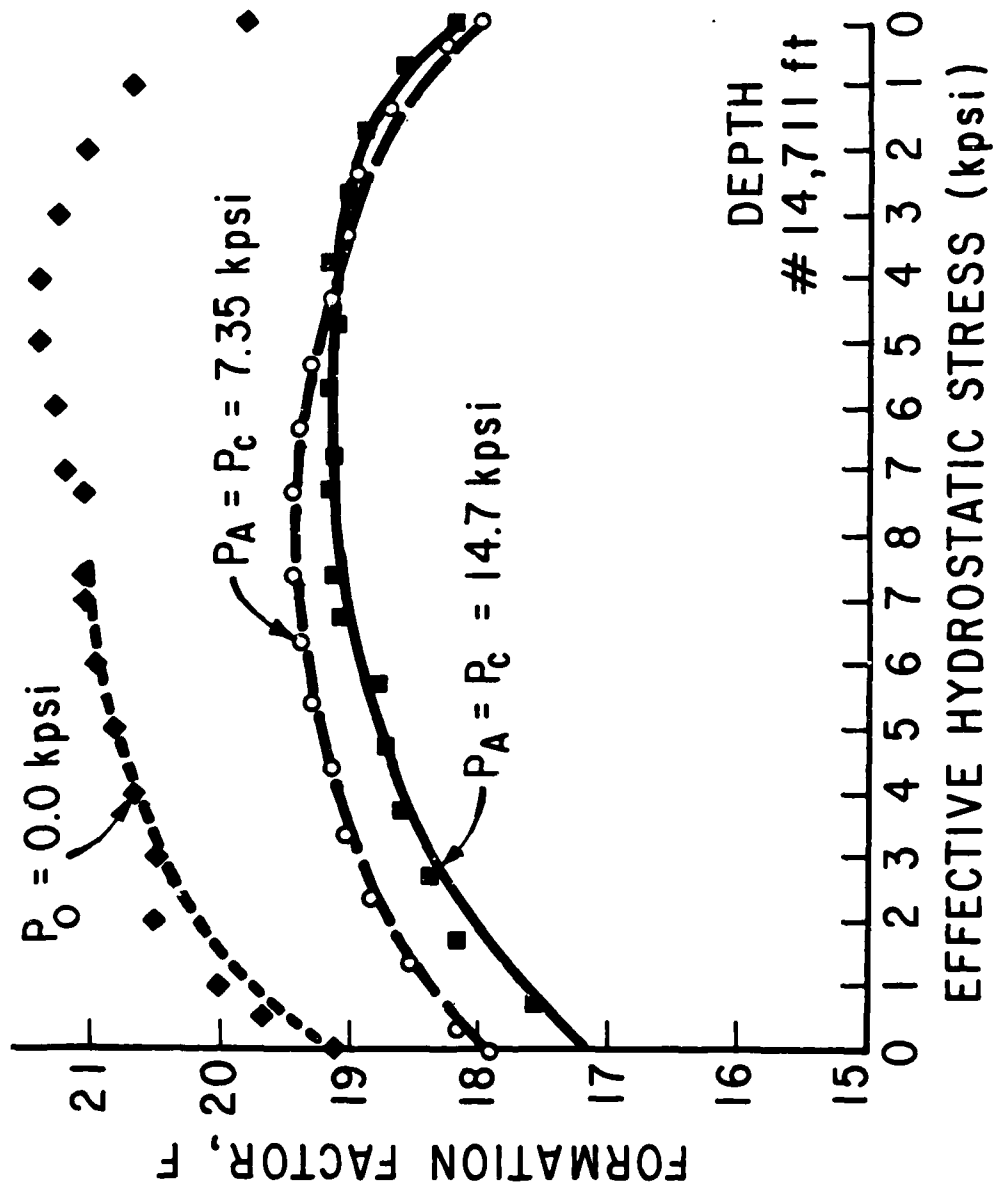


FIGURE 13 COMPARISONS OF VARIOUS HYDROSTATIC COMPRESSION TESTS (#14711)

the result was a larger more uniform change in F for tests run at elevated pore pressures.

The matrix compressibility and the microcracks of the samples do not significantly affect variations of F in the atmospheric pore pressure tests. The flatter curves at the higher effective stresses support this fact. Therefore, data gathered from compression tests under atmospheric pore pressure conditions may not be accurate enough for predicting rock properties under insitu rock conditions.

Offsetting among the curves could be attributed to several reasons: 1) Permanent set in the samples caused by loading and unloading cycles during different tests on the sample; 2) Temperature change between each test run. (Appendix I discusses that an average room temperature was used in determining the resistivity of the saturating fluid.)

Another comparison can be made between the hydrostatic compression test and the uniaxial compaction test. Figures 14 through 18 show typical plots of F verses effective hydrostatic stress, for compression tests at elevated pore pressures, and effective axial stress, for uniaxial compaction tests. The good agreement among the curve shapes demonstrates that the formation factor is similarly influenced in these two type tests by changes in the effective stress. The pressure level did not appear to be a strong factor influencing the data. This resulted because the pore pressures were high enough initially to open microcracks and to compress the rock matrix. Any offsetting of the curves was caused by the factors described above.

Since both of the triaxial loading tests under elevated pore

pressure conditions appeared to give comparable results, further analysis with other samples was conducted. Figures 19 through 24 show plots of F verses effective stress for the uniaxial compaction tests for many of the rocks tested. The graphs for each rock show that the triaxial loading tests at various elevated pore pressures give similar results. The near closeness of the curve shapes demonstrates the validity and accuracy of the effective stress concept.

The data obtained in the experiments showed that formation factors resulting from effective stress changes are nonlinear and could be represented by a polynomial expression in pressure. Curvilinear bivariate regression on the formation factor and effective stress data for each test was performed. A simple quadratic expression in pressure of the form

$$F = n_1 + n_2 P_E + n_3 P_E^2 \quad 5.1$$

where

n_1 = coefficients dependent upon the rock type

was tried but did not fit the data. A very good correlation for all rock samples was obtained by regressing $\ln F$ and P_E , resulting in a second degree polynomial of the form

$$\ln F = n_1 + n_2 P_E + n_3 P_E^2 \quad 5.2$$

Figure 25 shows a typical curve for one of the rock samples and demonstrates the goodness of fit of equation 5.2. Data curves for the remainder of the samples are given in Figures 26 through 36.

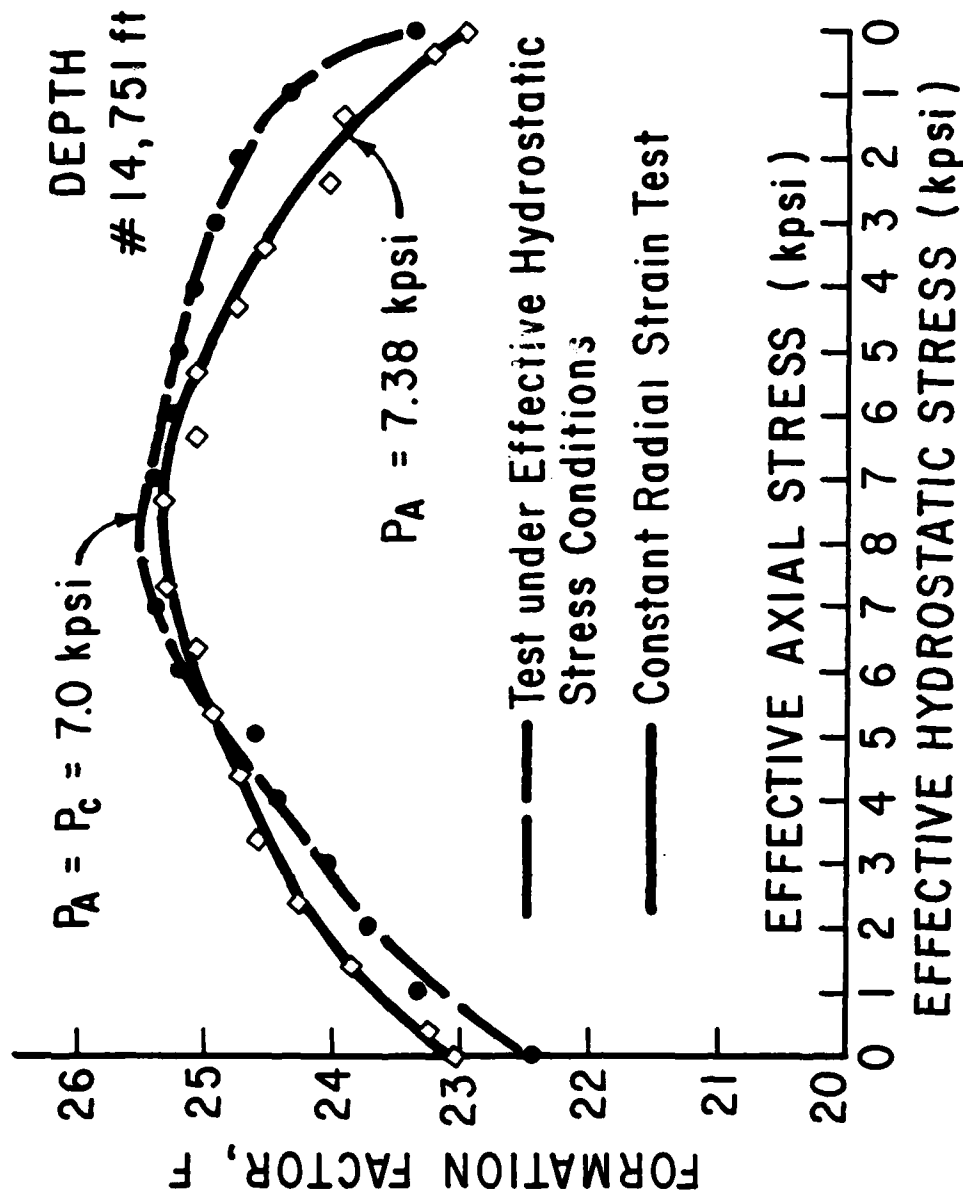


FIGURE 14 COMPARISONS OF HYDROSTATIC COMPRESSION TEST AND UNIAXIAL COMPRESSION TEST (#14751)

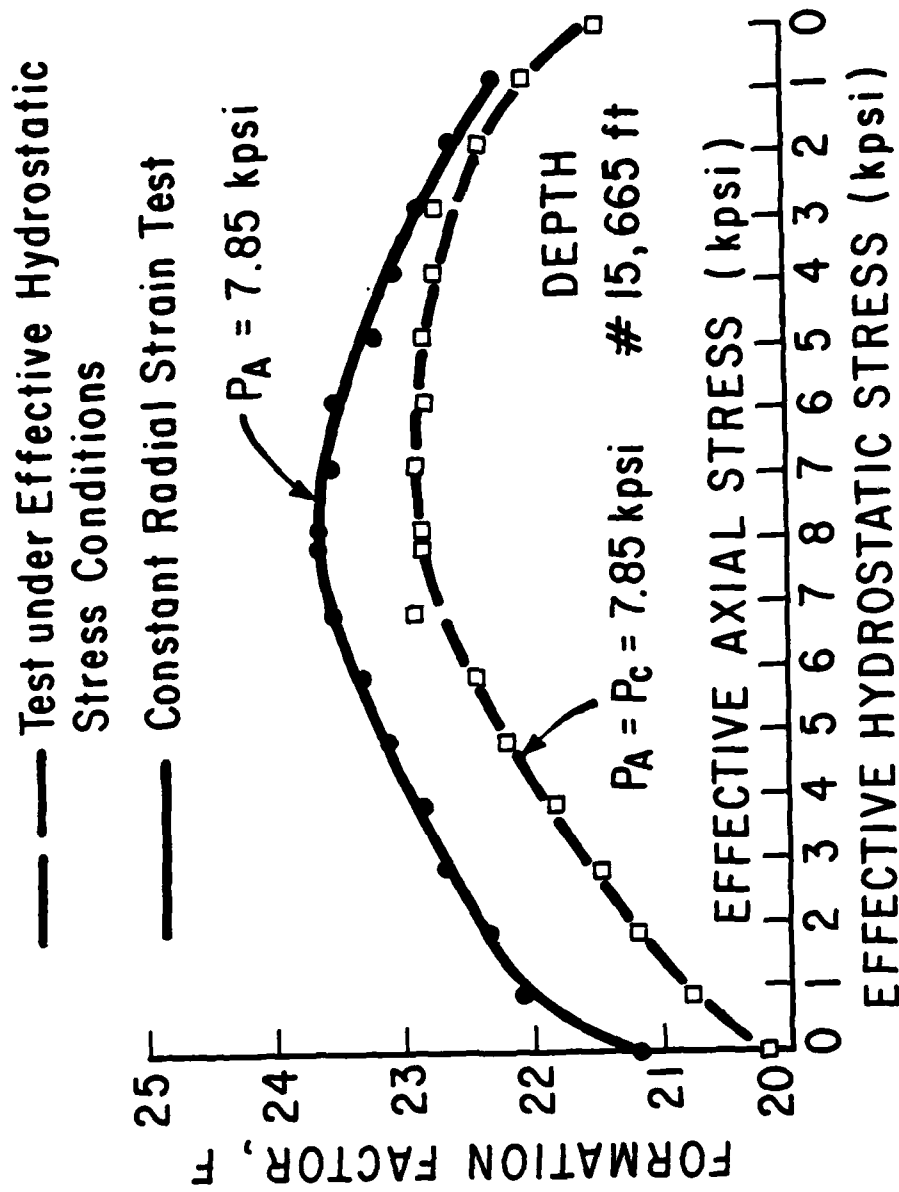


FIGURE 15 COMPARISONS OF HYDROSTATIC COMPRESSION TEST AND UNIAXIAL COMPACTION TEST (#15665)

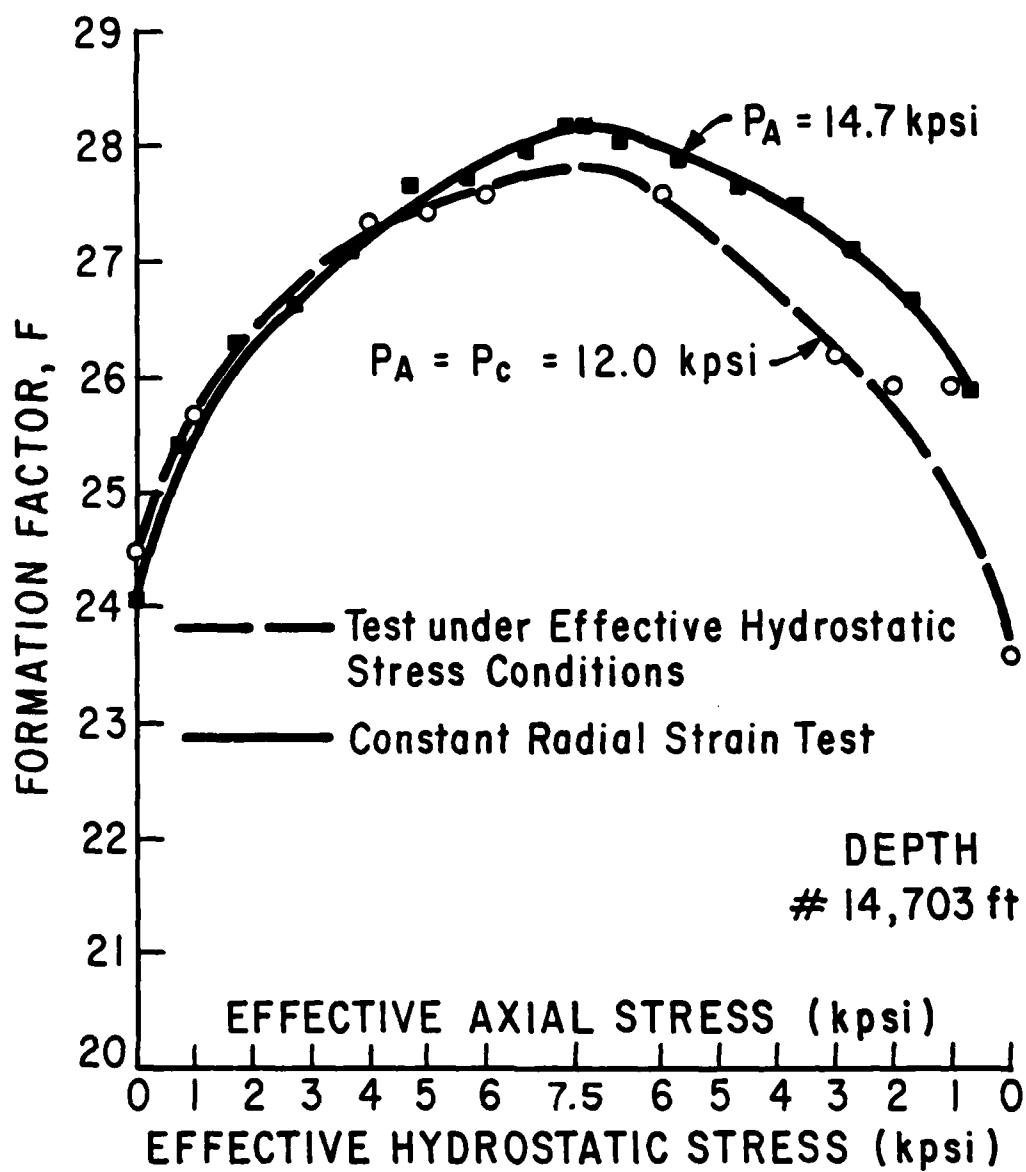


FIGURE 16 COMPARISONS OF HYDROSTATIC COMPRESSION TEST AND UNIAXIAL COMPACTION TEST (#14703)

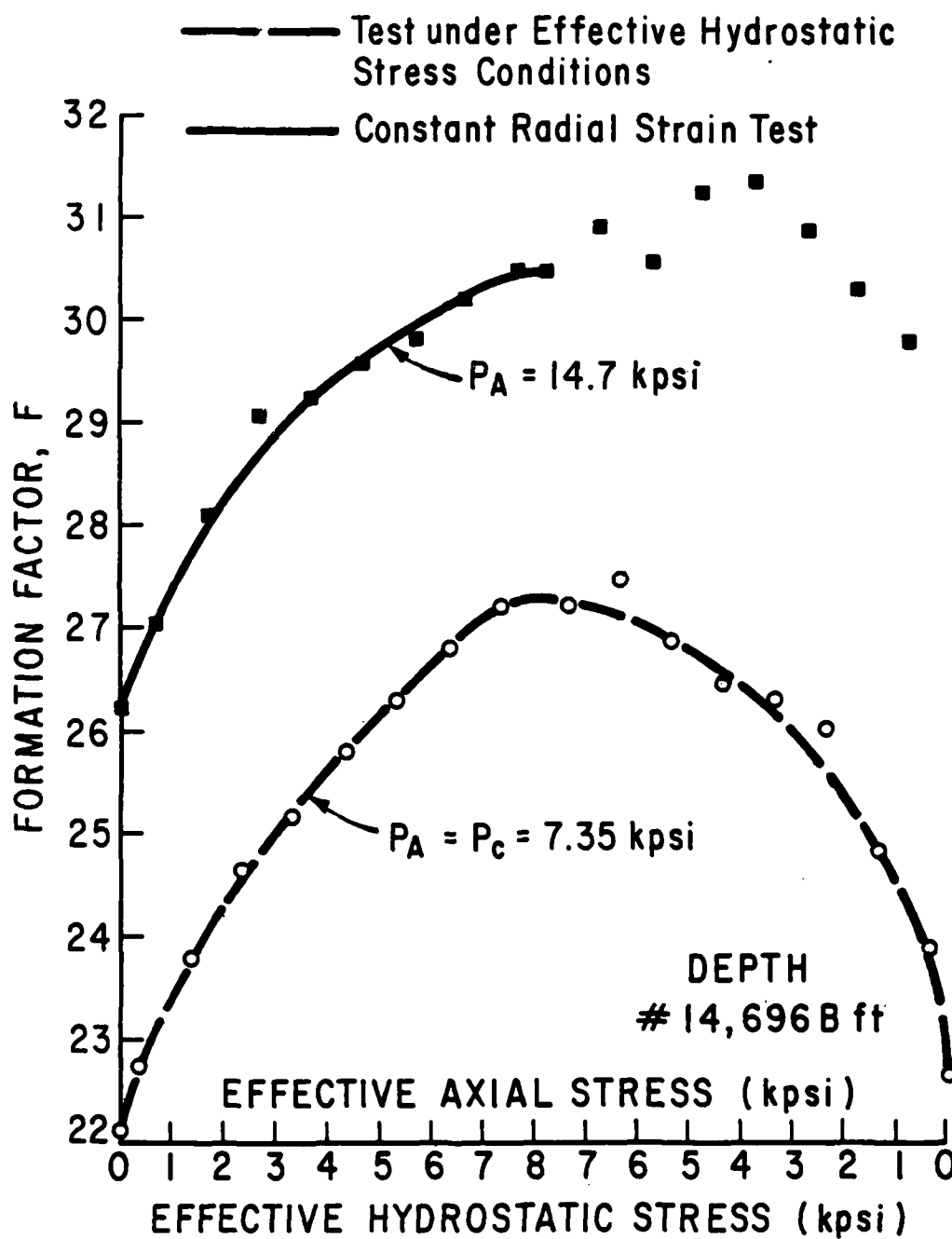


FIGURE 17 COMPARISONS OF HYDROSTATIC COMPRESSION TEST AND UNIAXIAL COMPACTION TEST (#14696B)

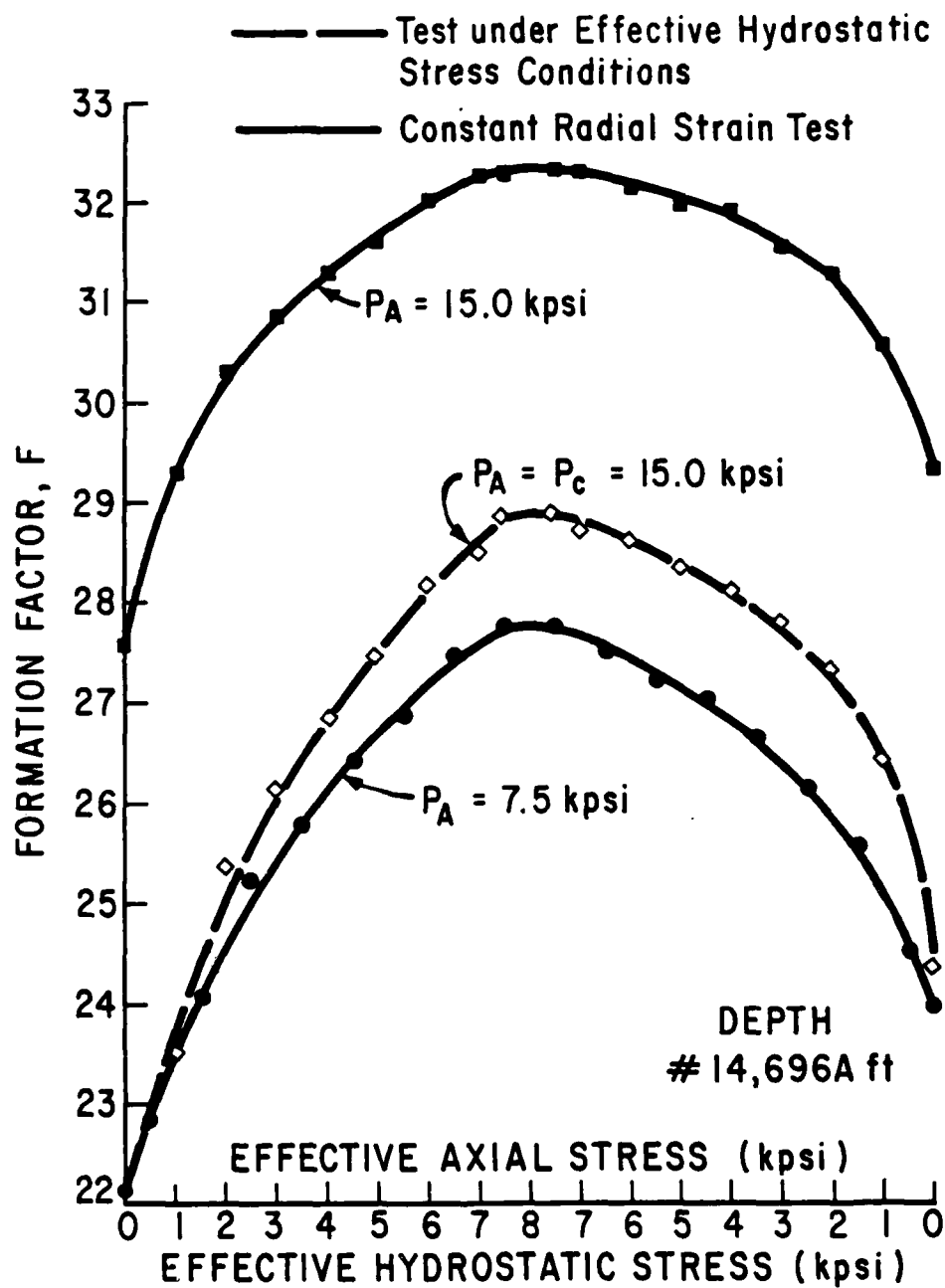


FIGURE 18 COMPARISONS OF HYDROSTATIC COMPRESSION TEST AND UNIAXIAL COMPACTION TEST (#14696A)

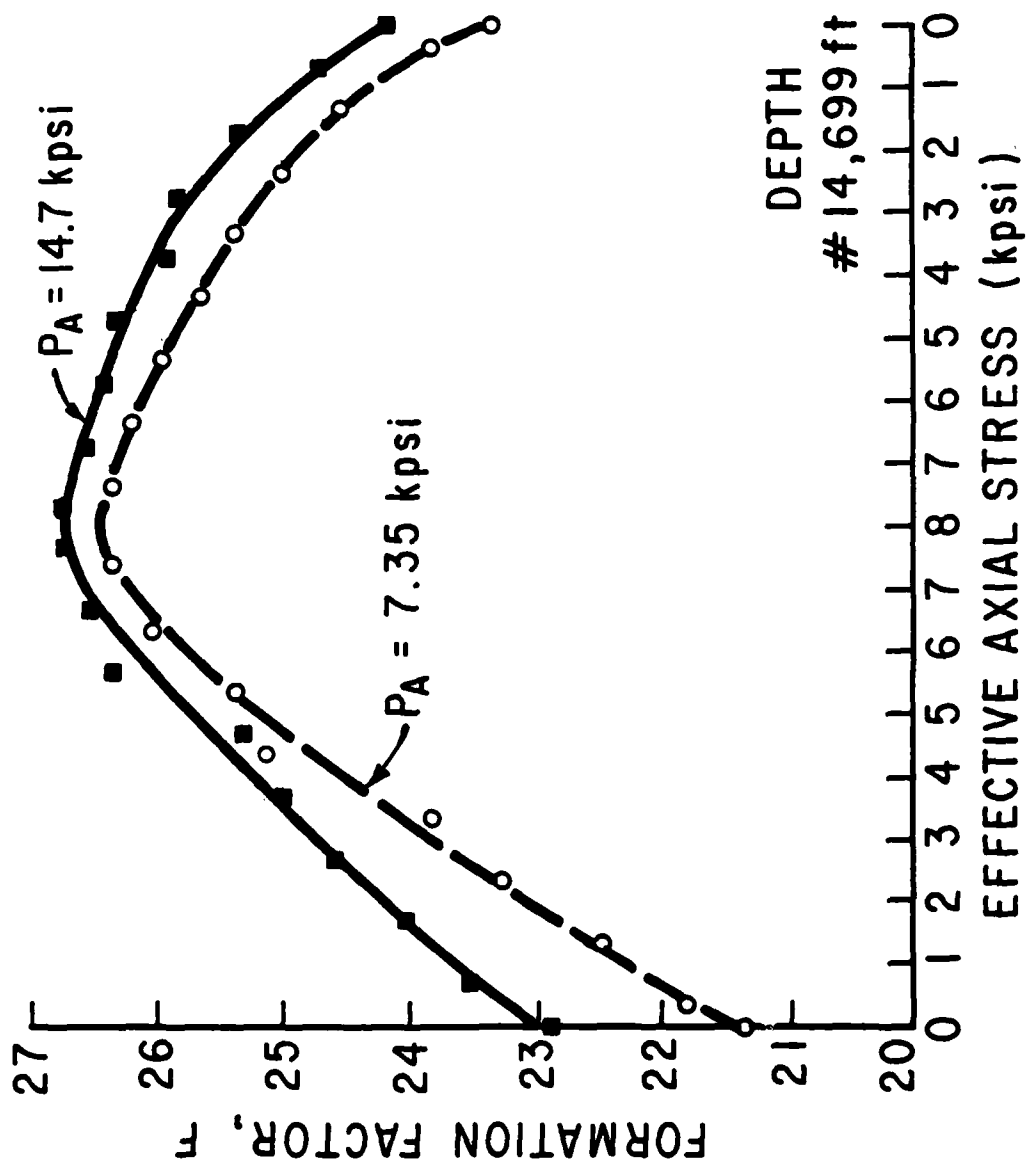


FIGURE 19 COMPARISONS OF VARIOUS UNIAXIAL COMPACTION TESTS (#14699)

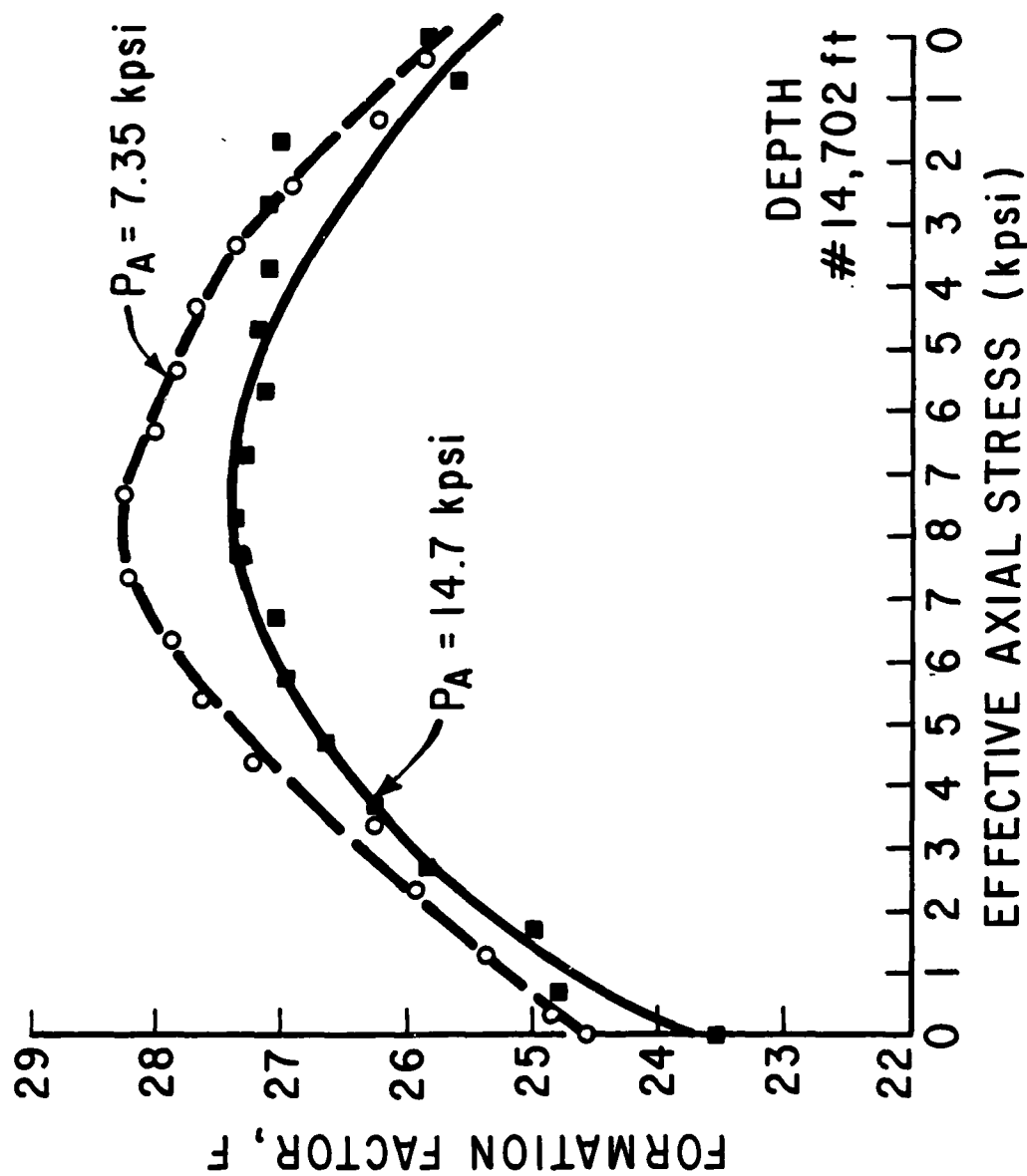


FIGURE 20 COMPARISONS OF VARIOUS UNIAXIAL COMPACTION TESTS (#14702)

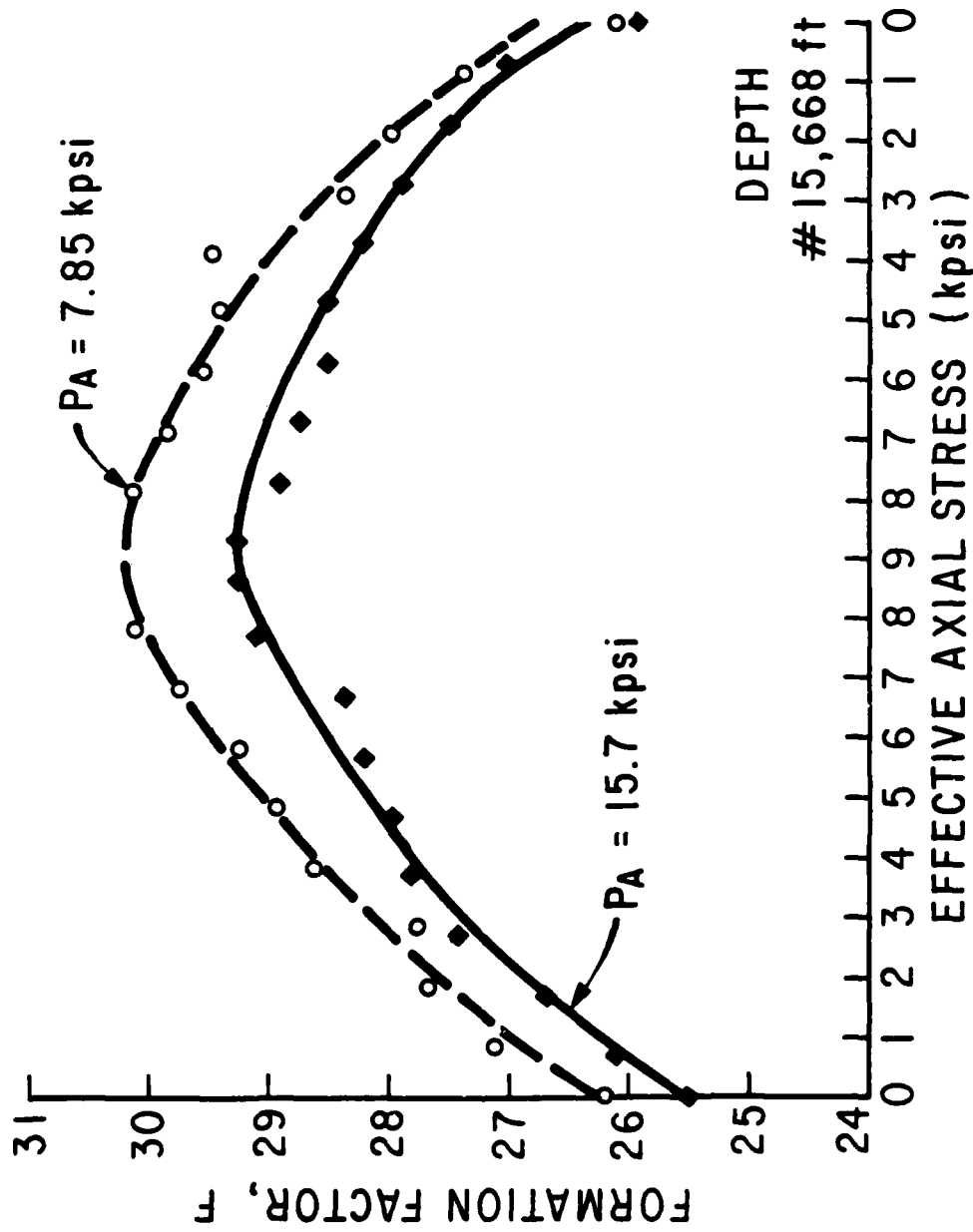


FIGURE 21 COMPARISONS OF VARIOUS UNIAXIAL COMPACTION TESTS (#15668)

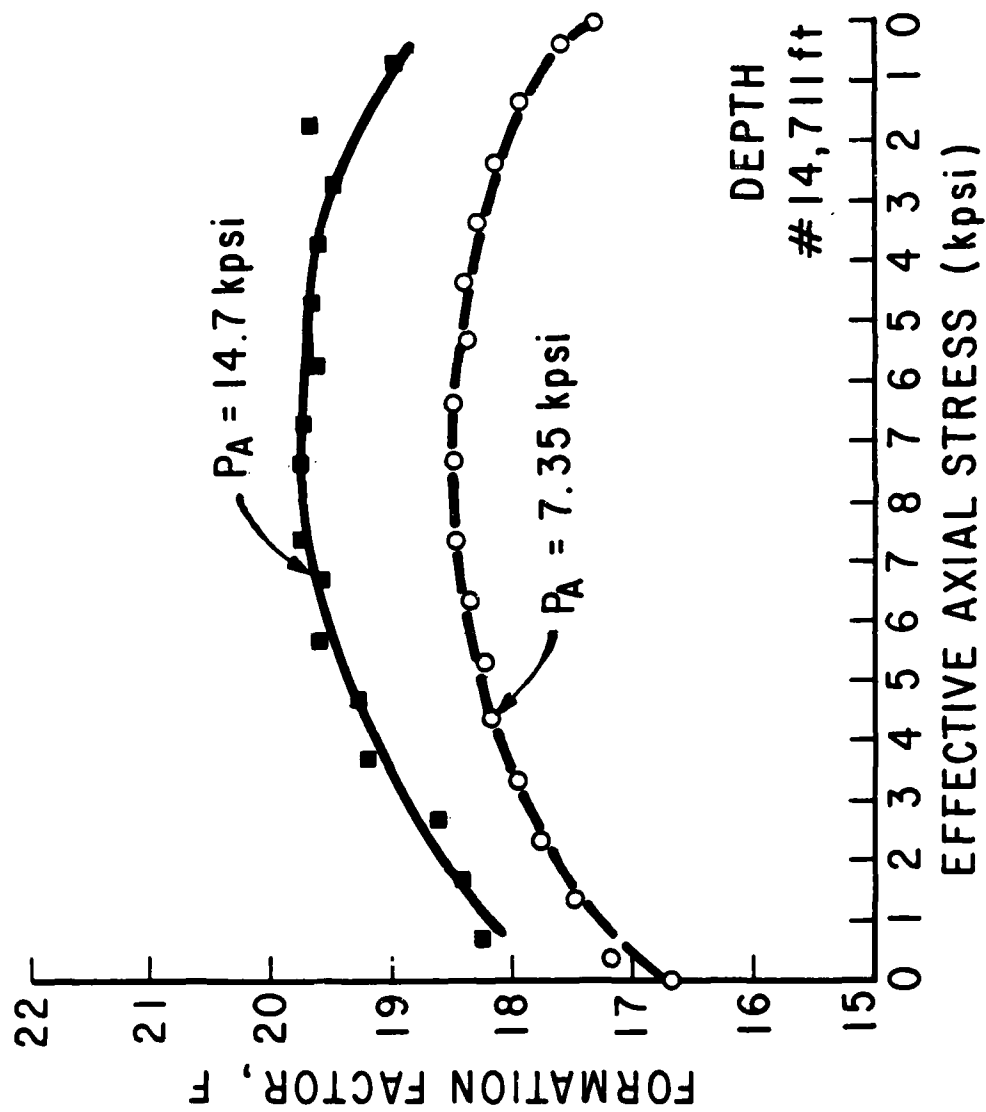


FIGURE 22 COMPARISONS OF VARIOUS UNIAXIAL COMPACTION TESTS (#14711)

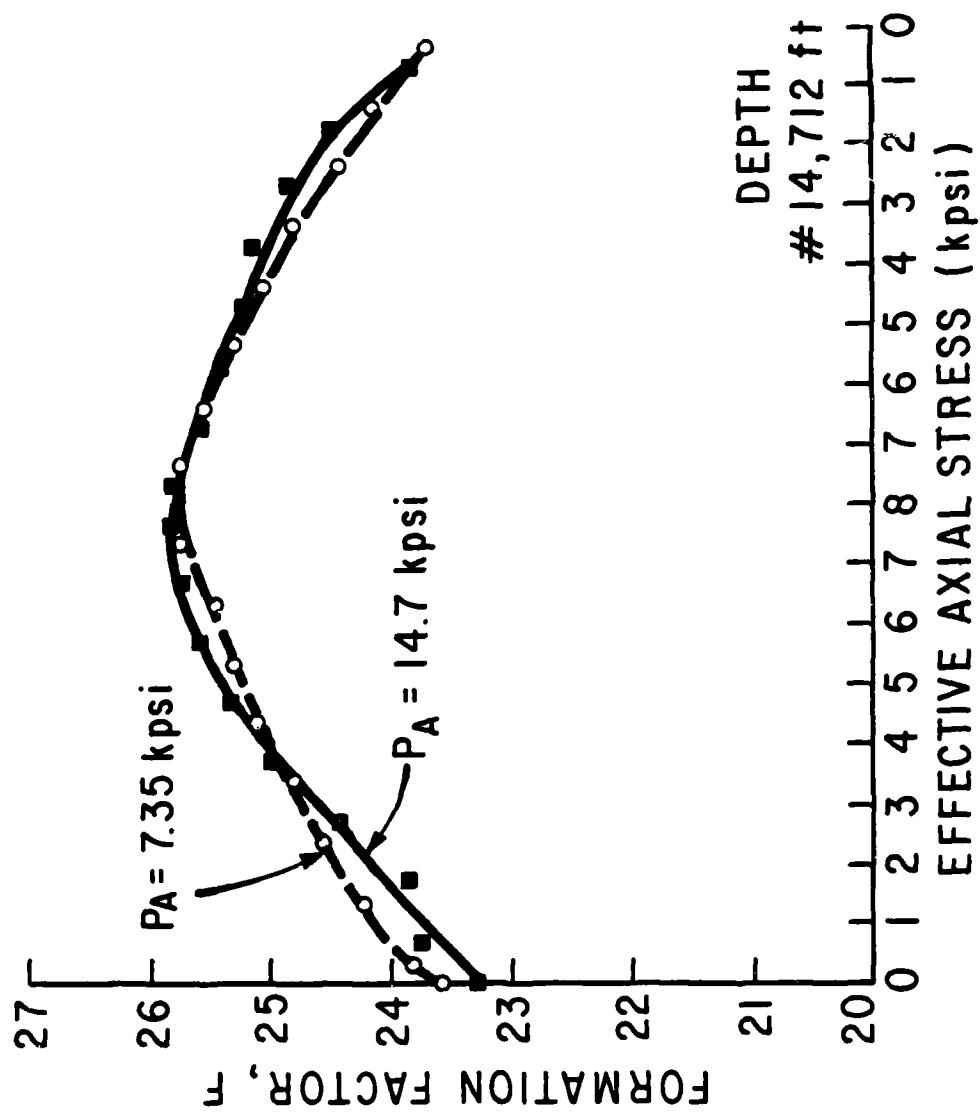


FIGURE 23 COMPARISONS OF VARIOUS UNIAXIAL COMPACTION TESTS (#14712)

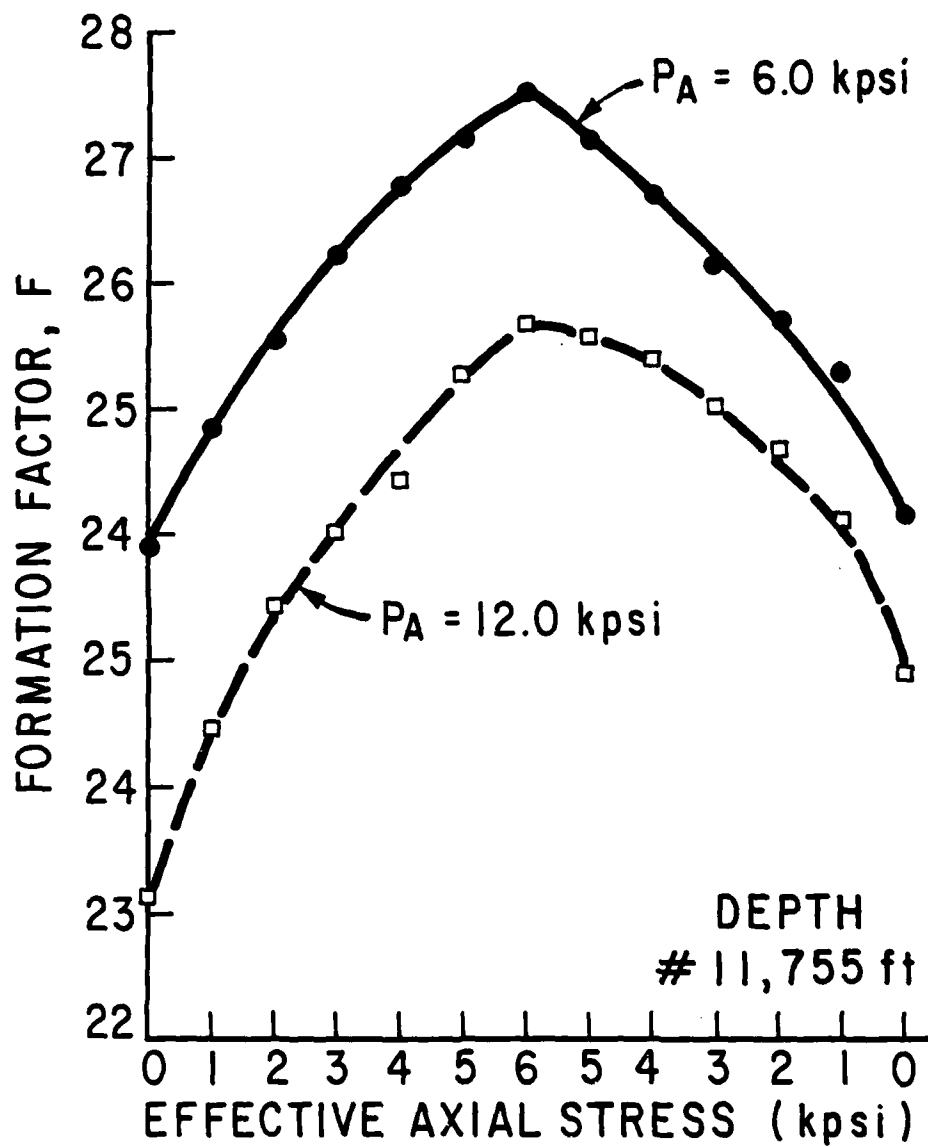


FIGURE 24 COMPARISONS OF VARIOUS UNIAXIAL COMPACTION TESTS (#11755)

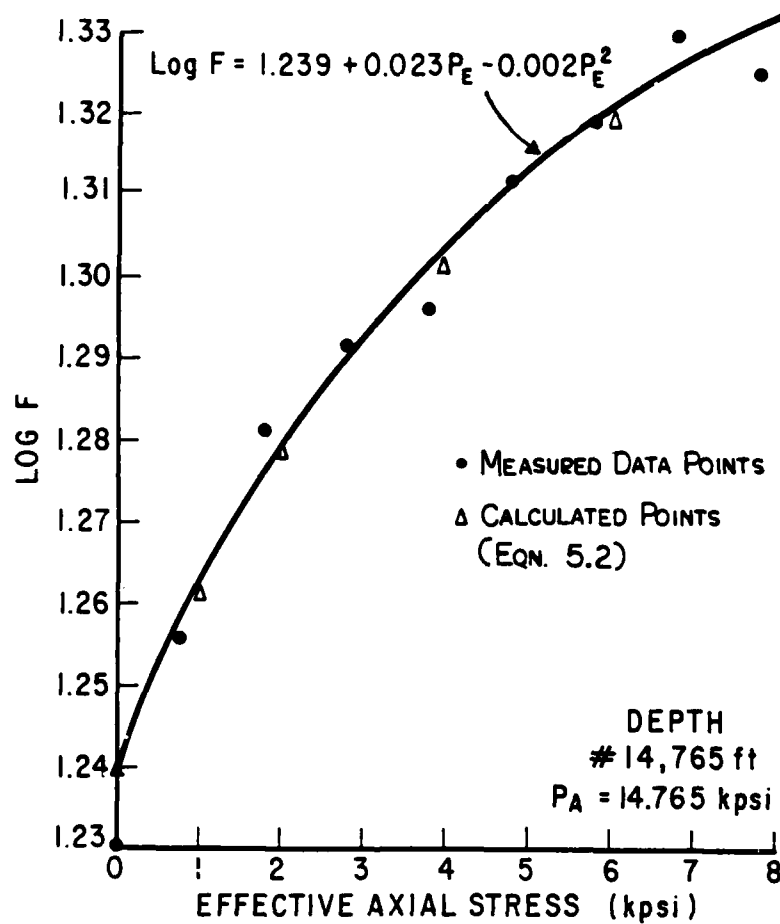


FIGURE 25 COMPARISON OF FORMATION FACTORS OBTAINED FROM MEASURED RESISTIVITY DATA AND FROM EQUATION 5.2 (#14765, UNI-AXIAL COMPACTION TEST)

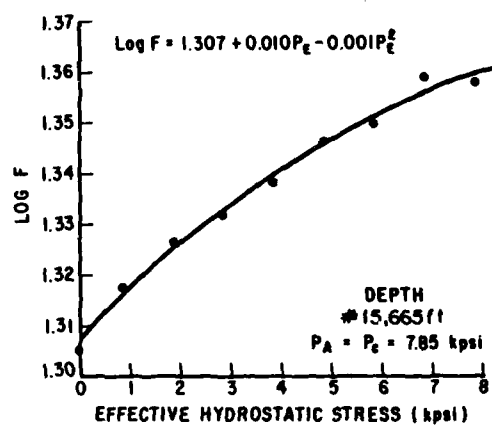


FIGURE 26A

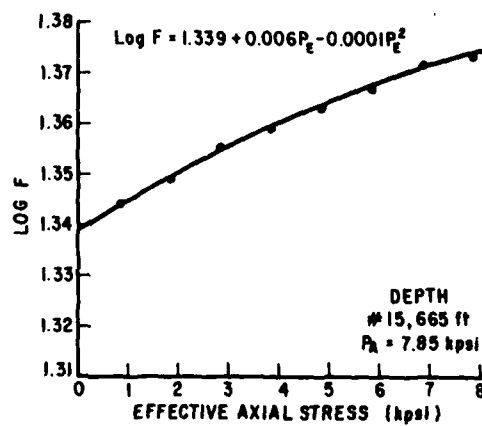


FIGURE 26B

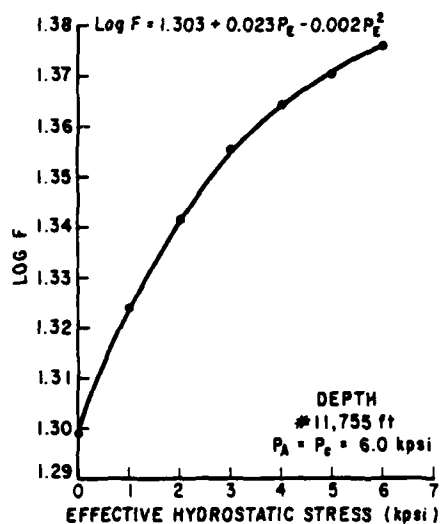


FIGURE 27A

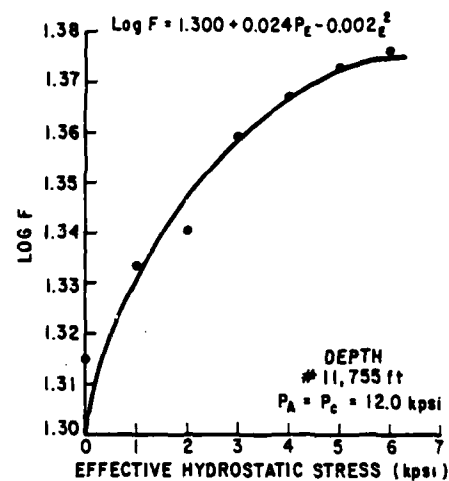


FIGURE 27B

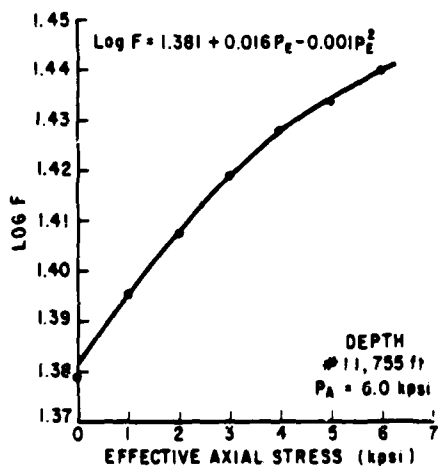


FIGURE 27C

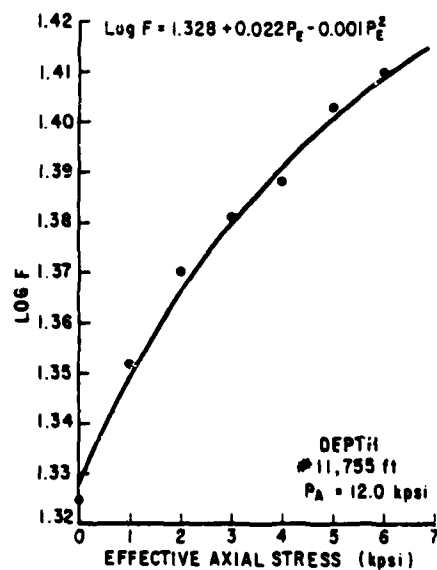


FIGURE 27D

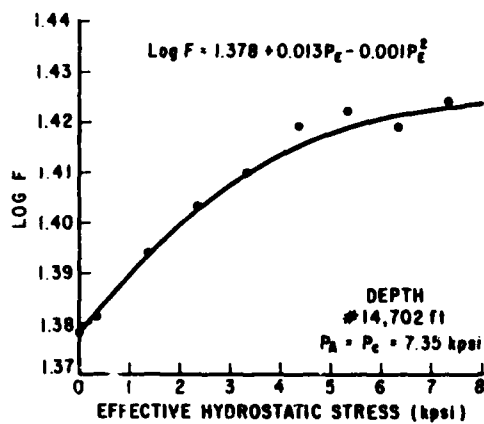


FIGURE 28A

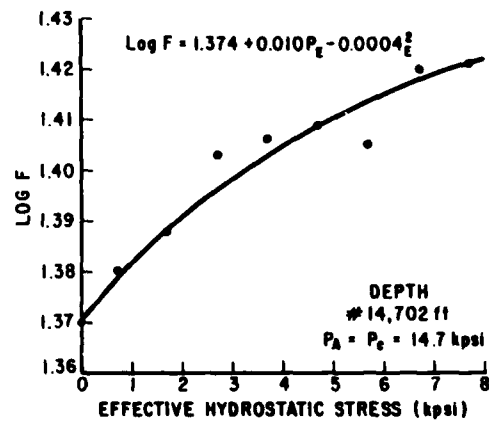


FIGURE 28B

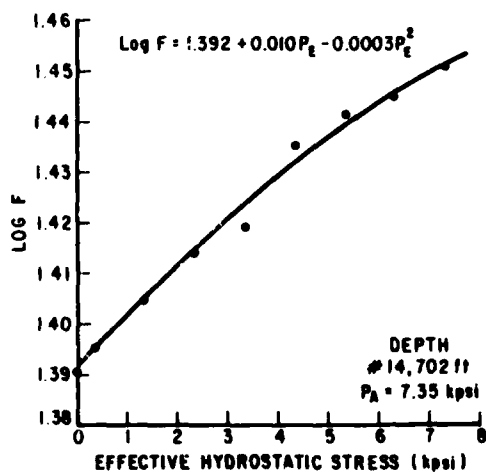


FIGURE 28C

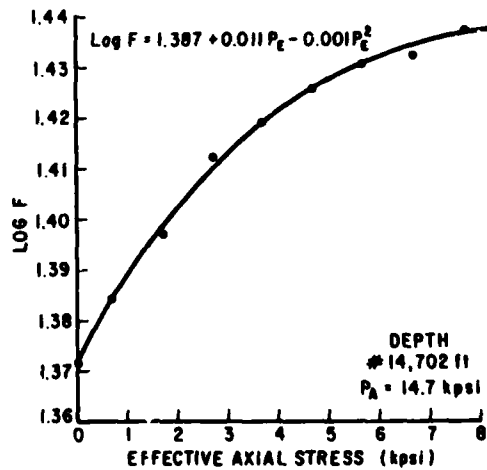


FIGURE 28D

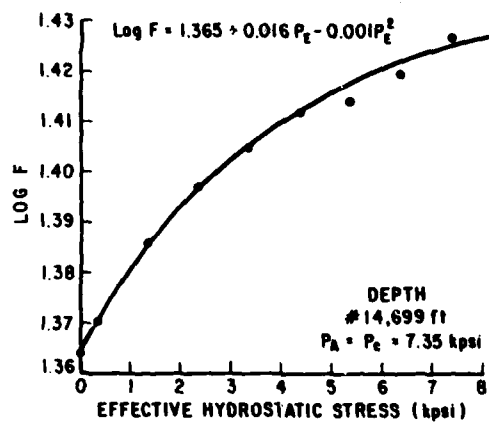


FIGURE 29A

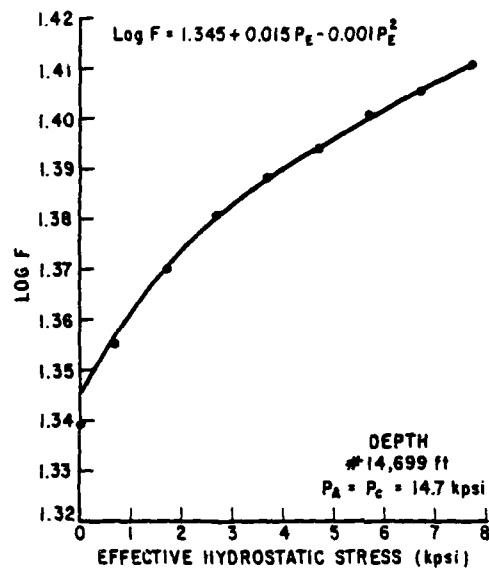


FIGURE 29B

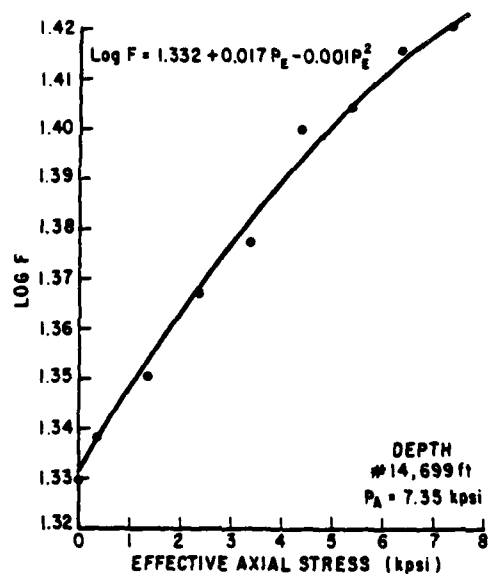


FIGURE 29C

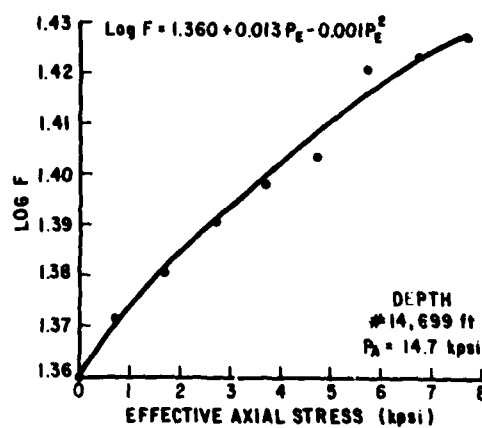


FIGURE 29D

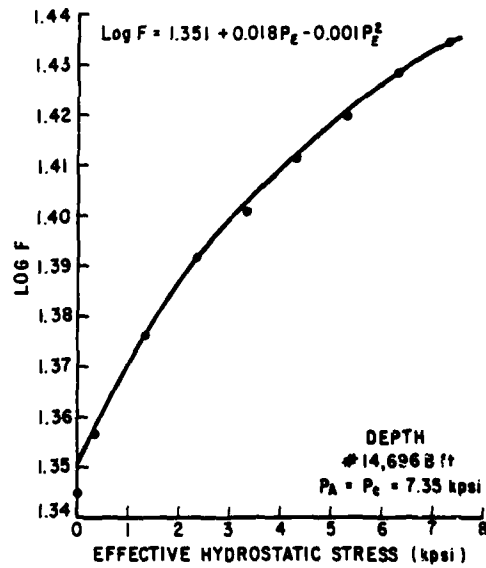


FIGURE 30A

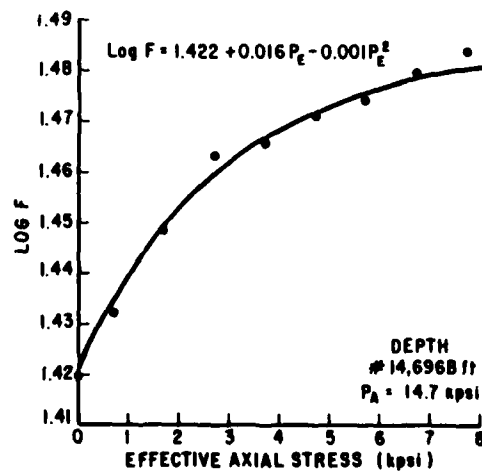


FIGURE 30B

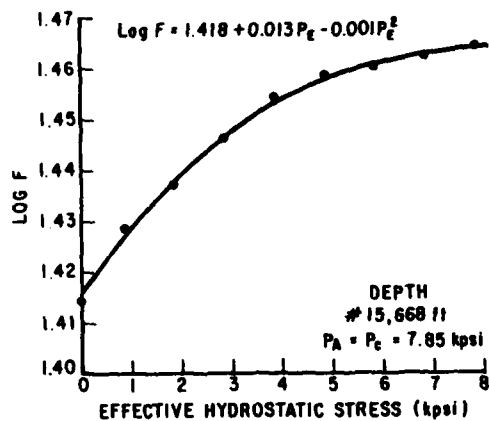


FIGURE 31A

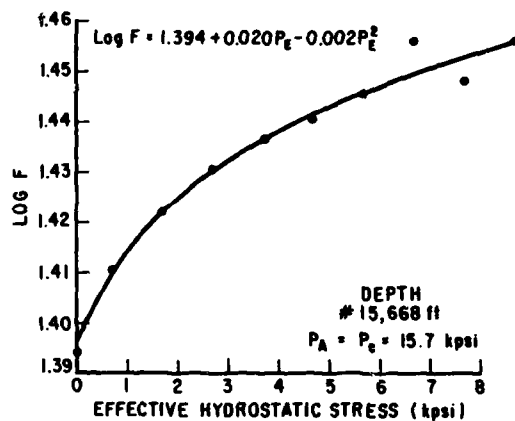


FIGURE 31B

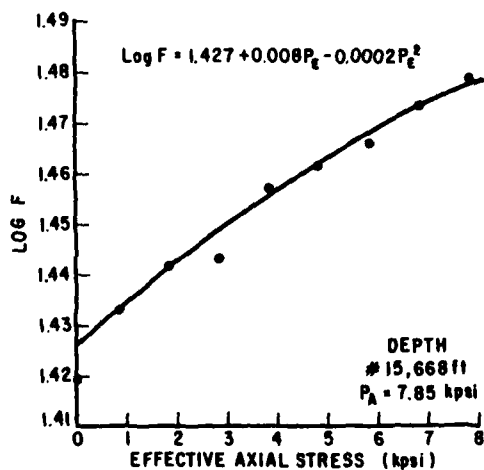


FIGURE 31C

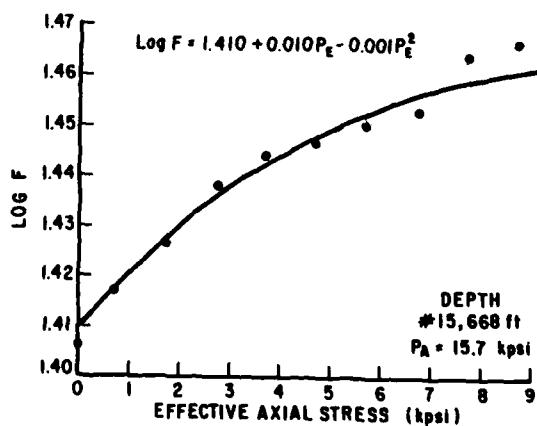


FIGURE 31D

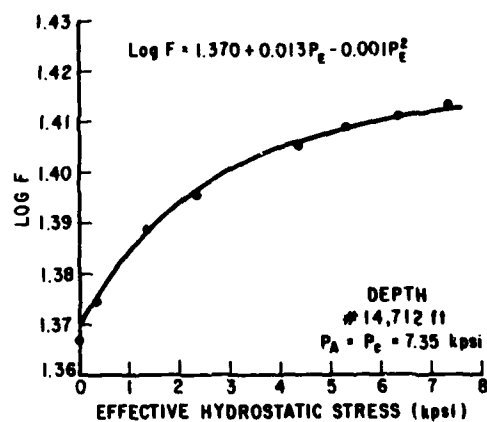


FIGURE 32A

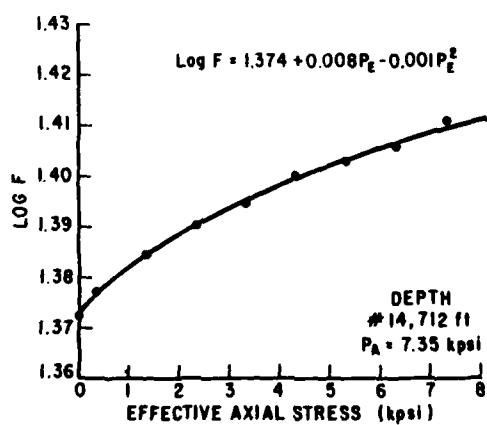


FIGURE 32B

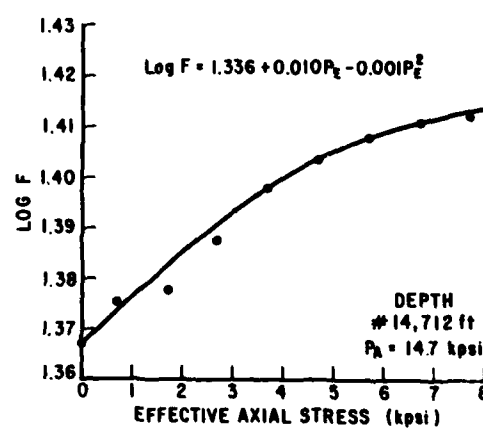


FIGURE 32C

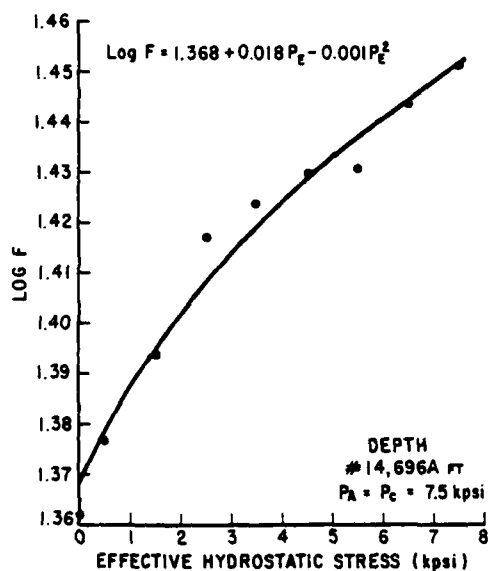


FIGURE 33A

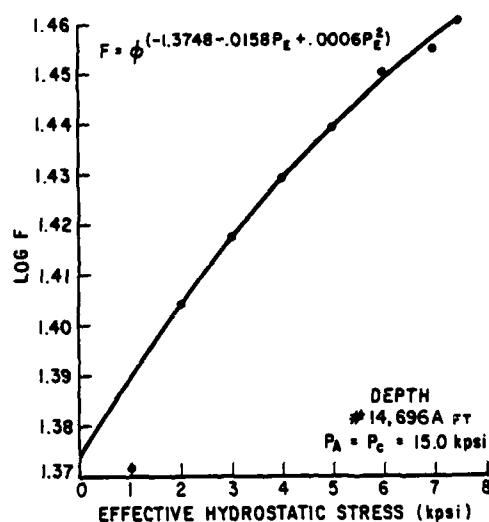


FIGURE 33B

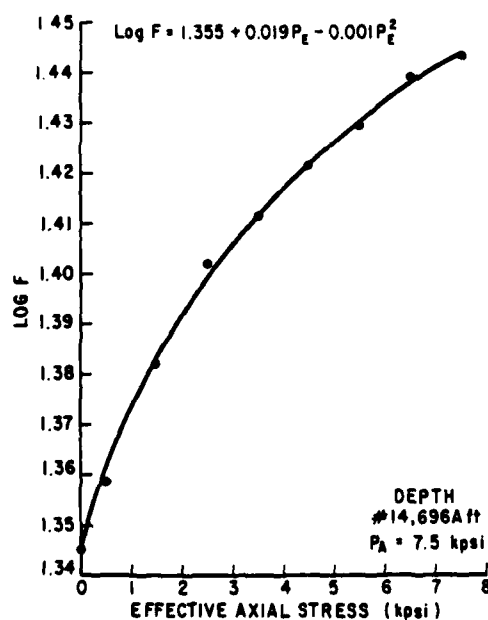


FIGURE 33C

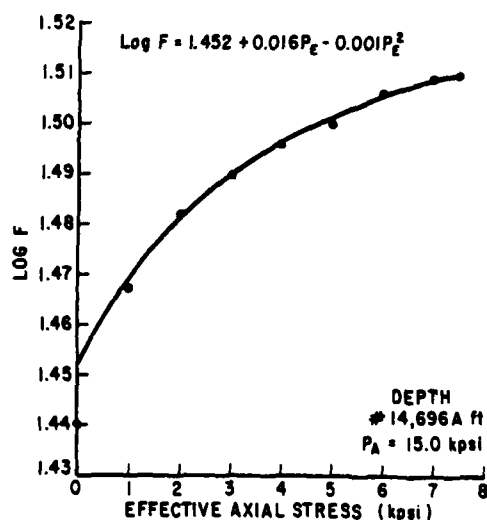


FIGURE 33D

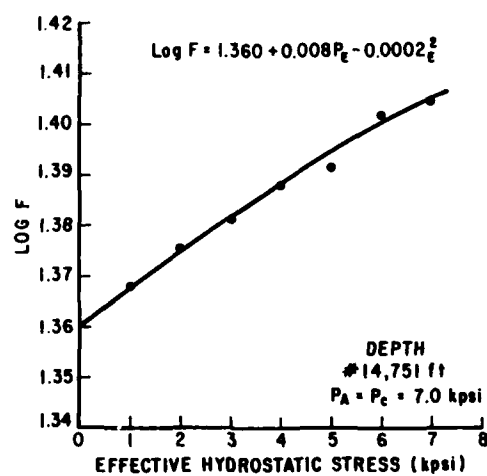


FIGURE 34A

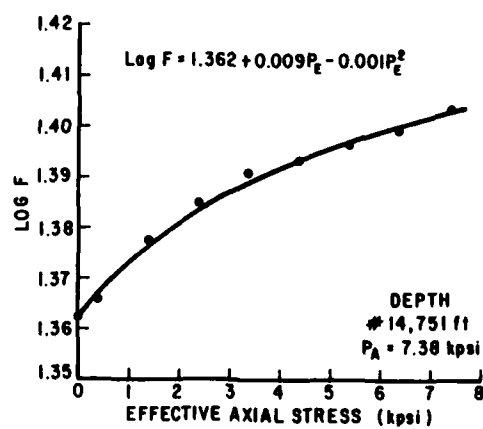


FIGURE 34B

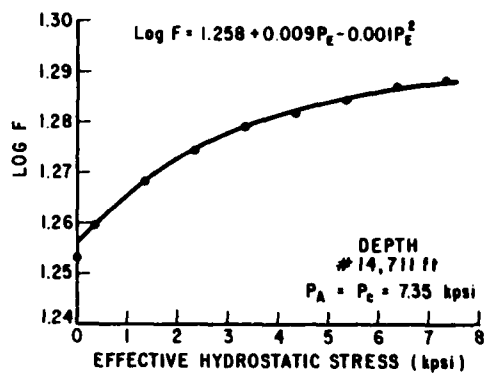


FIGURE 35A

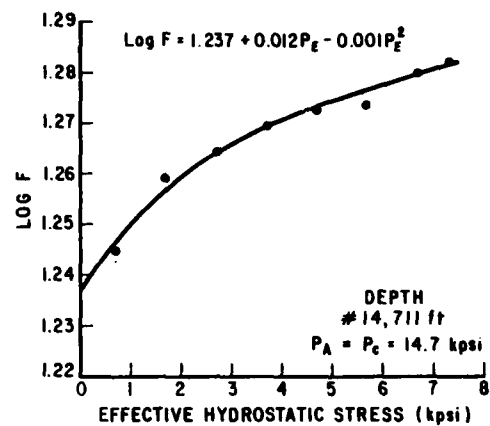


FIGURE 35B

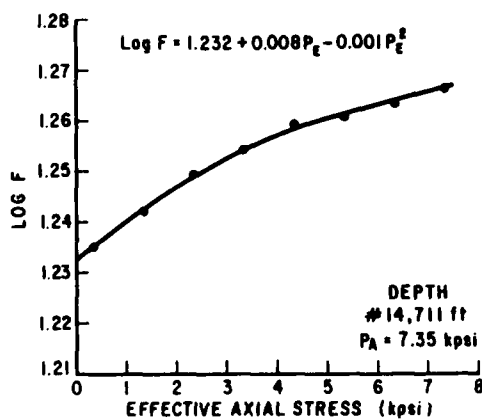


FIGURE 35C

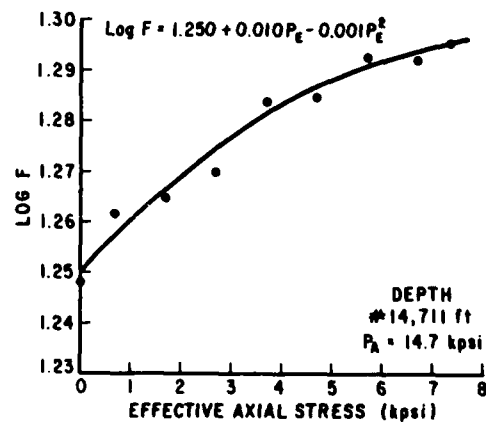


FIGURE 35D

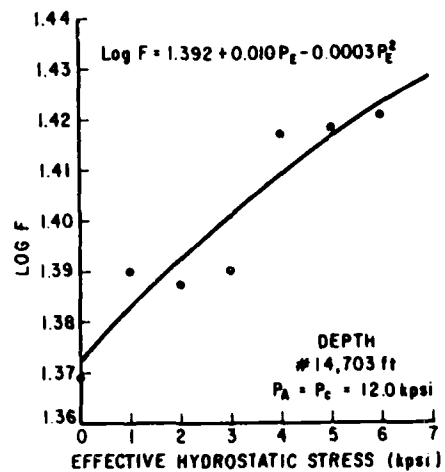


FIGURE 36A

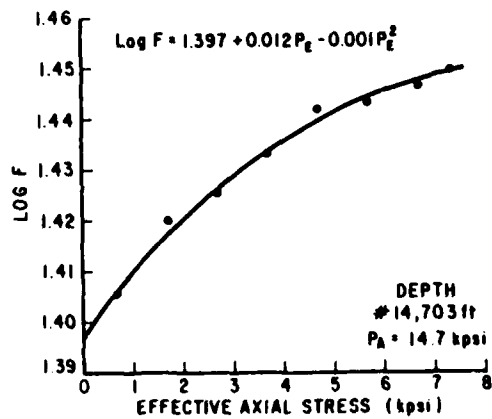


FIGURE 36B

The n_1 coefficients are dependent upon the rock matrix, amount of conductive solids in the matrix, shale content, tortuosity, and porosity. The coefficients varied from rock to rock, but for the sandstone samples representing the Pleasant Bayou reservoir, they had a low variation from the mean as discussed in Section V.4.

V.2 Porosity Changes with Effective Stress

During the compaction process, as discussed earlier, both the formation factor and the porosity change with the effective stress. In order to develop a proper relation between porosity and F , porosity changes were measured as the effective stress was varied. Porosity was obtained by both static and dynamic methods as described below.

A. Static Measurements

1. Porosity by Water Volume and Strain Measurement Method

In this method, expelled water volume measurements provided pore volume changes, and volumetric strain measurements represented bulk volume variations. The measurements were used to calculate porosity via the following expression:

$$\phi_1 = \frac{\phi_0 V_0 - \Delta V_w}{V_0 - \Delta_{eff}} \quad 5.3$$

where

ϕ_1 = measured porosity at each stress level

ϕ_0 = initial porosity of sample

V_0 = initial bulk volume

ΔV_w = expelled water volume from rock pores during deformation

Δ_{eff} = volumetric strain due to effective stress
(= $\epsilon_z + 2\epsilon_R$)

ϵ_z = axial strain

ϵ_R = radial strain

2. Porosity by Water Volume Measurement Method

Assuming that bulk volume changes are direct reflections of pore volume changes,⁶ porosity can be expressed by:

$$\phi_2 = \frac{\phi_0 V_0 - \Delta V_w}{V_0 - \Delta V_w} \quad 5.4$$

3. Porosity by Volumetric Strain Measurement Method

As a counterpart to method 2, assuming that pore volume changes are attributable mainly to bulk volume changes,⁶ the porosity can be calculated by using only measured strains:

$$\phi_3 = \frac{\phi_0 - \Delta_{eff}}{1 - \Delta_{eff}} \quad 5.5$$

4. Porosity by Resistivity Measurement Method

In this method, the Humble formula (equation 2.2), which is used for Gulf Coast sandstones, was utilized. It is given by:

$$F = \frac{0.62}{\phi^{2.15}} \quad 2.2$$

or upon rearrangement

$$\phi_4 = e^{\frac{\ln(0.62/F)}{2.15}} \quad 5.6$$

B. Dynamic Measurements

Porosity by Willie Time Average Method:³⁷

$$\phi_s = \frac{v_t(v_m - v_f)}{v_f(v_m - v_t)} \quad 5.7$$

where

v_t = p-wave velocity through the saturating fluid (for the 6% NaCl solution used, $v_f = 5195$ ft/sec)

v_f = measured p-wave velocity through the sample

v_m = p-wave velocity through the matrix material (for the sandstone samples selected, $v_m = 19,600$ ft/sec based on values obtained in the laboratory for fused quartz.²⁹)

Porosities obtained using these methods were plotted against the applied effective stress for each of the tests. Figures 37 through 48 show such plots for the various rock samples subjected to similar effective stress conditions. Each of the graphs shows that the percentage change in porosity per 1000 psi effective stress change is dependent upon the method of determination. Table 1 provides a relative comparison among the methods.

ϕ_s gave the largest percentage change. Variations in this method appear in general to be excessive. The greatest change occurred at low effective stress, however, and in the 4,000 to 7,000 psi range of effective stress, the variation with pressure decreased, providing values of porosity which for most rocks approximated porosities determined by other methods.

The porosity obtained by the water volume and volumetric strain method, ϕ_1 , was considered to be the most accurate measure of the true porosity. The calculations, which were corrected for brine compressibility variations according to Gibson,³¹ incorporated no assumptions beside

TABLE 1

Relative Comparisons of Porosity Reductions
With Effective Stress

| Method of Porosity Determination | Symbol | Average % Change in Porosity [*] per kpsi Effective Stress Change |
|---------------------------------------|----------|--|
| Water Volume and Volumetric Strain | ϕ_1 | 0.7 - 1.1 |
| Water Volume | ϕ_2 | 0.6 - 1.0 |
| Volumetric Strain | ϕ_3 | 0.1 - 0.3 |
| Resistivity | ϕ_4 | 0.5 - 0.9 |
| Time Average | ϕ_5 | 3.0 - 4.0 |

* Porosity range for the samples tested was 16 to 21%

rock isotropy and homogeneity.

In contrast, both the porosity by water volume, ϕ_2 , and the porosity by volumetric strain, ϕ_3 , methods were computed based on the simplifying approximation⁶ that if

$$C_R \ll C_B$$

where

C_R = rock matrix compressibility

C_B = rock bulk compressibility

then, pore volume changes approach bulk volume changes. Or more directly,

$$\Delta V_P \approx \Delta V_B$$

where

ΔV_P = change in pore volume

ΔV_B = change in bulk volume

The porosity as determined by the water volume method, ϕ_2 , has been used widely in literature^{6,19,20,21,22} to represent porosity variations with pressure. From a macroscopic viewpoint, the small difference between ϕ_2 and ϕ_1 shown in Table 1 could justify the use of the more easily obtainable ϕ_2 . However, this difference could be significant when modelling reservoirs of high initial porosity and abnormally high formation pressures.

The volumetric strain porosity, ϕ_3 , reflected percentage changes in porosity which, in relation to results from the other methods, were low. The actual variations in the rock porosity were masked by using re-

latively small percentage changes in the bulk volume to reflect pore volume changes.

Porosities calculated by the resistivity method using the Humble formula, ϕ_4 , reflected changes with effective stress which were less than those given by ϕ_1 . The Humble formula, then, did not appear to be completely accurate in providing porosities from resistivity data at the high effective stresses found in the geopressured reservoir.

Logically, since both resistivity and porosity vary with pressure, the cementation factor in the Humble formula and in Archie's equation should also change. As explained in Section III.2, several investigators^{20,21,22} found that the cementation factor was not constant with pressure. In view of this fact, a modified Archie's equation may be written as

$$F(P_E) = \phi(P_E)^{-m(P_E)} \quad 3.7$$

$$\text{or} \quad \ln F(P_E) = -m(P_E) \ln \phi(P_E) \quad 5.8$$

Formation factors were calculated using measured values of rock resistivity and pressure-corrected values of brine resistivity as explained in Appendix I. Porosities were determined by the expelled water volume and volumetric strain method (method 1).

Graphs of $\ln F$ versus $\ln \phi_1$ were nonlinear which reflected the pressure dependence of the cementation factor. Therefore, in order to evaluate $m(P_E)$ formation factors were plotted against ϕ_1 for the different rock samples tested under various loading conditions. Figure 49 through 60 show the results.

The data was best fitted by a second degree polynomial in P_E of the form

$$-m(P_E) = m_1 + m_2 P_E + m_3 P_E^2 \quad 5.9$$

where

$$m_i = \text{constant coefficients}$$

Substitution into equation 3.7 results in

$$F(P_E) = \phi(P_E)^{m_1 + m_2 P_E + m_3 P_E^2} \quad 5.10$$

Notice that for $P_E = 0$, Archie's equation is reproduced.

The coefficients in the quadratic expression of the cementation factor are a function of the rock type. Guyod¹⁶ explained that m itself is dependent upon the degree of cementation in the rock. The coefficients, m_i , are similarly dependent. Their values fluctuated slightly from sample to sample tested, but the statistical variation from the mean was low as shown in Table 2 and discussed in Section V.4

An expression for the porosity as a function of the effective stress was formulated using the mean values of the coefficients in the quadratic expression of m . From equation 5.10

$$\ln \phi(P_E) = \frac{\ln F(P_E)}{m_1 + m_2 P_E + m_3 P_E^2} \quad 5.11$$

Substituting equation 5.2 and solving for porosity results in

$$\phi = e^{\frac{n_1 + n_2 P_E + n_3 P_E^2}{m_1 + m_2 P_E + m_3 P_E^2}} \quad 5.12$$

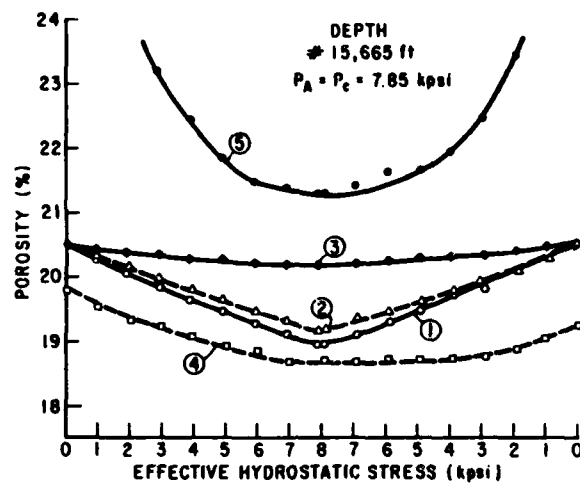


FIGURE 37A

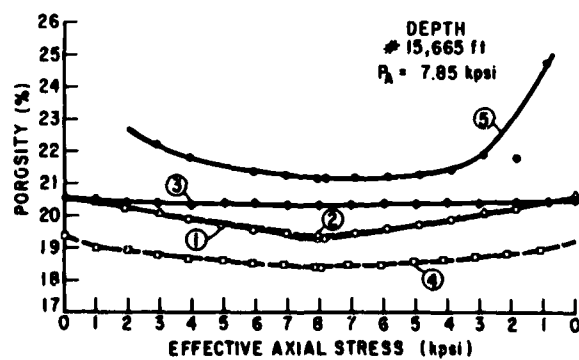


FIGURE 37B

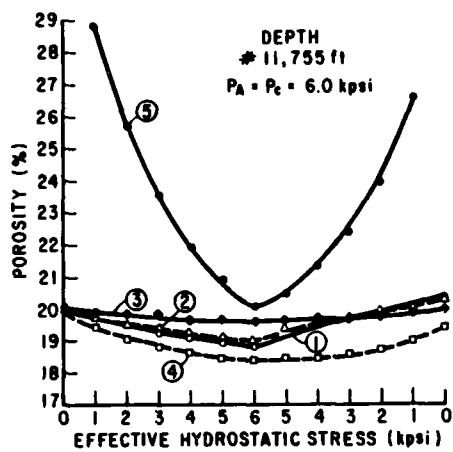


FIGURE 38A

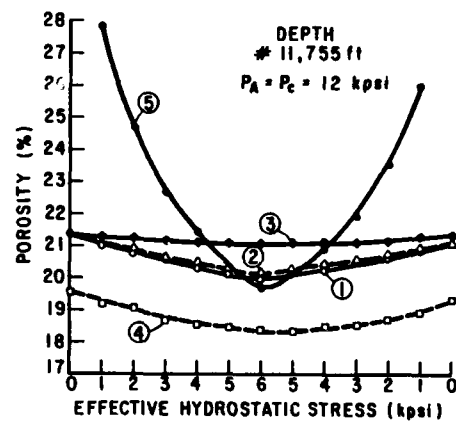


FIGURE 38B

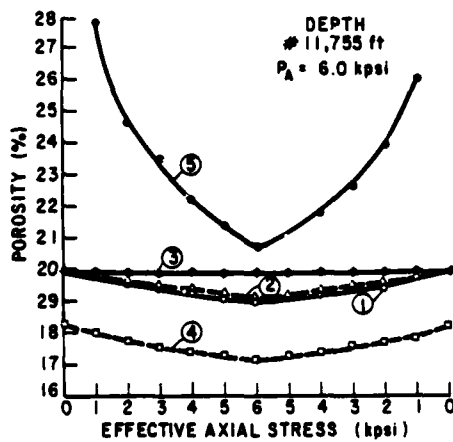


FIGURE 38C

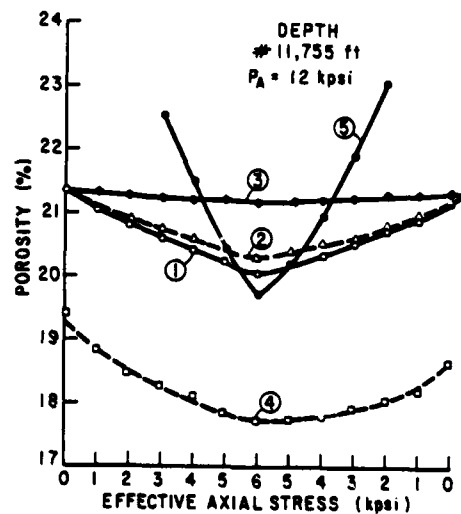


FIGURE 38D

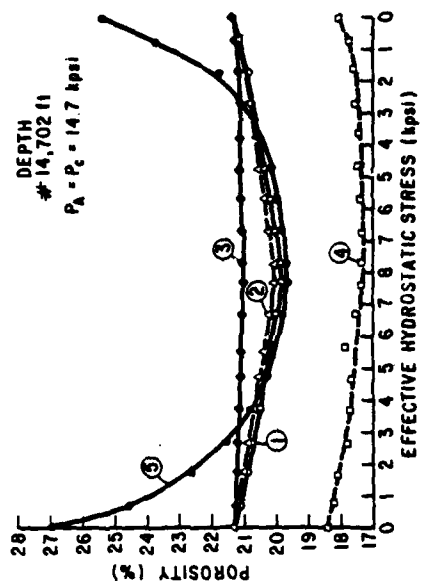


FIGURE 39B

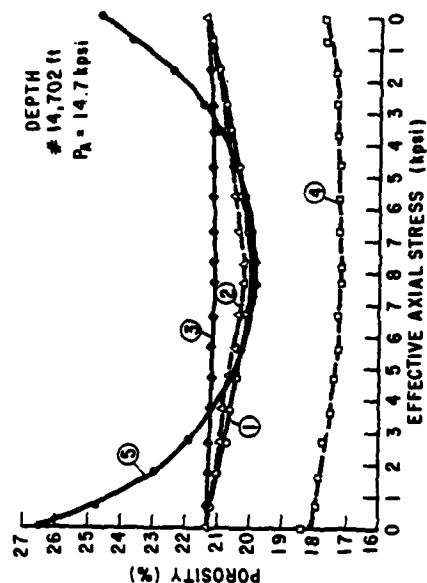


FIGURE 39D

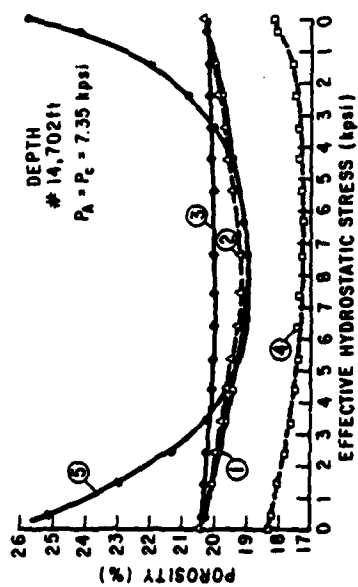


FIGURE 39A

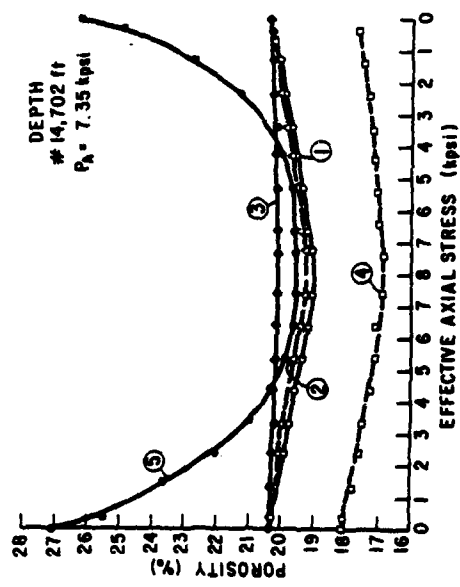


FIGURE 39C

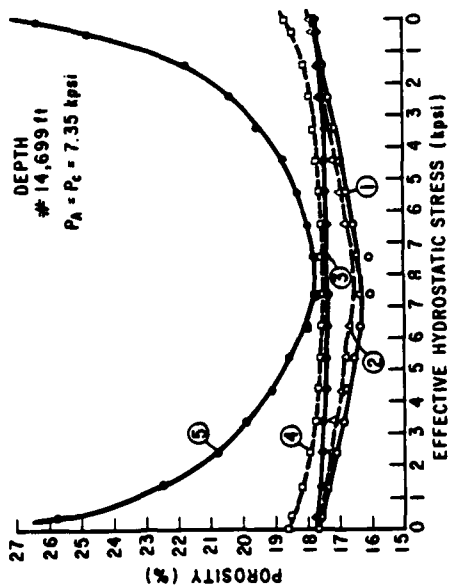


FIGURE 40A

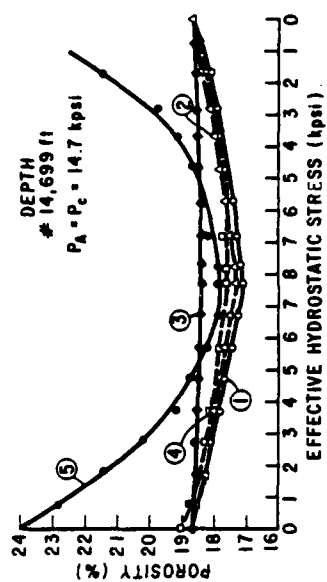


FIGURE 40B

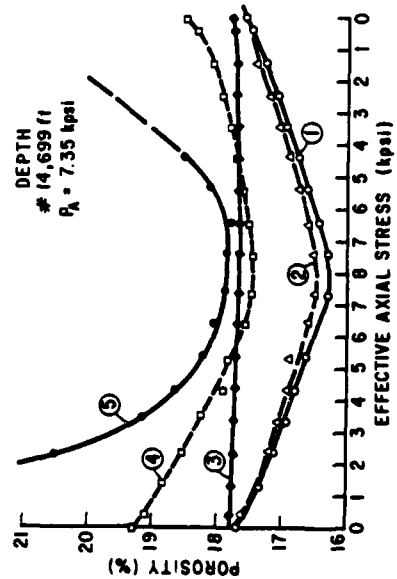


FIGURE 40C

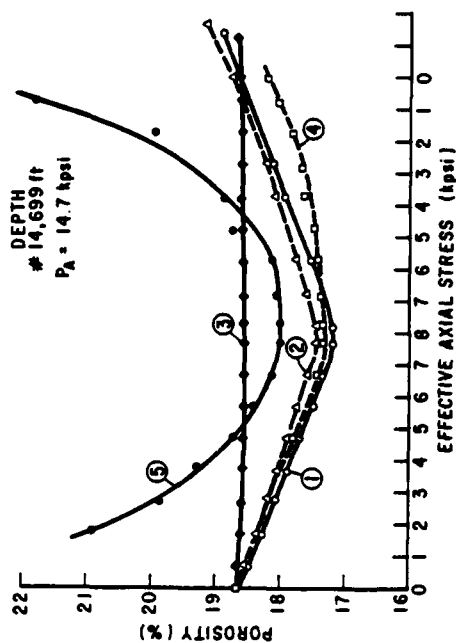


FIGURE 40D

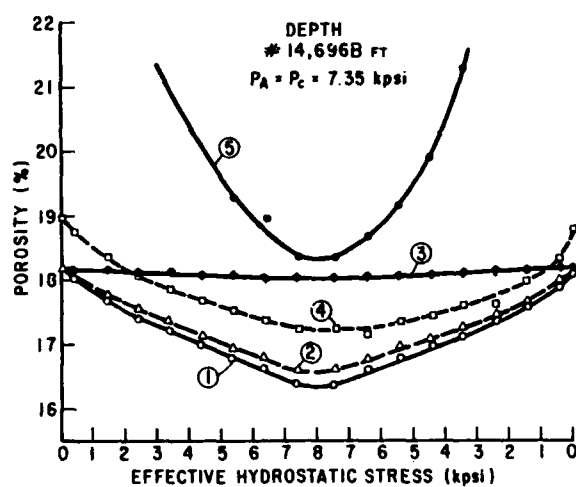


FIGURE 41A

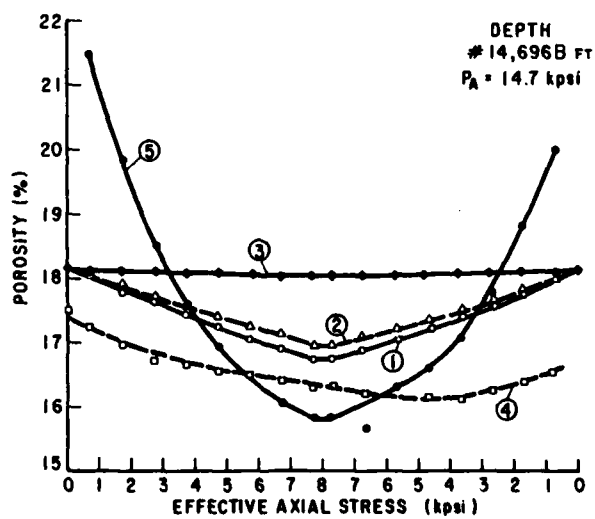


FIGURE 41B

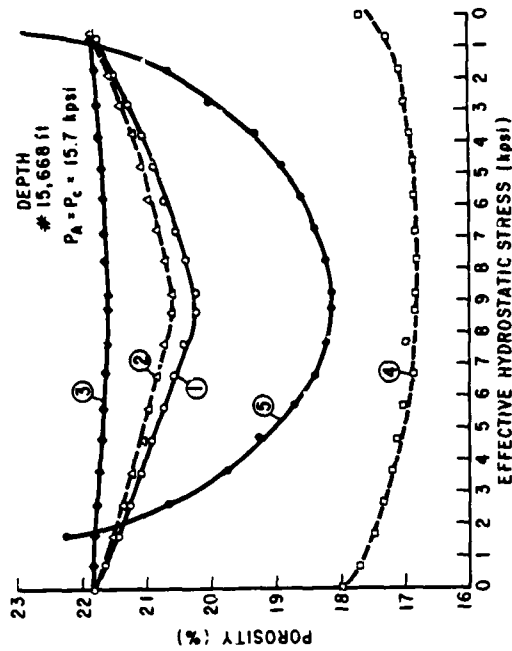


FIGURE 42B

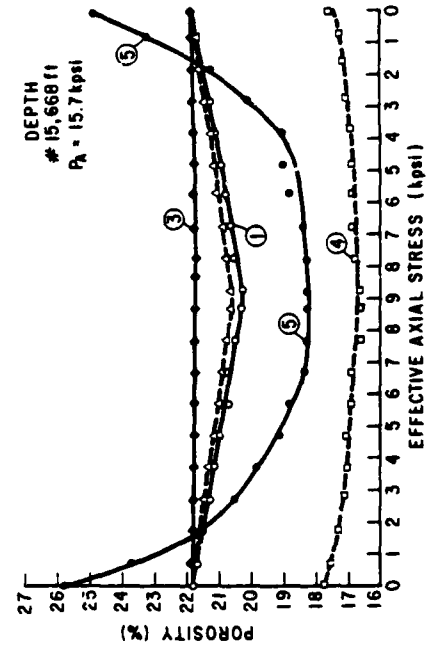


FIGURE 42D

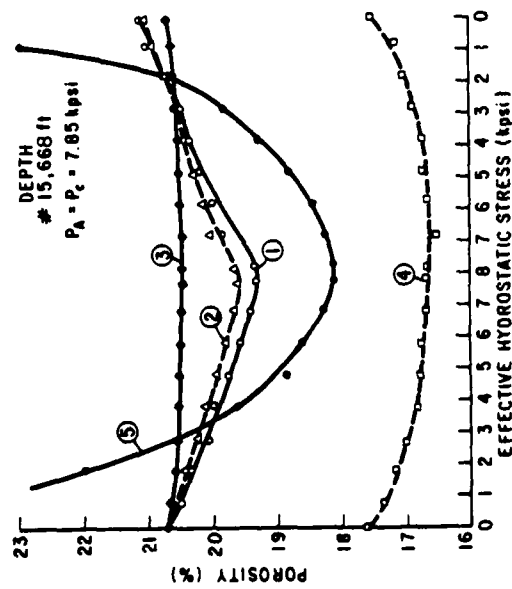


FIGURE 42A

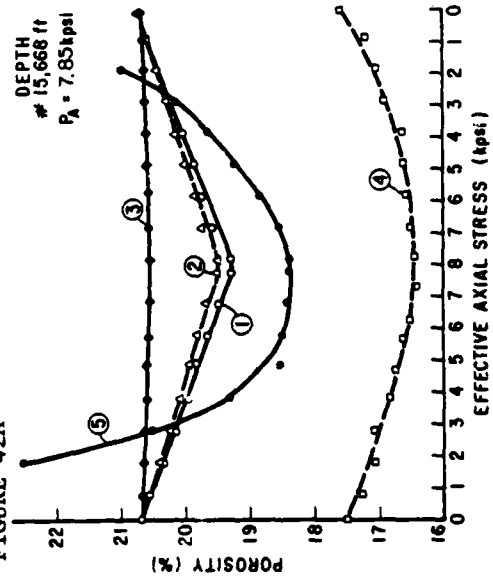


FIGURE 42C

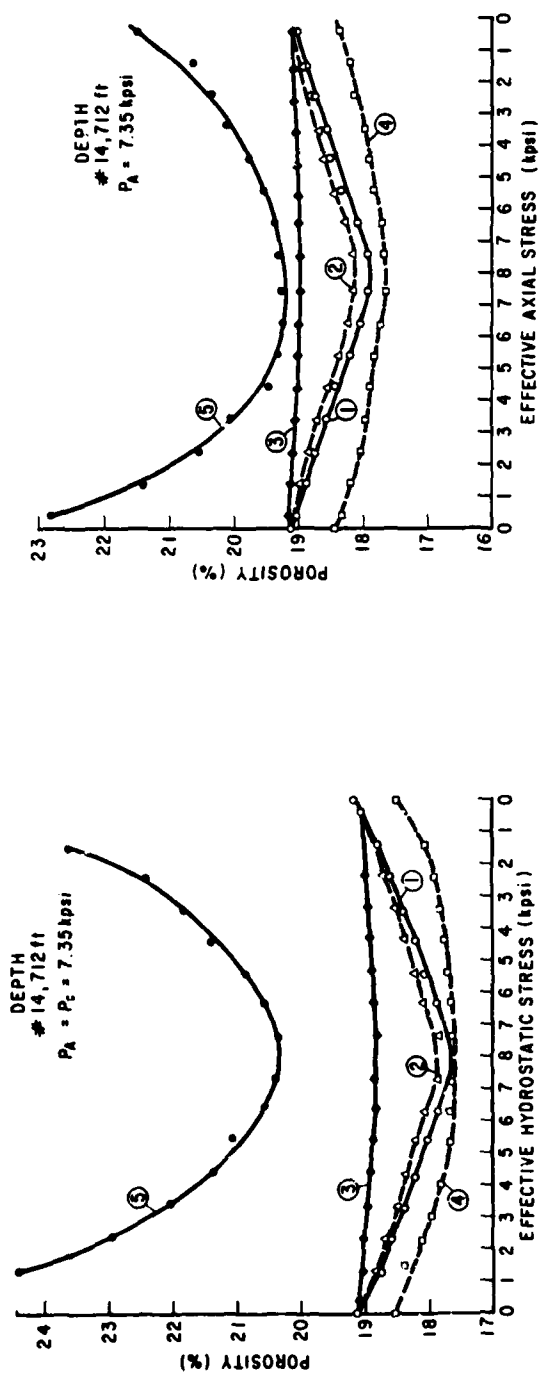


FIGURE 43A

FIGURE 43B

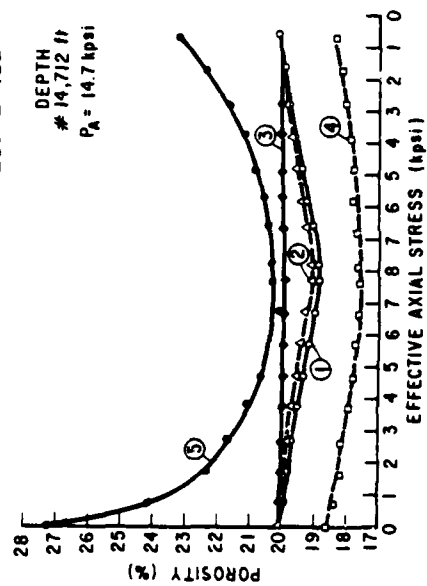


FIGURE 43C

AD-A108 116

AIR FORCE INST OF TECH WRIGHT-PATTERSON AFB OH
THE INTERRELATIONSHIPS AND VARIATIONS OF THE RESISTIVITY, POROS--ETC(U)
AUG 81 T R ASHMAN
AFIT-CI-81-617

F/G 8/7

NL

UNCLASSIFIED

2 of 2

3086



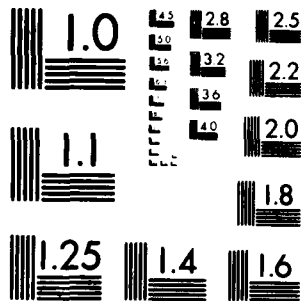
END

DATE

FILMED

1 4 2

DTIC



MICROCOPY RESOLUTION TEST CHART
NATIONAL BUREAU OF STANDARDS - 1963-A

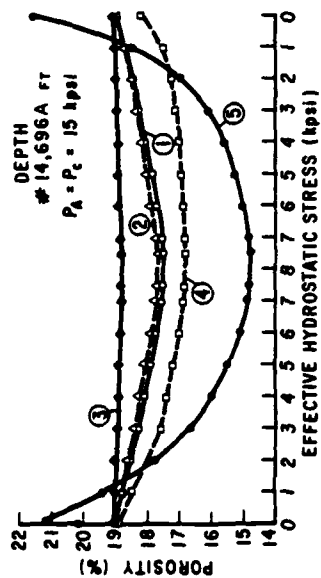


FIGURE 44A

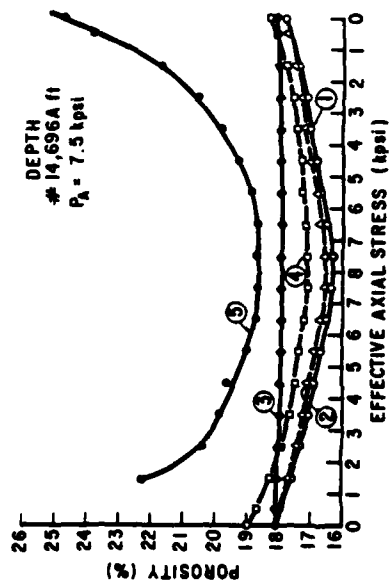


FIGURE 44B

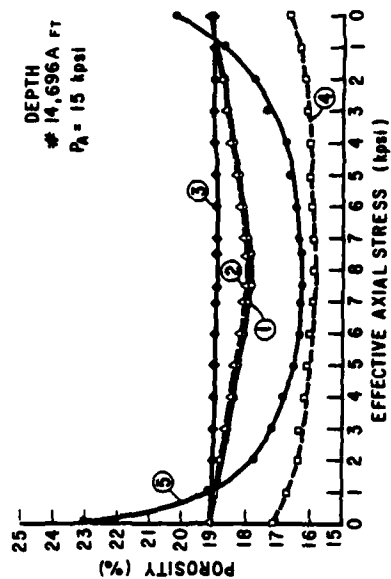


FIGURE 44C

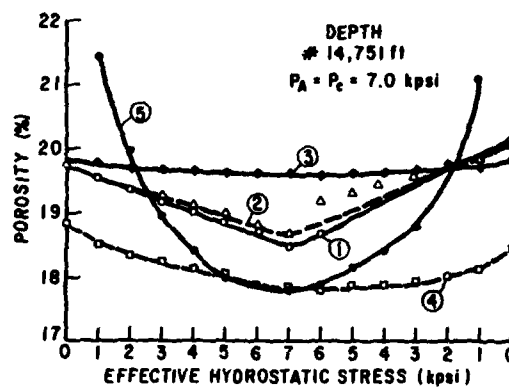


FIGURE 45A

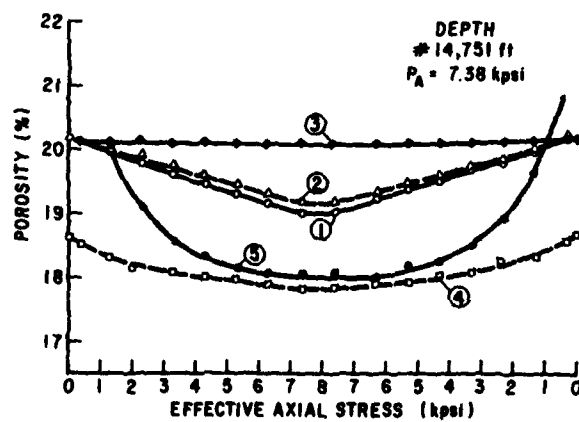


FIGURE 45B

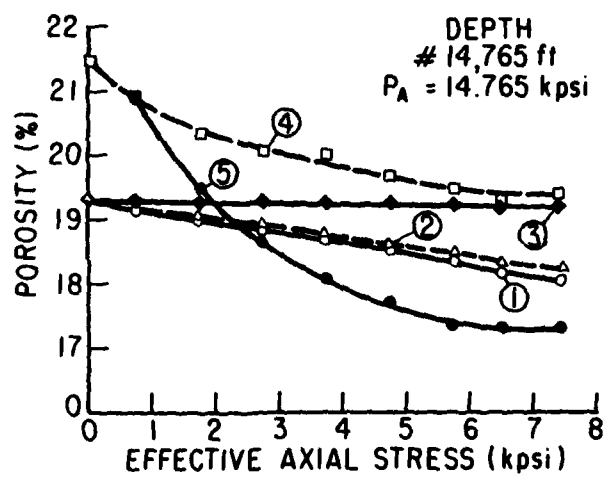


FIGURE 46

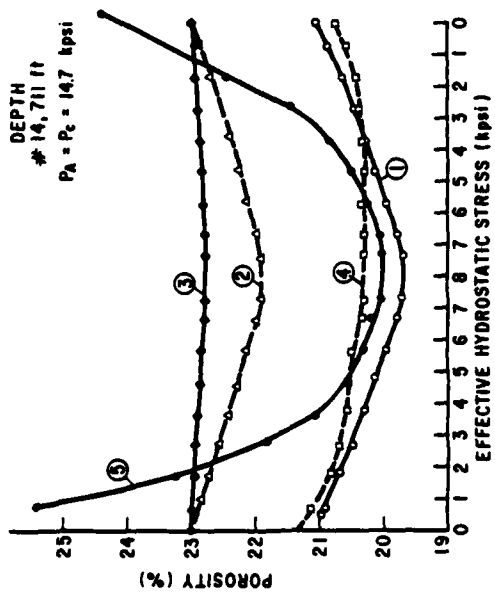


FIGURE 47B

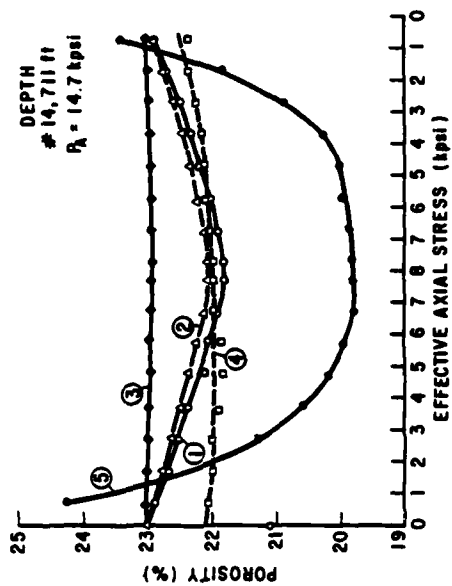


FIGURE 47D

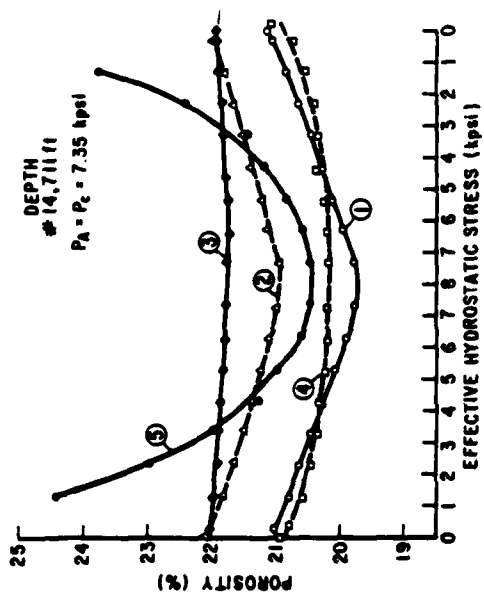


FIGURE 47A

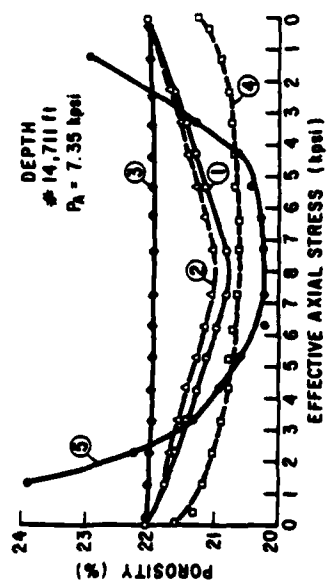


FIGURE 47C

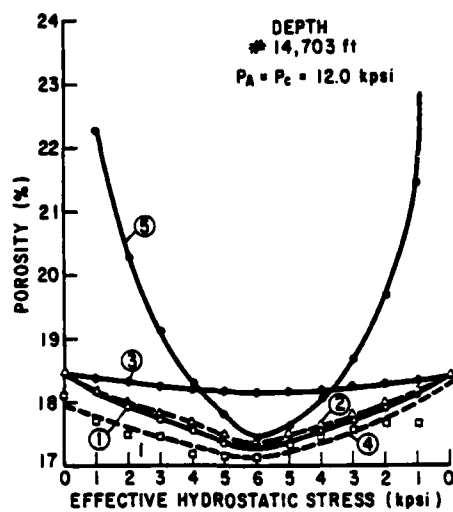


FIGURE 48A

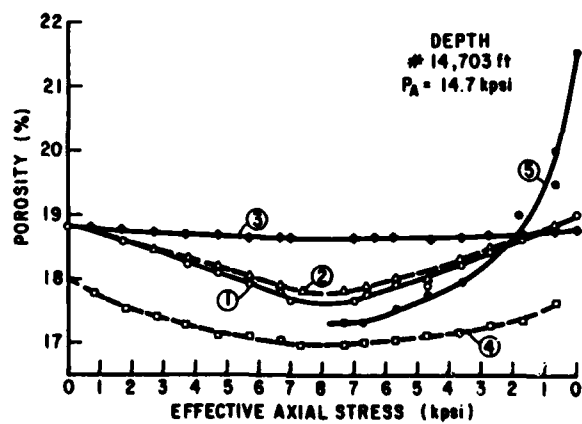


FIGURE 48B

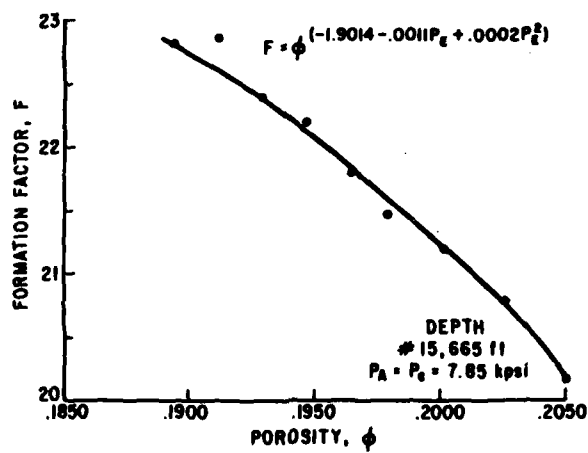


FIGURE 49A

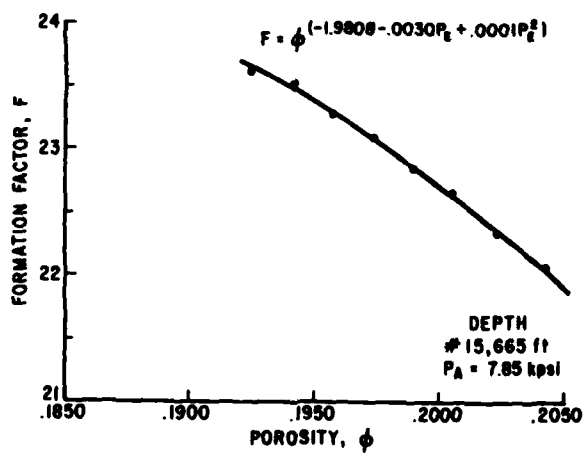


FIGURE 49B

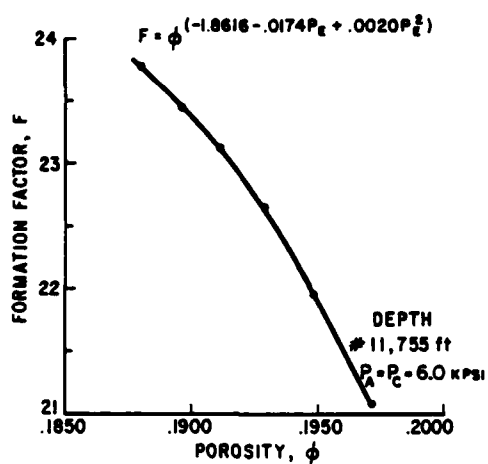


FIGURE 50A

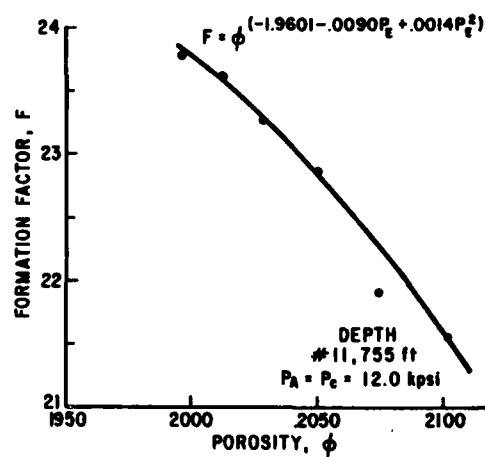


FIGURE 50B

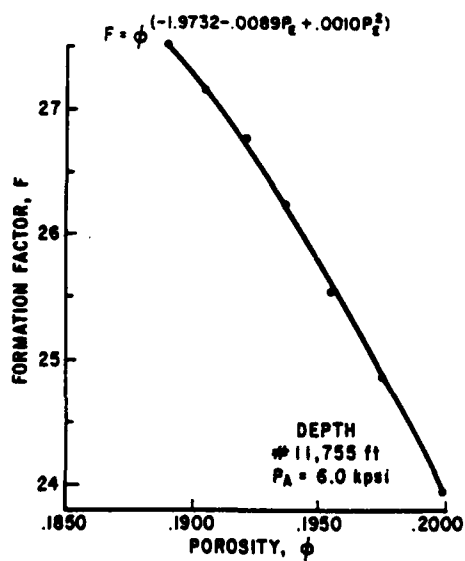


FIGURE 50C

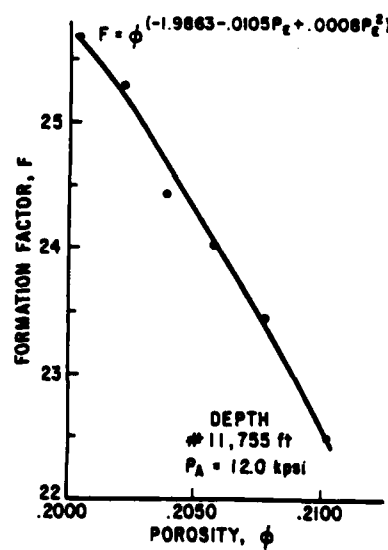


FIGURE 50D

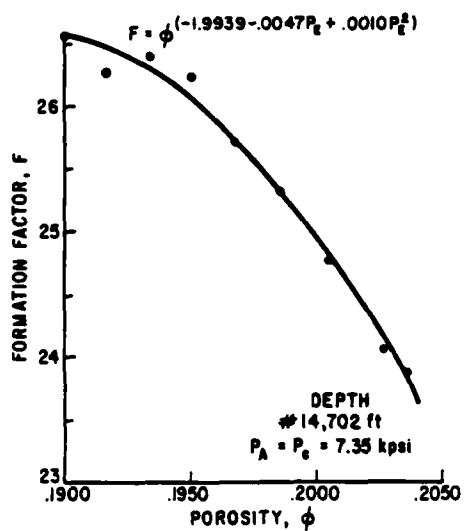


FIGURE 51A

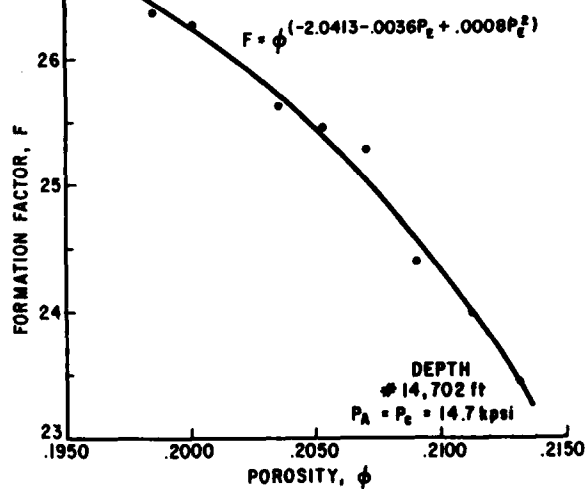


FIGURE 51B

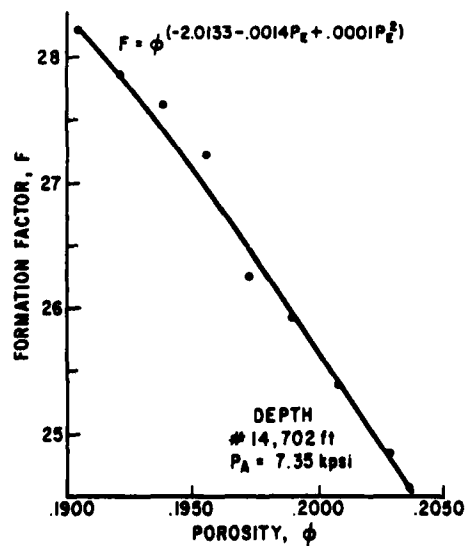


FIGURE 51C

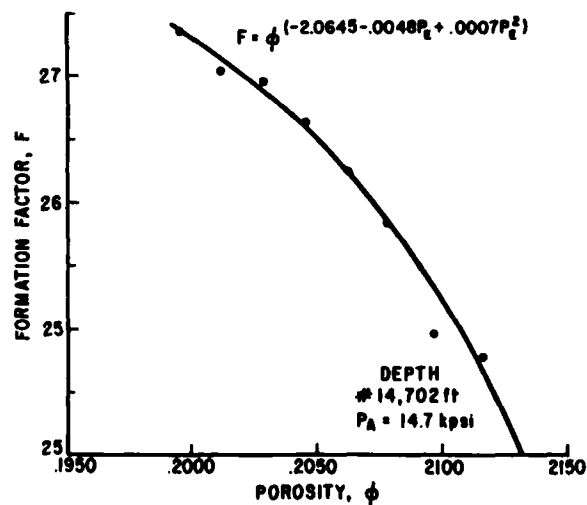


FIGURE 51D

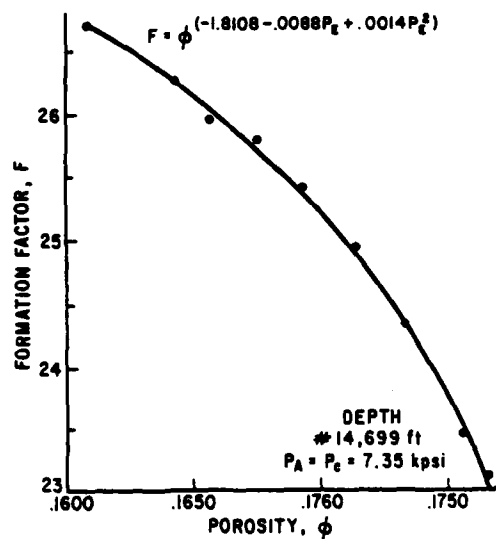


FIGURE 52A

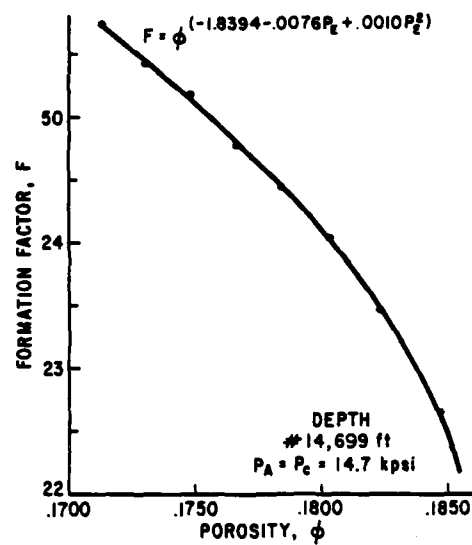


FIGURE 52B

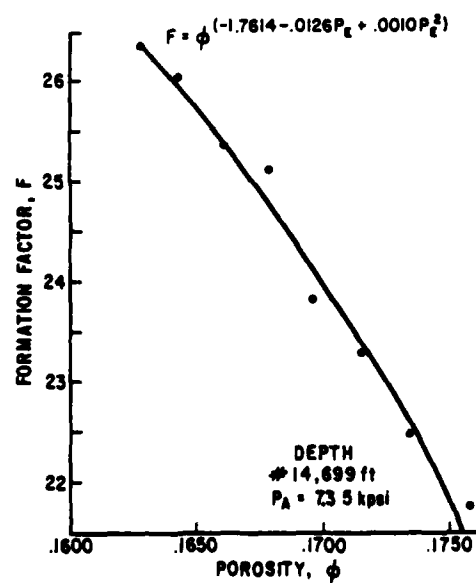


FIGURE 52C

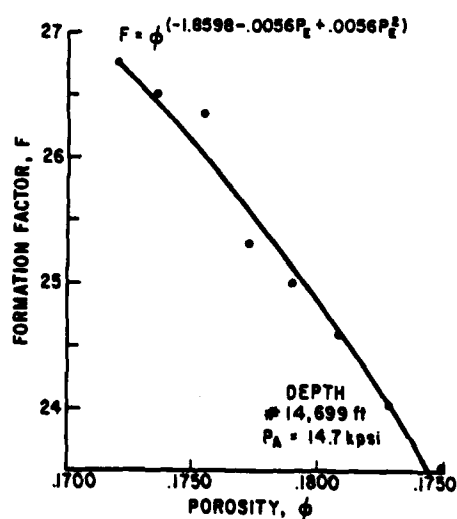


FIGURE 52D

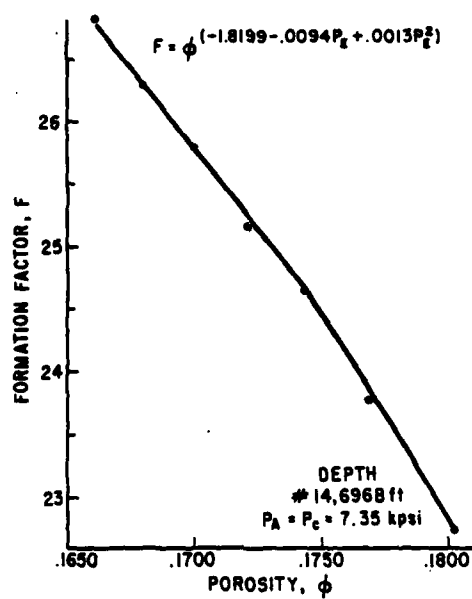


FIGURE 53A

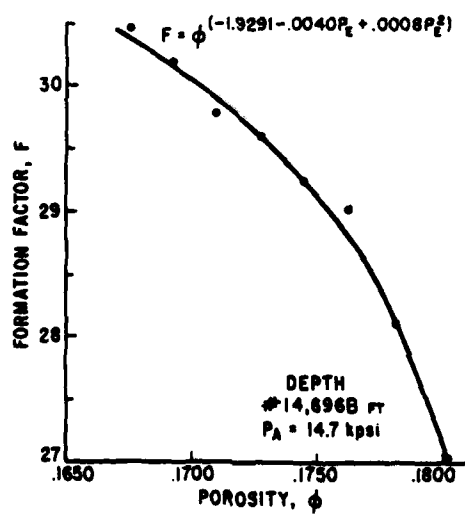


FIGURE 53B

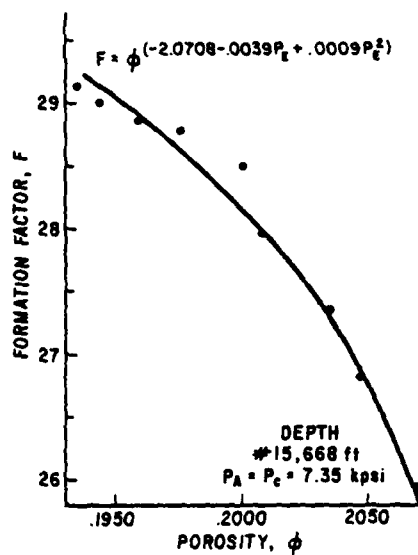


FIGURE 54A

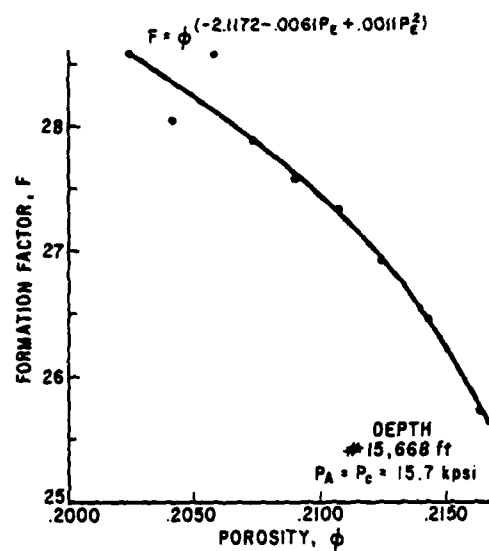


FIGURE 54B

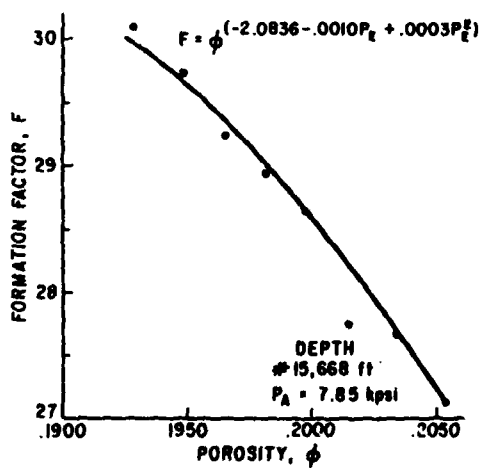


FIGURE 54C

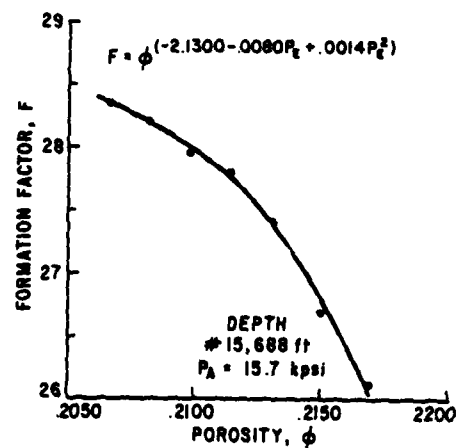


FIGURE 54D

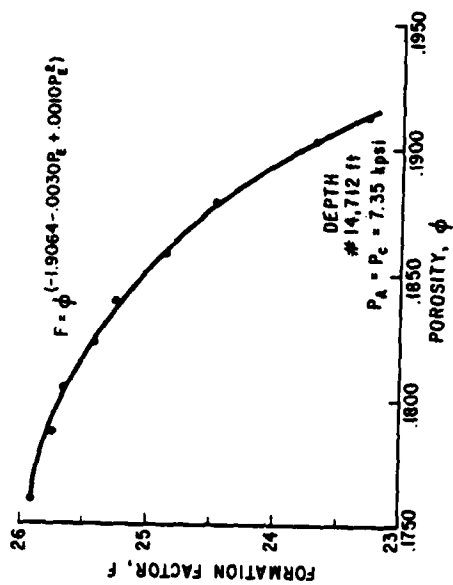


FIGURE 55A

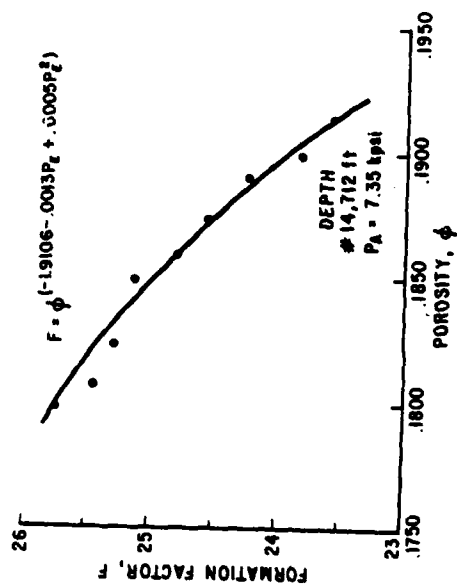


FIGURE 55B

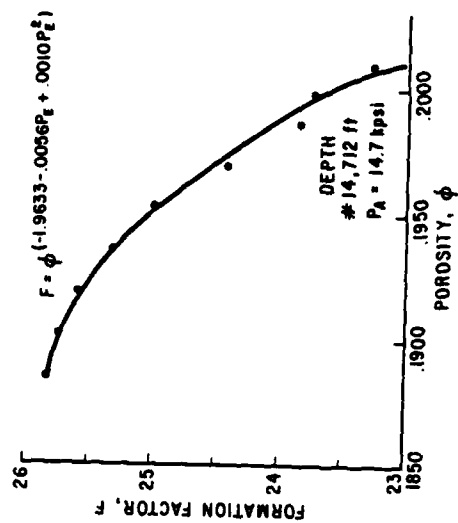


FIGURE 55C

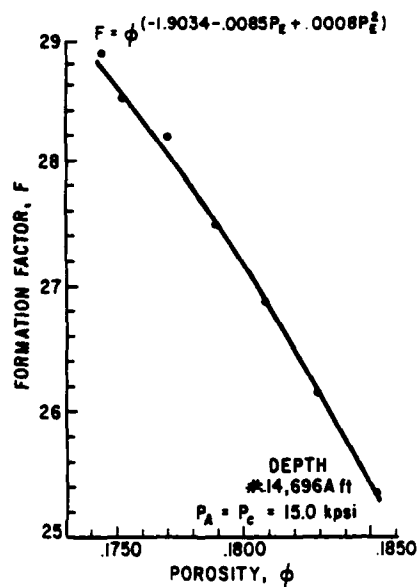


FIGURE 56A

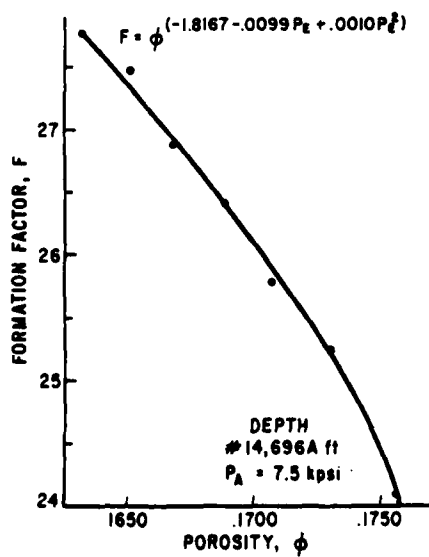


FIGURE 56B

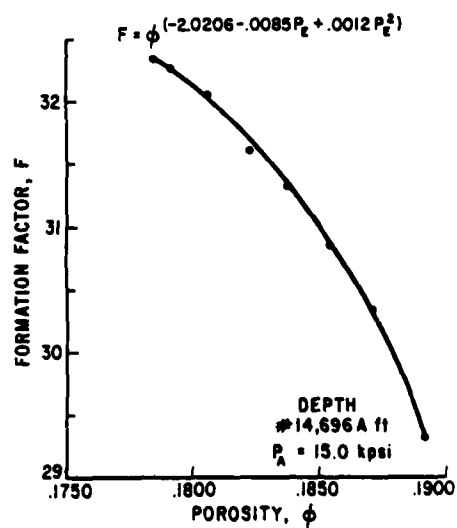


FIGURE 56C

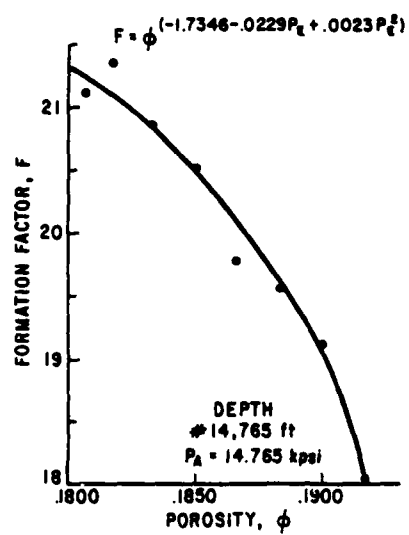


FIGURE 57

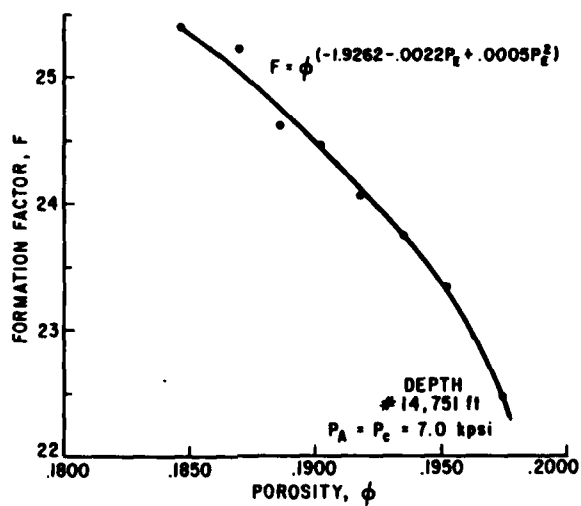


FIGURE 58A

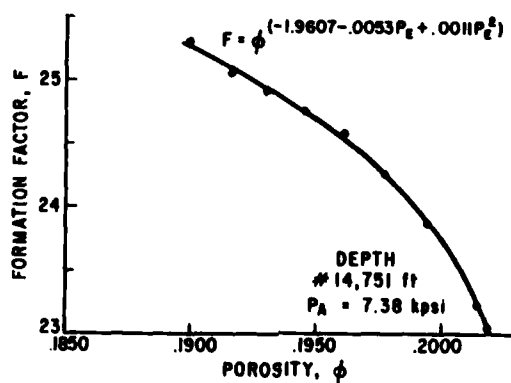


FIGURE 58B

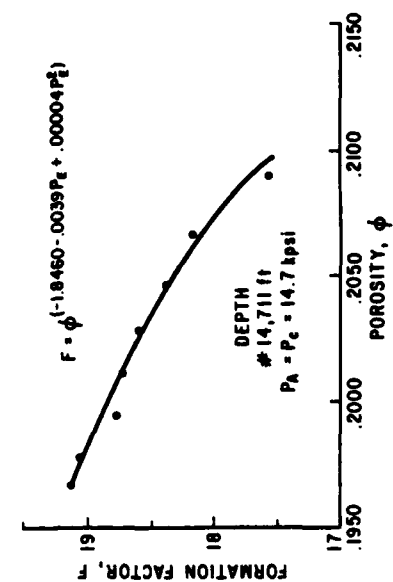


FIGURE 59A

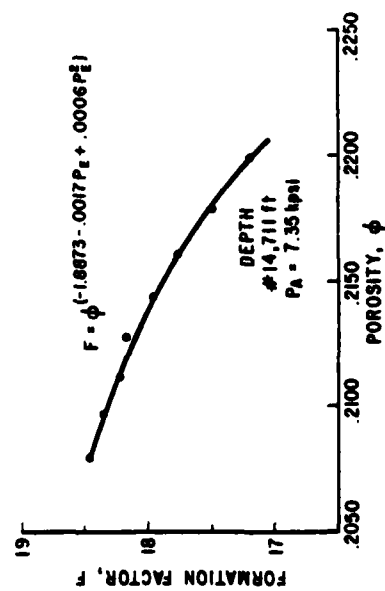


FIGURE 59C

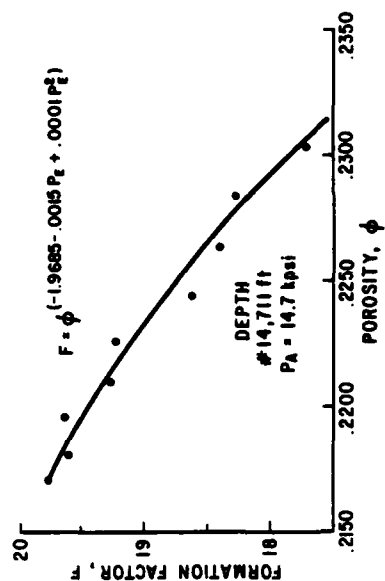


FIGURE 59D

FIGURE 59B

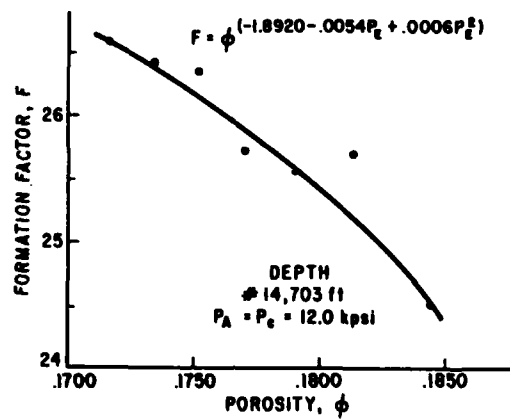


FIGURE 60A

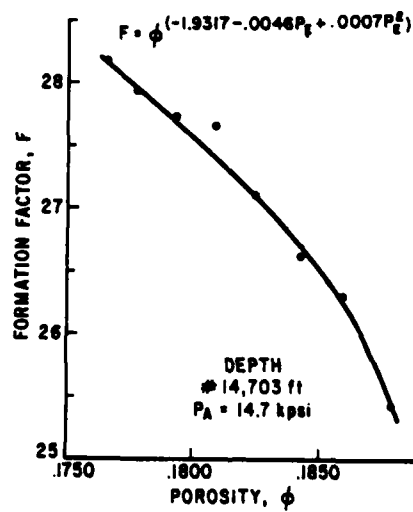


FIGURE 60B

A change in porosity, $d\phi$, as a result of an effective stress change, dP_E , therefore is given by

$$d\phi = \left\{ \left[\frac{(n_1 + 2n_2P_E)}{(m_1 + m_2P_E + m_3P_E^2)} - \frac{(m_2 + 2m_3P_E)(n_1 + n_2P_E + n_3P_E^2)}{(m_1 + m_2P_E + m_3P_E^2)^2} \right] \frac{n_1 + n_2P_E + n_3P_E^2}{m_1 + m_2P_E + m_3P_E^2} \right\} dP_E \quad 5.13$$

Results produced by equation 5.13 were comparable to experimentally obtained data. Figure 63 shows calculated and measured values of porosity for a typical sample. An analysis of the results is provided in Section V.4.

V.3 Permeability Changes with Effective Stress

The permeability changes with effective stress observed in this work were qualitatively similar to those found by other investigators^{9,10,12,22,27}. Permeability, k , was found to decrease significantly with increases in effective stress. Figure 61 shows such a dependence for one of the rocks tested. All other samples gave similar results.

A general polynomial expression of k in P_E was not feasible because of the non-uniform variations of the permeability with effective stress. A more practical and obtainable relationship was found when permeability was related to resistivity.

Wyllie and Spangler²³ and Boggus²⁴ have shown that resistivity increased with decreasing permeability for clean sandstones. Since resistivity is the reciprocal of electrical conductivity and permeability

has been labelled the hydraulic conductivity, this relationship seems to be natural.

Wyllie and Spangler, however, concluded that this relationship might not be so apparent for rocks containing shale inclusions, mica flakes, or secondary cementation effects. Rock samples selected for this work from the producing horizon of Pleasant Bayou wells #1 and #2, were relatively clean sandstones and, therefore, should not have been influenced greatly by these factors.

Data was analyzed using the hydraulic - electrical conductivity analog developed in Chapter III and reflected in equation 3.10:

$$F \times k = \text{constant} \quad 3.10$$

The product of permeability and formation factor at each stress level for each rock sample was normalized in analysis to permit comparisons between various samples. Since experimental data were not always available at the zero effective stress condition, a 5,000 psi effective stress level was used as the reference for normalization.

Figure 62 shows the normalized Fk product plotted against effective stress for the twelve rock samples tested. Results were regressed linearly and are represented by the equation

$$y = 1.000 - 0.002x \quad 5.14$$

where

$$y = \frac{(F \times k)}{(F \times k)_{\text{reference level}}}$$

Equation 5.14 shows that the product Fk is essentially independent of the effective stress, thereby indicating that

$$F \times k = (F \times k)_{\text{reference level}} \quad 5.15$$

Since $(F \times k)_{\text{reference level}}$ for each rock is a constant, equation 5.15 reduces to the form of equation 3.10. That is

$$F \times k = \text{constant} \quad 3.10$$

Since $\ln F$ can be represented by a quadratic expression in P_E (equation 5.2), the permeability, upon rearrangement of equation 3.10, can be given by

$$\begin{aligned} \ln k &= C - (n_1 + n_2 P_E + n_3 P_E^2) \\ &= C' - n_2 P_E - n_3 P_E^2 \end{aligned} \quad 5.16$$

where C & C' are constants

The permeability, therefore, becomes a function of the rock type and the effective stress. The constant, C' , can be evaluated using permeability data for a core at atmospheric pressure where $P_E = 0$, resulting in

$$C' = [\ln k]_{P_E=0} \quad 5.17$$

Equation 3.10 can also be used to obtain a relation between permeability and porosity. Substituting equation 5.10 into 3.10 results in

$$k \times \phi^{m_1 + m_2 P_E + m_3 P_E^2} = \text{constant} = C \quad 5.18$$

where the constant, C , depends on the rock characteristics. Therefore, permeability is a function of the porosity, effective stress, and rock type.

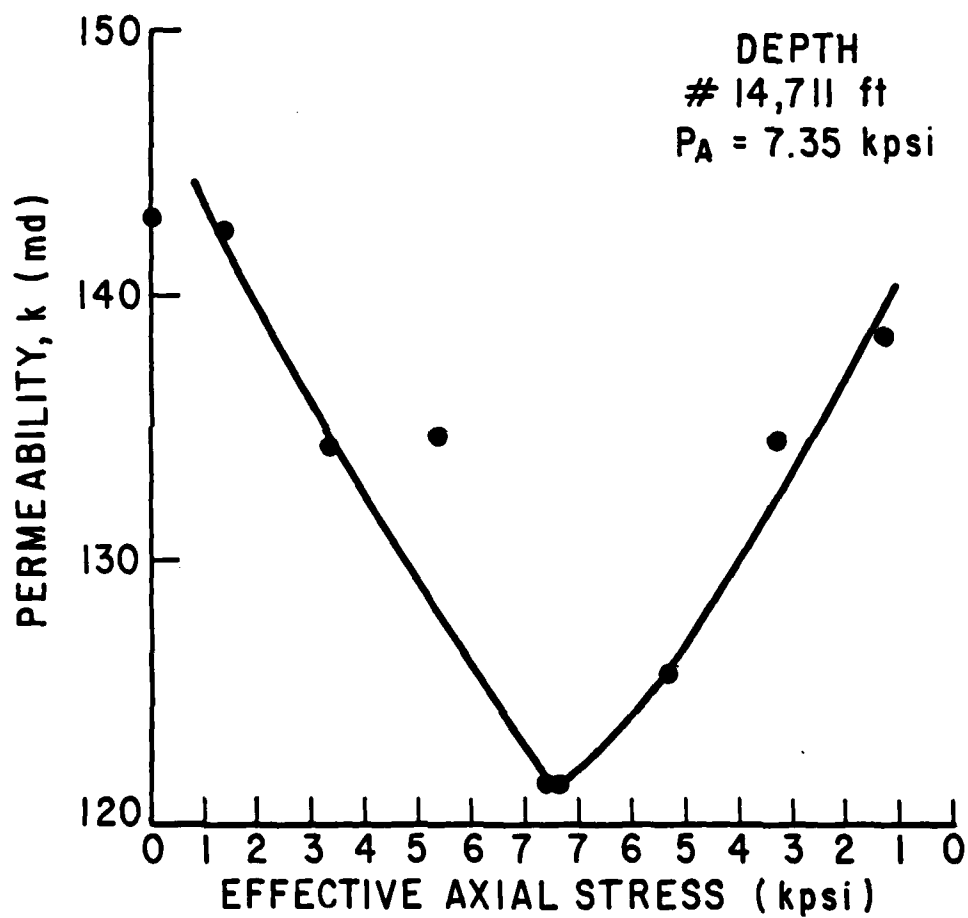


FIGURE 61 GENERAL PERMEABILITY TREND WITH EFFECTIVE STRESS
(#14711)

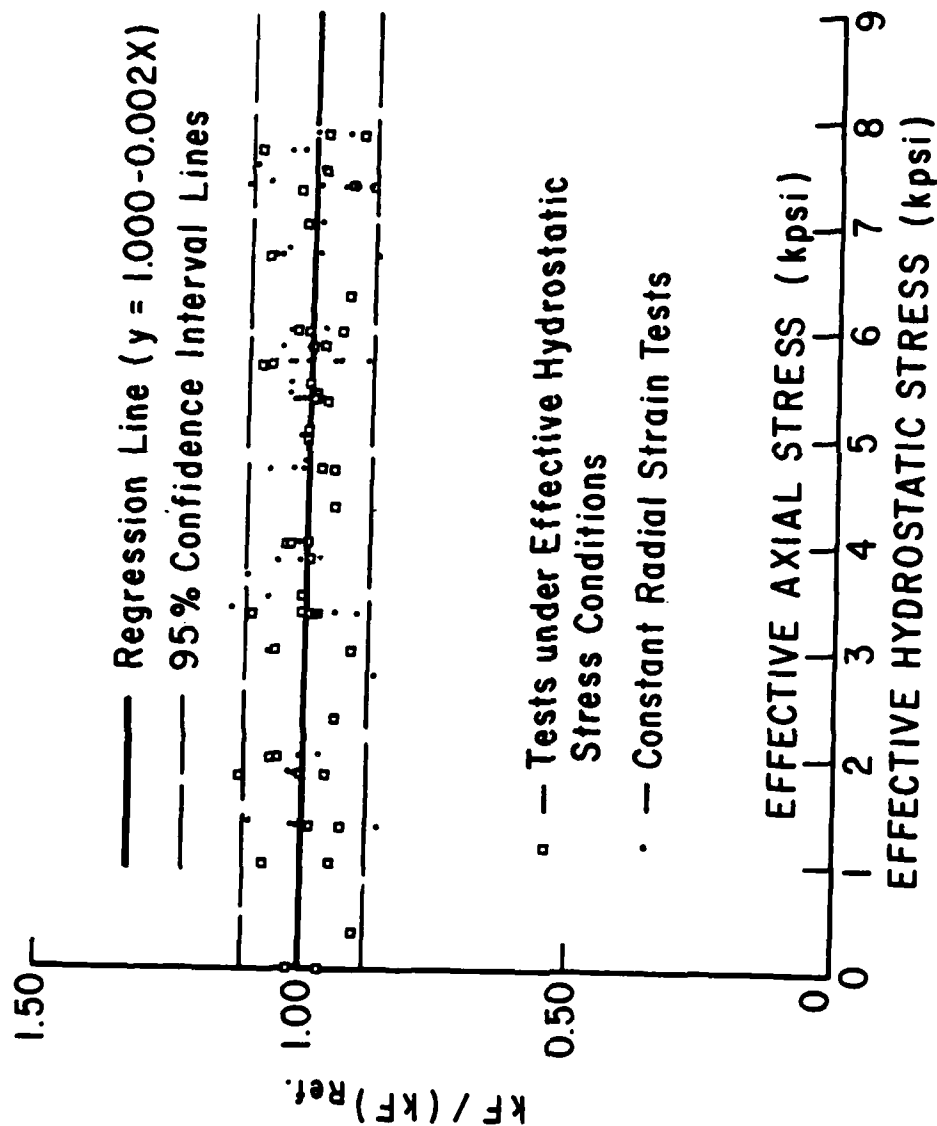


FIGURE 62 REGRESSION LINE OF NORMALIZED $k \times F$ PRODUCT AS A FUNCTION OF EFFECTIVE STRESS (ALL TESTS)

Comparisons between permeabilities obtained from actual experimental results and those predicted by equation 5.18 are given in Table 6 and Figure 64.

V.4 Discussion of Results

Values for coefficients n_1 and m_1 as expressed in equations 5.2 and 5.9 respectively were calculated for each test (the loading procedures for which are described in Chapter III) on all rock samples. Table 2 lists the results. One can observe that when $P_E = 0$, the cementation factor expression reduces to a constant, m_1 , with a value in the range 1.7 - 2.1. These values are consistent with those given by Archie and other investigators.^{16,17}

A statistical analysis of the results provided a basis for comparison. Since the porosity range among the samples was small (16% - 21%), the arithmetic mean, standard deviation, and variation were computed for each coefficient. Because different stress loadings were imposed in the various tests, results were grouped accordingly, and the variations from the mean compared. Table 3 depicts these variations for the data in total and for the individual tests. In general, the lowest variations for the six coefficients occurred for the uniaxial compaction test.

Since uniaxial compaction loading can be considered to best represent the stress conditions in a depleting reservoir, the mean and actual m_1 and n_1 values for this test were used to back-calculate reservoir parameters, ϕ and k . Changes in porosity were calculated via equation 5.13 and compared to actual experimental data. All comparisons were made using ϕ_1 data since porosity determined by the water volume and

volumetric strain measurement method was most reflective of the true rock porosity as discussed earlier. Tables 4 and 5 and Figure 63 show excellent agreement between calculated and measured porosity changes for several rock samples when the actual m_1 and n_1 values were used. Although some offsetting occurred when mean coefficient values were utilized, porosity changes with effective stress variations were approximately the same.

Permeabilities, back-calculated using the mean and actual m_1 and n_1 values in equation 5.18, provided a method of verifying the permeability-porosity relationship. Comparisons were made with experimentally measured permeabilities. Results given in Table 6 show good agreement between measured k 's and k 's calculated from actual coefficient values. Some discrepancy occurs, however, when mean coefficient values are used. Figure 64 clearly depicts these results for a typical sample during a uniaxial compaction test.

In general, a modified Archie's equation and a permeability-porosity relationship as given by equations 5.13 and 5.18 have the capability to estimate both porosity and permeability variations with effective stress.

$$d\phi = \left\{ \begin{aligned} &\frac{n_2 + 2n_3 P_E}{(m_1 + m_2 P_E + m_3 P_E^2)} - \frac{(m_2 + 2m_3 P_E)(n_1 + n_2 P_E + n_3 P_E^2)}{(m_1 + m_2 P_E + m_3 P_E^2)} \\ &\frac{n_1 + n_2 P_E + n_3 P_E^2}{m_1 + m_2 P_E + m_3 P_E^2} \end{aligned} \right\} dP_E \quad 5.13$$

$$k \times \phi^{\frac{m_1 + m_2 P_E + m_3 P_E^2}{m_1 + m_2 P_E + m_3 P_E^2}} = C \quad 5.18$$

Their use for geopressured, geothermal reservoirs should be helpful in more accurately predicting fluid recovery.

TABLE 2
Coefficients of the Cementation Factor and Formation Factor Expressions

| Sample* | Test Type** | $-m(P_E) = m_1 + m_2 P_E + m_3 P_E^2$ | | | $\log F(P_E) = n_1 + n_2 P_E + n_3 P_E^{2.44}$ | | |
|---------|--------------------|---------------------------------------|--------|-----------------------|--|-------|--------|
| | | m_1 | m_2 | m_3 | n_1 | n_2 | n_3 |
| 15665 | $P_A = P_C = 7.85$ | -1.9014 | .0011 | .0002 | 1.3069 | .0104 | -.0005 |
| | $P_A = 7.85$ | -1.9508 | .0030 | .0001 | 1.3394 | .0056 | -.0001 |
| 11755 | $P_A = P_C = 12.0$ | -1.9601 | -.0090 | .0014 | 1.3004 | .0239 | -.0019 |
| | $P_A = P_C = 6.0$ | -1.8616 | -.0174 | .0020 | 1.3031 | .0225 | -.0017 |
| | $P_A = 12.0$ | -1.9863 | -.0105 | .0008 | 1.3279 | .0223 | -.0015 |
| | $P_A = 6.0$ | -1.9732 | -.0089 | .0010 | 1.3808 | .0156 | -.0010 |
| 14702 | $P_A = P_C = 14.7$ | -2.0413 | -.0036 | .0008 | 1.3735 | .0096 | -.0004 |
| | $P_A = P_C = 7.35$ | -1.9939 | -.0047 | .0010 | 1.3776 | .0133 | -.0010 |
| | $P_A = 7.35$ | -2.0133 | -.0014 | .0001 | 1.3919 | .0100 | -.0003 |
| | $P_A = 14.7$ | -2.0645 | -.0040 | .0007 | 1.3869 | .0107 | -.0005 |
| 14699 | $P_A = 14.7$ | -1.8598 | -.0056 | .0006 | 1.3596 | .0129 | -.0005 |
| | $P_A = 7.35$ | -1.7614 | -.0126 | .0010 | 1.3319 | .0173 | -.0007 |
| | $P_A = P_C = 14.7$ | -1.8394 | -.0076 | .0010 | 1.3450 | .0146 | -.0008 |
| | $P_A = P_C = 7.35$ | -1.8108 | -.0088 | .0014 | 1.3647 | .0162 | -.0011 |
| 14696B | $P_A = P_C = 7.35$ | -1.8199 | -.0094 | .0013 | 1.3506 | .0178 | -.0009 |
| | $P_A = 7.35$ | -1.9291 | -.0040 | .0008 | 1.4217 | .0163 | -.0011 |
| 15668 | $P_A = 7.85$ | -2.0836 | -.0010 | .0003 | 1.4266 | .0080 | -.0002 |
| | $P_A = 15.7$ | -2.1300 | -.0080 | .0014 | 1.4095 | .0103 | -.0005 |
| | $P_A = P_C = 7.85$ | -2.0708 | -.0039 | .0009 | 1.4181 | .0129 | -.0009 |
| | $P_A = P_C = 15.7$ | -2.1172 | -.0061 | .0011 | 1.3941 | .0199 | -.0019 |
| 14712 | $P_A = P_C = 7.35$ | -1.9064 | -.0030 | .0010 | 1.3699 | .0133 | -.0011 |
| | $P_A = 7.35$ | -1.9106 | -.0013 | .0005 | 1.3745 | .0077 | -.0005 |
| | $P_A = 14.7$ | -1.9633 | -.0056 | .0010 | 1.3665 | .0099 | -.0005 |
| 14696A | $P_A = 7.5$ | -1.8167 | -.0099 | .0010 | 1.3549 | .0195 | -.0010 |
| | $P_A = 15.0$ | -2.0206 | -.0085 | .0012 | 1.4525 | .0156 | -.0011 |
| | $P_A = P_C = 15.0$ | -1.9034 | -.0085 | .0008 | 1.3748 | .0158 | -.0006 |
| | $P_A = P_C = 7.5$ | - | - | - | 1.3680 | .0177 | -.0009 |
| 14751 | $P_A = P_C = 7.0$ | -1.9262 | -.0022 | -.0005 | 1.3601 | .0079 | -.0002 |
| | $P_A = 7.38$ | -1.9607 | -.0053 | .0011 | 1.3624 | .0094 | -.0005 |
| 14765 | $P_A = 14.765$ | -1.7346 | -.0229 | .0023 | 1.2390 | .0235 | -.0017 |
| 14711 | $P_A = P_C = 7.35$ | -1.8598 | .0033 | .0055 | 1.2566 | .0087 | -.0006 |
| | $P_A = P_C = 14.7$ | -1.8460 | .0039 | 4.40×10^{-5} | 1.2366 | .0117 | -.0008 |
| | $P_A = 7.35$ | -1.8773 | -.0017 | .0006 | 1.2321 | .0083 | -.0005 |
| | $P_A = 14.7$ | -1.9665 | .0015 | .0001 | 1.2502 | .0103 | -.0006 |
| 14703 | $P_A = P_C = 12.0$ | -1.8920 | .0054 | -.0006 | 1.3917 | .0104 | -.0003 |
| | $P_A = 12.7$ | -1.9317 | -.0046 | .0007 | 1.3967 | .0124 | -.0007 |

* Sample number reflects depth (ft.) from which sample obtained.

** Test type is described by the initial hydrostatic or axial stress level, reflecting respectively a hydrostatic compression or uniaxial compaction test as discussed in Chapter III.

*** n_1 values are based upon a log₁₀ derivation. To obtain values for use in \ln calculations, multiply listed values by 2.3.

TABLE 3
Statistical Parameters for the Coefficients of the Cementation
Factor and Formation Factor Expressions

| Group Analysis | Statistic* | m ₁ | m ₂ | m ₃ | n ₁ | n ₂ | n ₃ |
|---|------------|----------------|----------------|----------------|----------------|----------------|----------------|
| All Tests | μ | -1.934 | -0.005 | 0.001 | 1.353 | 0.014 | -0.001 |
| | σ | 0.096 | 0.006 | 0.001 | 0.055 | 0.005 | 0.001 |
| | V (%) | 5 | 104 | 111 | 4 | 34 | 63 |
| Uniaxial Compaction Tests @ 1.0 psi/ft Initial Overburden Pressure | μ | -1.959 | -0.007 | 0.001 | 1.361 | 0.014 | -0.001 |
| | σ | 0.103 | 0.006 | 0.001 | 0.067 | 0.005 | 0.0004 |
| | V (%) | 5 | 85 | 60 | 5 | 33 | 44 |
| Uniaxial Compaction Tests @ 0.5 psi/ft Initial Overburden Pressure | μ | -1.928 | -0.005 | 0.001 | 1.355 | 0.011 | -0.001 |
| | σ | 0.093 | 0.004 | 0.0004 | 0.051 | 0.005 | 0.0003 |
| | V (%) | 5 | 83 | 61 | 4 | 41 | 57 |
| Hydrostatic Com- pression Tests (Elevated Pore Pressure) @ 1.0 psi/ft Initial Stress | μ | -1.943 | -0.004 | 0.001 | 1.345 | 0.015 | -0.001 |
| | σ | 0.096 | 0.006 | 0.001 | 0.003 | 0.005 | 0.001 |
| | V (%) | 5 | 151 | 98 | 4 | 32 | 65 |
| Hydrostatic Com- pression Tests (Elevated Pore Pressure) @ 0.5 psi/ft Initial Stress | μ | -1.906 | -0.005 | 0.001 | 1.348 | 0.014 | -0.0009 |
| | σ | 0.079 | 0.006 | 0.002 | 0.044 | 0.004 | 0.0004 |
| | V (%) | 4 | 117 | 112 | 3 | 31 | 43 |

* Statistical Parameters Are: μ = Arithmetic Mean
 σ = Standard Deviation
 V = Coefficient of Variation = $\frac{\sigma}{\mu} \times 100$

TABLE 4
Comparison of Measured and Calculated Porosities
For Several Rock Samples

| Sample | Test | P_o | ϕ_m | ϕ_c | ϕ_c | $\Delta\phi_m$ | $\Delta\phi_c$ | $\Delta\phi_c$ |
|----------|--------------|-----------------|---------------------------------|-------------------------------|-------------------------------|---------------------------------|-------------------------------|-------------------------------|
| | | | $m_1 \text{ \& } n_1$ Actual | $m_1 \text{ \& } n_1$ Mean | $m_1 \text{ \& } n_1$ Mean | $m_1 \text{ \& } n_1$ Actual | $m_1 \text{ \& } n_1$ Mean | $m_1 \text{ \& } n_1$ Mean |
| 14702 | $P_A = 14.7$ | 14.7 ± 7.0 | .1995 | .2002 | .1906 | -.0136 | -.0133 | -.0167 |
| 14711 | $P_A = 14.7$ | 14.7 ± 7.35 | .2180 | .2171 | .1902 | -.0123 | -.0224 | -.0159 |
| 14703 | $P_A = 14.7$ | 14.7 ± 7.35 | .1766 | .1769 | .1902 | -.0115 | -.0150 | -.0159 |
| 14699 | $P_A = 14.7$ | 14.7 ± 7.0 | .1720 | .1716 | .1906 | -.0145 | -.0142 | -.0167 |
| 14696B | $P_A = 14.7$ | 14.7 ± 7.0 | .1697 | .1687 | .1906 | -.0107 | -.0204 | -.0167 |
| Average: | | | .1872 | .1869 | .1904 | -.0125 | -.0171 | -.0164 |

- Notes: 1.) ϕ_m & $\Delta\phi_m$ - Measured Data Values
 2.) ϕ_c & $\Delta\phi_c$ - Calculated Values Using Eqns. 5.12 & 5.13 Respectively
 3.) Porosities Are Given @ $P_E|_{max}$.
 4.) Porosity Changes Are Given For $\Delta P_E|_{max}$.

TABLE 5
Comparison of Measured and Calculated Porosities
For a Typical Rock Sample (#14696B)

| Sample | Test | P_0 (kpsi) | ϕ_m | ϕ_c | ϕ_c |
|--------|--------------|-----------------|----------|-------------------------|-----------------------|
| | | | | m_i & n_i Actual | m_i & n_i Mean |
| 14696B | $P_A = 14.7$ | 14.7 | .1817 | .1832 | .2019 |
| | | 12 | .1762 | .1763 | .1967 |
| | | 10 | .1727 | .1723 | .1935 |
| | | 7 | .1675 | .1687 | .1906 |
| | | 10 | .1724 | .1723 | .1935 |
| | | 12 | .1757 | .1763 | .1967 |
| | | 14.7 | .1808 | .1832 | .2019 |

Notes: 1.) ϕ_m → Measured Data Values

2.) ϕ_c → Calculated Values

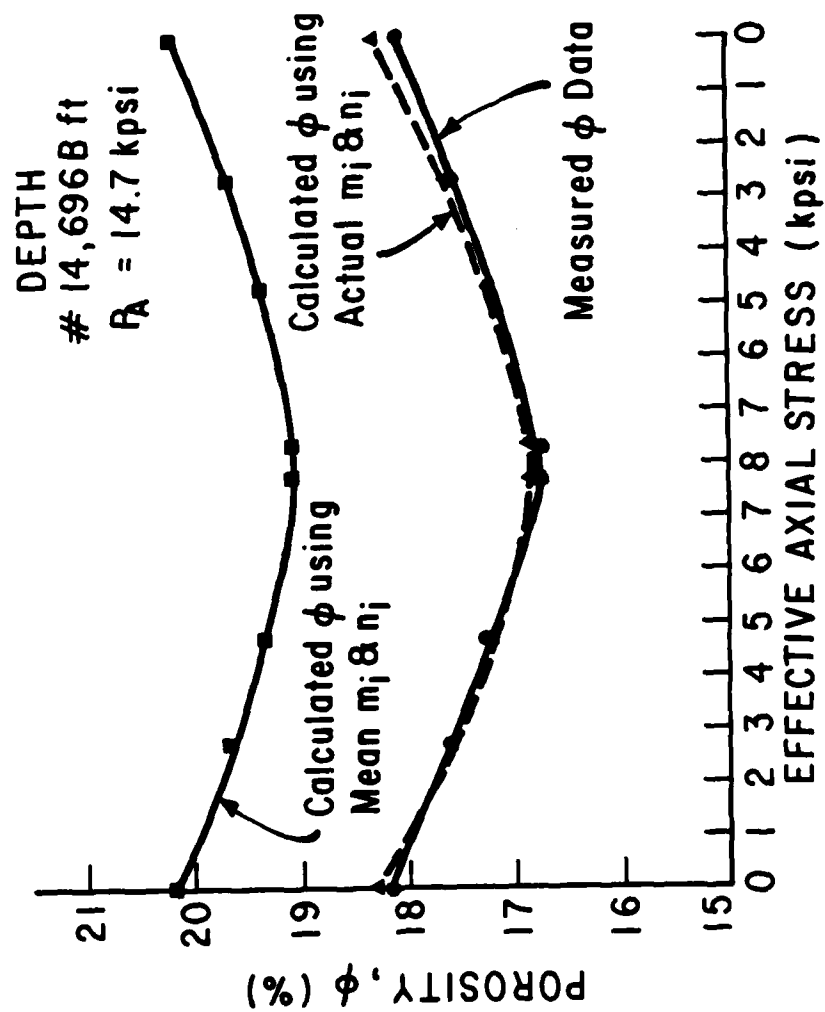


FIGURE 63 COMPARISONS OF POROSITIES OBTAINED FROM MEASURED DATA & FROM EQUATION 5.12 (#14696B ,
UNIAXIAL COMPACTION TEST)

TABLE 6

Comparison of Measured and Calculated Permeabilities
For Several Rock Samples

| Sample | Test | P_0 (kpsi) | k_m (md) | k_c | k_c | Value of Constant C |
|--------|--------------|-------------------------|---------------|-------------------------|-----------------------|---------------------------|
| | | | | n_1 & n_1 Actual | n_1 & n_1 Mean | |
| 14703 | $P_A = 14.7$ | $14.7 \rightarrow 7.35$ | 20 | 20 | 21 | 550 |
| 14711 | $P_A = 14.7$ | $14.7 \rightarrow 8.0$ | 156 | 134 | 103 | 2635 |
| 14696B | $P_A = 14.7$ | $14.7 \rightarrow 7.0$ | 87 | 87 | 102 | 2635 |
| 14699 | $P_A = 14.7$ | $14.7 \rightarrow 7.0$ | 85 | 96 | 99 | 2550 |
| 14699 | $P_A = 7.35$ | 6 | 116 | 113 | 107 | 2550 |
| | | 4 | 107 | 106 | 102 | 2550 |
| | | 2 | 101 | 100 | 100 | 2550 |
| | | 0 | 95 | 97 | 99 | 2550 |
| | | 2 | 100 | 100 | 100 | 2550 |
| | | 4 | 104 | 106 | 102 | 2550 |
| | | 6 | 108 | 113 | 107 | 2550 |

Notes: 1.) $k_m \rightarrow$ Measured Data Values

2.) $k_c \rightarrow$ Calculated Values using Eqn. 5.18 and Calculated Porosities from Table 5

3.) k 's are given @ $P_E|_{\max}$.

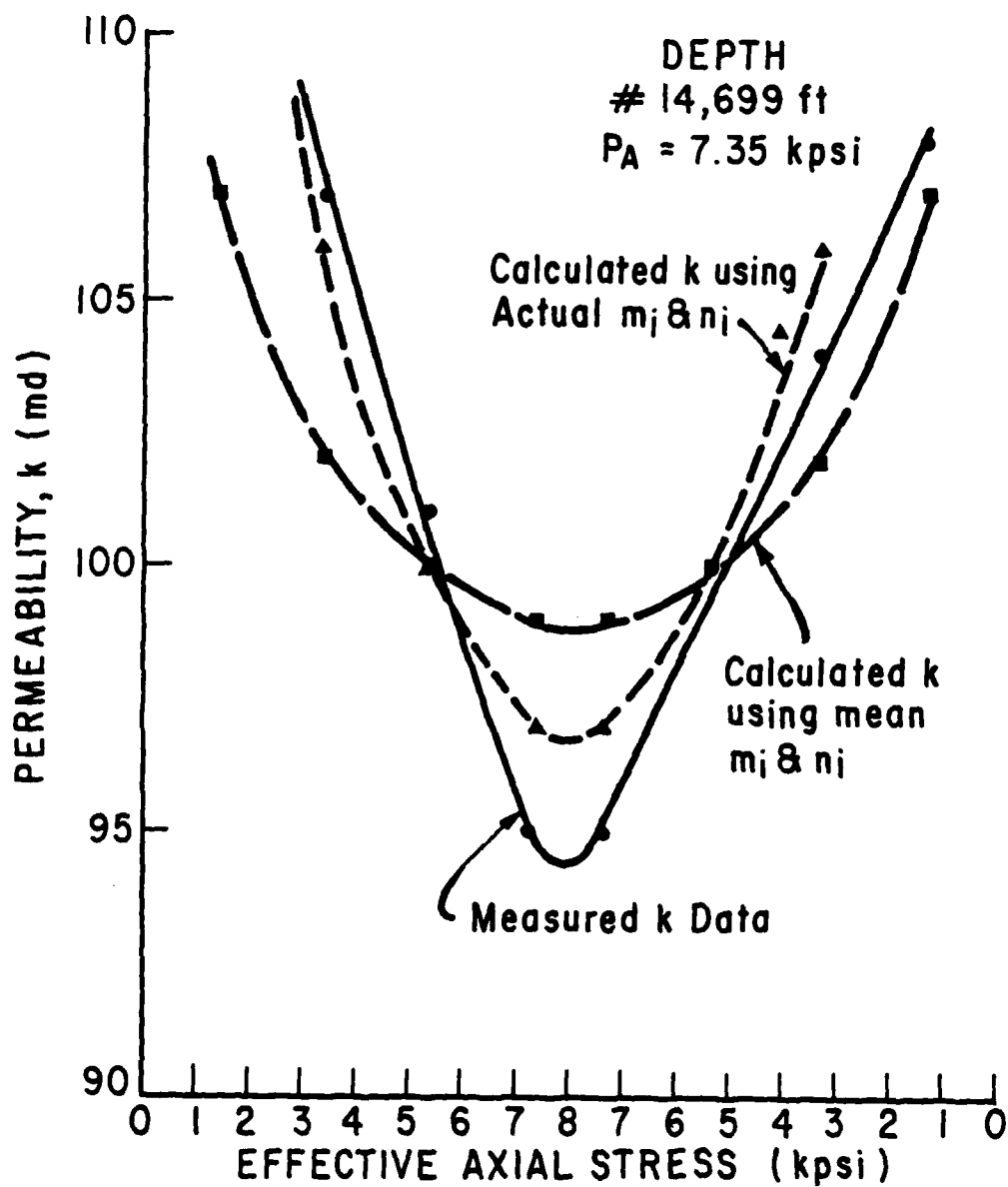


FIGURE 64 COMPARISONS OF PERMEABILITIES OBTAINED FROM MEASURED DATA AND FROM EQUATION 5.18 (#14699, Uniaxial Compaction Test)

VI. CONCLUSIONS AND RECOMMENDATIONS

VI.1 Conclusions

1. The effective stress concept is a valid and very good approximation of the stress conditions in a porous rock. However, effective stresses under atmospheric pore pressure conditions do not adequately reflect insitu rock conditions and may not be accurate in predicting actual reservoir parameter changes with pressure if the rock matrix compressibility is not taken into account.

2. Porosity changes determined by using only measured variations in the pore fluid volume adequately approximate actual porosity changes in medium and low porosity rocks under normal stress conditions. However, for highly porous rocks or for a more accurate indication of the true porosity in medium porous (~ 20%) rocks, porosity calculated with both volumetric strain and pore fluid volume measurements should be used.

3. Resistivity, porosity, and permeability are functions of the effective stress and vary as the stress conditions change. Resistivity and permeability are more sensitive to this change than porosity and showed a 10-15% variation over a 7,000 psi pressure range. Porosity changes reflected a 5-7% variation over the same range for the sandstones tested.

4. The cementation factor is a function of pressure. In logging interpretation, therefore, a modified form of the Archie equation, as developed in this research for the clean sandstone rocks tested, must be used.

5. Electrical and hydraulic conductivities are analogous for clean, nonconductive sandstones. The F_{Xk} product is independent of pressure for a given rock. This relation was found to be useful in predicting permeability changes with pressure. In general, such predictions can be made only if the constant of proportionality (equation 3.10) between F and $1/k$ can be evaluated.

6. For the geopressured zones of Pleasant Bayou wells #1 and #2, the permeability-porosity relationship is log linear (equation 5.18) and may be useful for modelling purposes.

VI.2 Recommendations

Based upon the experience gained in the present study, the following suggestions for possible improvements are made:

1. The pore fluid temperature should be isothermally controlled in order to prevent discrepancies in the formation factor calculations due to pore fluid resistivity changes.

2. Rocks with a wider range of porosity and permeability should be tested in the SPS in order to verify the qualitative results of this work.

3. An improved method of permeability measurement should be developed to more easily evaluate changes in the permeability with effective stress.

4. High temperatures reflecting insitu thermal conditions should be incorporated into the SPS. Additional tests on rock samples should be conducted in equipment presently under development.

APPENDIX I

A. Resistivity Measurement Method

Resistivity measurements in this study were made from observed potential drops across the flow heads as described earlier. These potential drops are a function of not only the rock, saturating fluid, and current flow but also any contact resistance that exists between the electrodes and the rock and any polarization of charges.

In order to obtain an accurate measurement of the rock resistivity, both contact resistance and charge polarization must be eliminated. Dunlap et al.³² used a four-electrode type circuit to remove the phenomena.

In this method current was passed axially through the sample using end plates as current electrodes. Potential drops were measured using additional probes or electrodes dispersed along the sample length. Dunlap measured and allowed for any appreciable contact resistance by inserting a high impedance resistor of the same size as the input impedance of the voltmeter in series with the meter. (Figure A1-1 simply depicts the circuitry.) If the contact resistance were negligible, the new voltage after insertion of the resistor would be one half the previously measured value. If the contact resistance were significant, the new voltage would be greater than one half the previously measured value.

Later work as described by Rust³³ used a two-electrode method in which the same electrodes were utilized for both current flow and potential drop measurements. Contact resistance between the electrodes

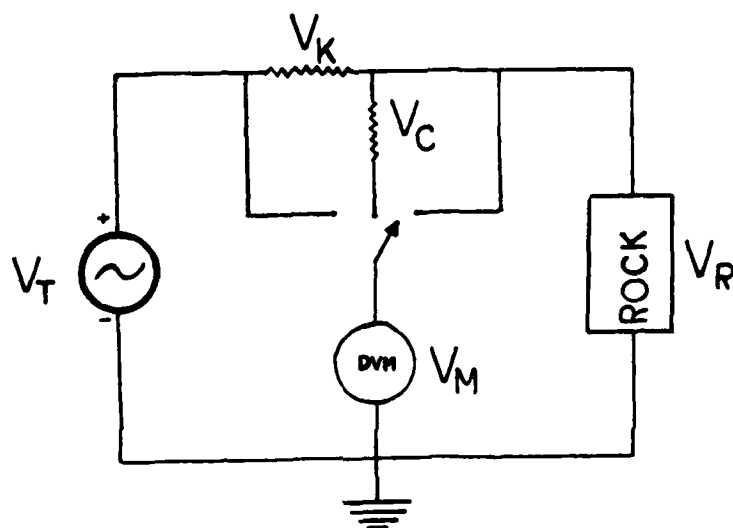


FIGURE A1-1 RESISTIVITY CIRCUITRY DIAGRAM SHOWING
VOLTAGE DROPS WITHIN THE SYSTEM

and the brine saturated rock sample was negated by several methods with varying degrees of success. Rust used conducting silver paint on the electrodes to reduce the contact resistance. His results showed that provided proper techniques were employed either the two-electrode or four-electrode method yielded reliable resistivity values.

Dunlap noted that polarization within the sample could affect the accuracy of the measured voltage drops. Although alternating current and the four-electrode method eliminate any significant polarization problems, AC flow introduces frequency as a variable influencing the resistivity.

In this work the need to measure potential voltage drops radially across the sample required that the two-electrode method be employed. Experiments conducted with Berea sandstone samples tested with the Simultaneous Property System showed that the problems of contact resistance and frequency dependence could be minimized by coating either the electrode or sample faces with conductive silver paint and by selecting an operating frequency above 700 hertz.

Figure A1-2 shows calculated resistivities as functions of frequency obtained using the two-electrode method. All the test runs show axial resistivities decreasing with increasing frequency. For the Berea samples with ends coated with conductive silver paint, resistivity values become essentially independent of frequency for frequencies greater than about 700 hertz. Similar results were obtained when the axial heads of the SPS were silver painted instead of the sample ends.

Resistivities measured using a two-electrode circuit were checked for accuracy against resistivities obtained from a four-electrode con-

figuration. Two-electrode resistivity values were measured across Berea samples coated on the ends with silver paint. Four-electrode resistivity values were obtained on the samples using rings of conductive paint on the cylinder circumference as measurement probes. Figure A1-3 shows the set-up.

A comparison of the results obtained from the two-electrode and four-electrode methods is given in Figure A1-4. Resistivities at 1,000 hertz calculated from potential drops measured using both methods are plotted against each other. The relationship is linear with an equation of the form $y = a + bx$. The regression coefficients were obtained by least squares. Values for "a" and "b" were 0.119 and 0.930 respectively. The coefficient of correlation for the regression analysis was 0.99. This close agreement between the two-electrode and four-electrode methods demonstrates that two-electrode contact resistance can be minimized and that potential drops obtained at 1,000 hertz are representative of the true resistivity of the brine saturated samples.

In order to apply the results obtained in the axial resistivity measurements to radial resistivity experiments, a more practical and durable electrode than silver painted stainless steel was required. Tests with hard industrial chromium plating on stainless steel radial pass-through shoes were successful and, as with the axial measurements, gave resistivities which were essentially independent of frequency when frequencies were greater than 700 hertz. The chromium plated passthrough shoes were molded into a polyurethane core jacket, and the resultant jacket-shoe arrangement was used to contain each of the rock samples.

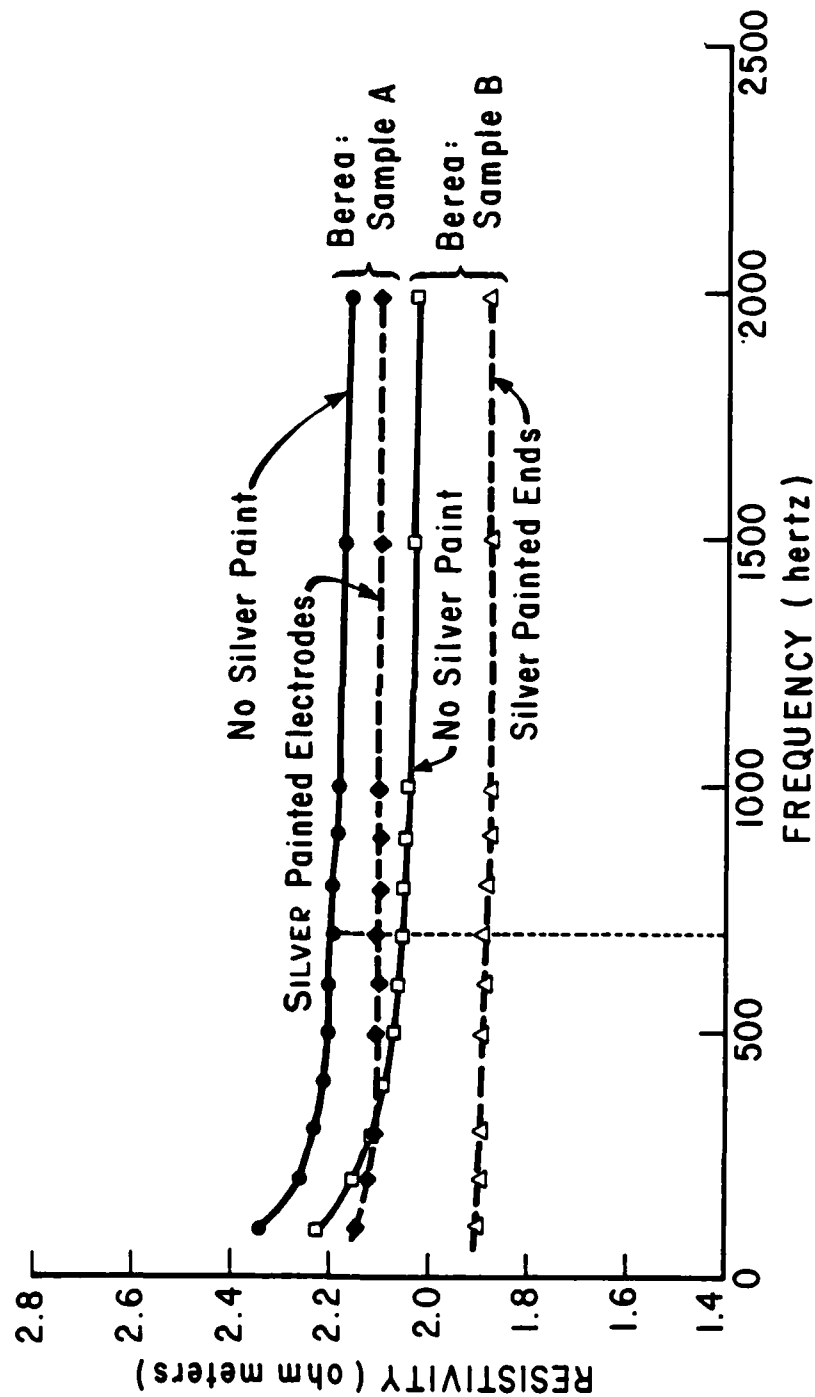


FIGURE A1-2 FREQUENCY DEPENDENCE OF RESISTIVITY MEASUREMENTS MADE ON TWO BEREA SANDSTONE SAMPLES

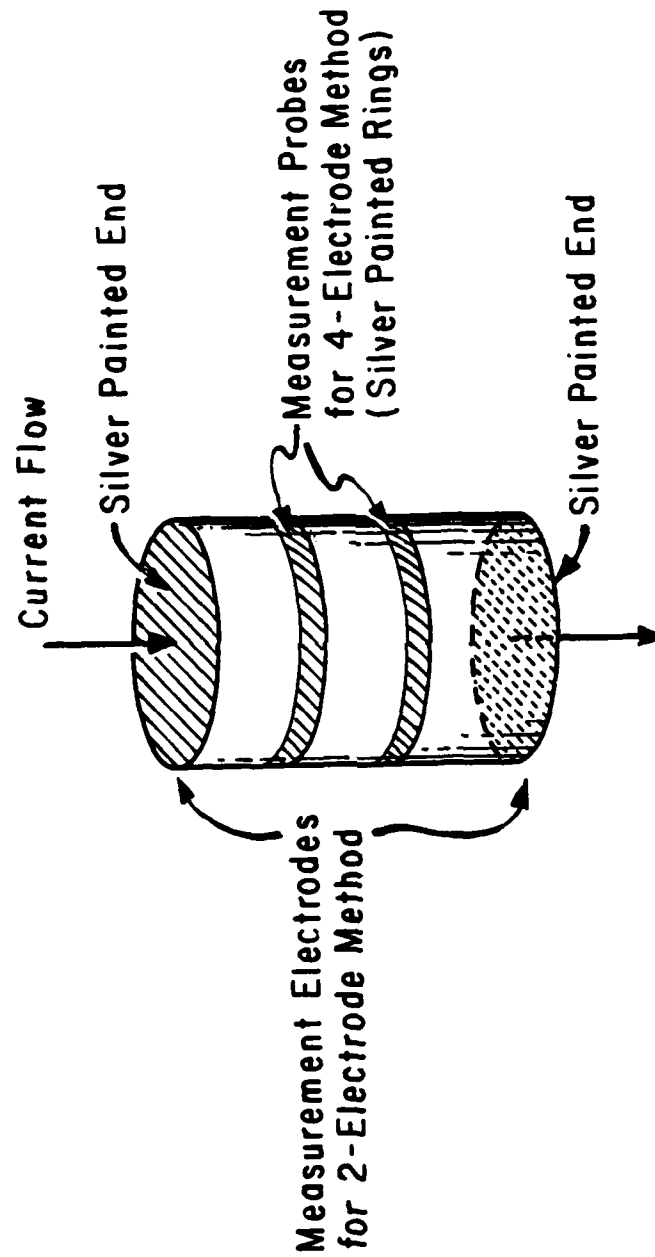


FIGURE A1-3 ARRANGEMENT OF MEASUREMENT PROBES ON A BERE A SAMPLE USED FOR TWO-ELECTRODE AND FOUR-ELECTRODE RESISTIVITY TESTS

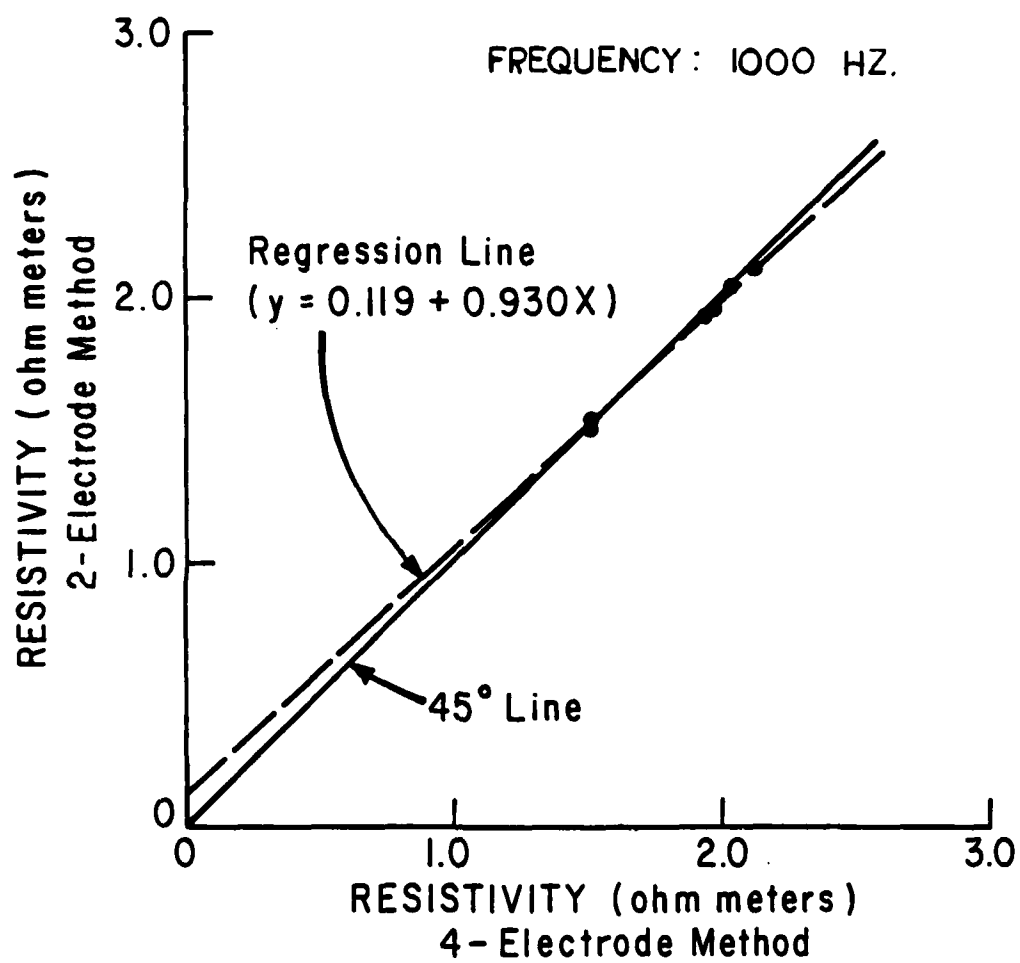


FIGURE A1-4 COMPARISON OF RESISTIVITIES OBTAINED FROM TWO-ELECTRODE AND FOUR-ELECTRODE METHODS

B. Application of Radial Resistivity Measurements

For axial measurement through a cylindrical rock sample only the current, voltage drop, and core dimensions are necessary for resistivity calculations. However, for radial measurement through a cylindrical sample, an analog to the permeability formula for a whole core type permeameter²⁸ was utilized. Equation 3.9 is such an analog:

$$\frac{1}{R_R} = \frac{1}{(\Delta V)(L)(R_f)} \left(\frac{K_e}{K_e'} \right) (100) \quad 3.9$$

The geometric and decreased current flow correction factors are based on ratio values of passthrough length and diameter to sample length and diameter. For this work $K_e/K_e' = 1.00$ and $R_f = 0.94$.

Two cut samples of a Berea sandstone rock were used to test the reliability of resistivity measurements calculated from this method. Berea, if properly selected, can be nearly isotropic and homogeneous for all practical purposes. However, for comparison, two clean Berea cores were cut, one perpendicular, the other parallel to the general bedding plane orientation. Each sample was saturated with brine, inserted into the core jacket, placed within the SPS, and subjected to current flow axially and radially. Figure A1-5 depicts the flow directions. Axial resistivities were calculated using

$$R_R = \frac{\Delta V}{i} \times \frac{A}{L} \quad A1.1$$

where A = area perpendicular to current flow (cm^2)

Radial resistivities were calculated using equation 3.9. Results showed that axial resistivities of Sample A were within 2% of the radial re-

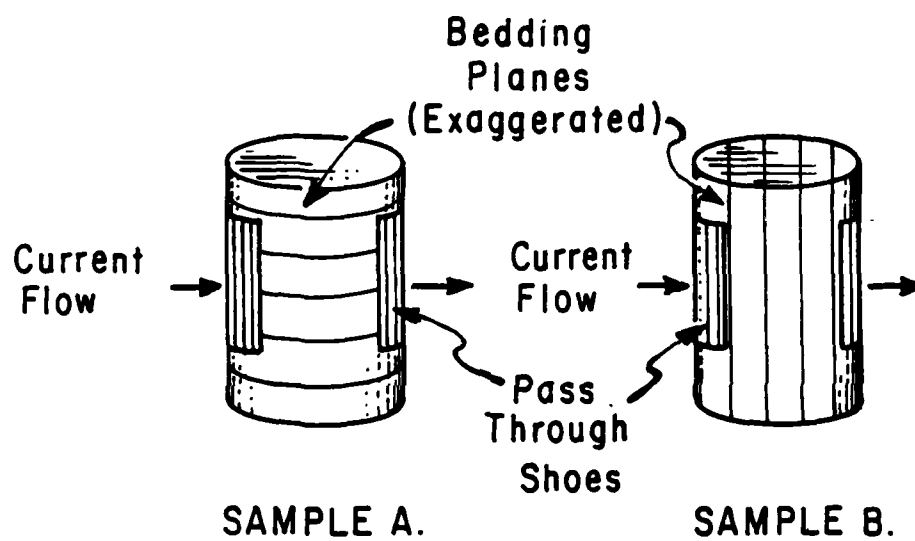


FIGURE A1-5 CUT SAMPLES OF BEREIA SANDSTONE USED FOR TESTING RADIAL RESISTIVITY MEASUREMENTS (EQUATION 3.9)

sistivities of Sample B. No trend existed and resistivities were taken at 1,000 hertz. The results verify that equation 3.9 provides reliable resistivity values.

Rock resistivity data in its basic form has limited use because of its dependency on the saturating fluid. The formation factor concept developed by Archie¹⁴ normalizes the rock resistivity and renders it independent of the pore fluid resistivity. The formation factor as defined by equation 3.4 is an intrinsic property of the rock at a specified effective stress state. It is extremely useful so far as it can be related to other rock parameters such as porosity and permeability as discussed in Chapter III.

C. Pressure Dependence of Resistivity Measurements

Pressure effects on the resistivity of formation brines usually are not significant. Guyod¹⁶ explained that for the usual formation waters an increase in pressure from 0 to 5,000 psi results in a decrease in resistivity of less than 5% at 70°F.

In this work, however, resistivity measurements were taken at various effective stress states and at pore pressures as high as 15,000 psi. For this reason and since the change in resistivity of the rock with effective stress was the variable of interest, pressure effects on the resistivity of the saturating fluid had to be taken into consideration.

Quist and Marshall³⁴ measured electrical conductances of aqueous sodium chloride solutions from 0° to 800°C and at pressures to 58,000 psi. However, their work was limited to solution concentrations up to only 0.7 molar (0.58%). Therefore, resistivities as functions of pressure under

isothermal conditions for NaCl brines of 6% concentration, which was the saturating fluid of the samples, had to be obtained through experiment.

The experimentation consisted of placing a volume of 6% NaCl solution in a Perspex, thick-walled cylinder equipped with brass end pieces for measuring voltage drops. A two-electrode method for fluid resistivity determination was employed. Current introduced at one of the brass end pieces flowed through the brine and out the other end piece. The voltage drop across the brine was obtained utilizing the same end pieces as measurement electrodes.

Testing occurred at various pressures up to 15,000 psi. To achieve such pressures, the Perspex apparatus was placed into the SPS. The confining pressure generated by the SPS was conveyed to the brine solution through a 1/16 inch tubing piece extended with a 12 inch long, 1/16 inch ID hose. This configuration acted merely as an oil/water separator. Figures A1-6A and A1-6B show the apparatus between the heads of the SPS.

Voltage drops across the brine in the Perspex cylinder were measured with digital volt meters. The potential drops together with the current flow and the dimensions of the cylinder were used to calculate the brine resistivity. The length and diameter of the fluid column in the Perspex cylinder changed with pressure due to fluid compressibility and deformation of the container. The dimensional change of the fluid column was corrected for in the resistivity computations by measuring the strain of the hollow cylinder under the hydrostatic stress conditions. Rosette strain gauges cemented to the walls of the cylinder provided the strain measurements. Since Perspex is an isotropic, homogeneous elastic



FIGURE A1-6B



FIGURE A1-6A

medium, strain can be expressed as

$$\epsilon = \frac{1 - 2\nu}{E} P \quad A1.2$$

where ϵ = strain (inches/inch)

ν = Poisson's Ratio (= 0.36 for Perspex)³⁵

E = Young's Modulus (psi) (= 4.5×10^5 psi for Perspex)³⁵

P = hydrostatic pressure (psi)

Therefore, the internal radius and length of the brine container are given by:

$$r = r_0 \left(1 - \frac{1 - 2\nu}{E} P\right) \quad A1.3$$

and

$$L = L_0 \left(1 - \frac{1 - 2\nu}{E} P\right) \quad A1.4$$

where r_0 = original cylinder internal radius (inches)

L_0 = original cylinder length (inches)

With the dimensions of the fluid column corrected for deformation, the resistivity of the brine at various pressures was calculated using equation A1.1. The results, which gave resistivities of 6% NaCl solution as a function of pressure (temperature constant), are shown in Figure A1-7. Linearly regressing the results gave the following relationship:

$$R_B = 0.1215 - 0.714P \quad A1.5$$

where R_B = resistivity of the brine (ohm-meters)

P = applied pressure (psi)

Absolute values of brine resistivities are very temperature sen-

sitive as shown by Guyod¹⁶. It was found during this experiment that temperature primarily influenced the intercept of the resistivity verses pressure line. The slope of the line remained essentially constant for the room temperature variations which occurred during the rock testing experiments.

The rock resistivities at different elevated pore pressures were corrected only for the pressure dependence of the brine resistivity. To compensate for pressure, formation factors were calculated using brine resistivities adjusted for pressure effects.

Temperature was not a factor within each individual rock test since each test was conducted under essentially isothermal conditions. The temperature dependence of the calculated formation factors did arise, however, when comparisons were made between individual rock tests. As explained above, though, the slight room temperature variations merely changed the absolute value of F and did not influence relative values. Therefore, within each test cycle, variations of F with effective stress could be compared without error.

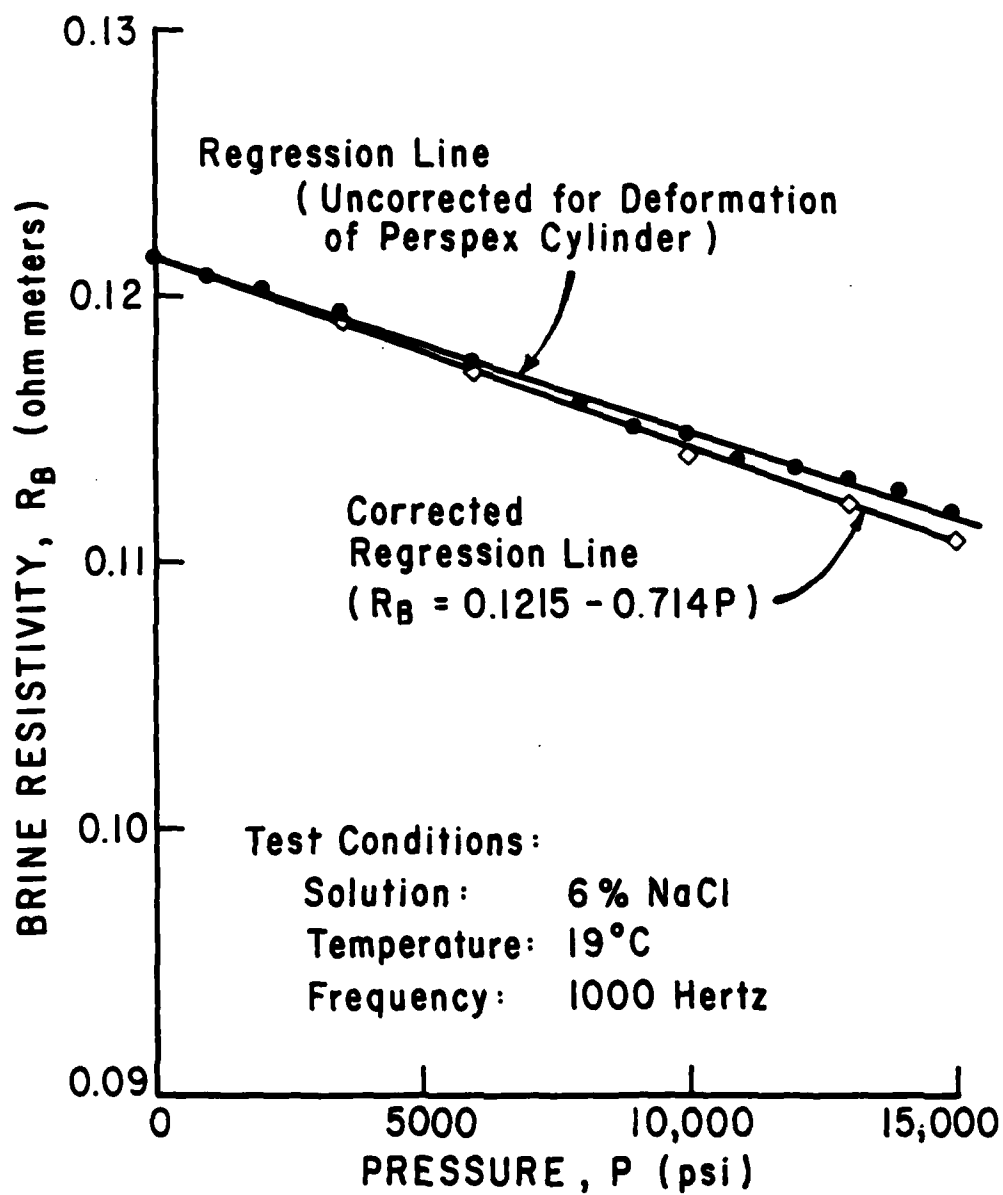


FIGURE A1-7 GRAPH OF 6% NaCl SOLUTION RESISTIVITY AS A FUNCTION OF PRESSURE

APPENDIX II

Equipment Calibration and Sensitivities

Various components of the Simultaneous Property System (SPS) required calibration. The internal axial load cell, strain gauges, pore fluid tubing, and wave transducer cell heads were affected by the pressure and, consequently, were calibrated as functions of the confining, pore, or axial pressure. The functions were essentially linear as reflected in the calibration equations provided in Table A2-1.

The waves generated and received by the transducer cell heads (Figure 3) were also affected by the epoxy coatings applied to the ends of the sample cores. In order to correct measured p-wave propagation times through the rock samples for the epoxy, a correction factor was determined using an aluminum cylinder. The cylinder was placed in the SPS, and p-wave propagation times measured at various pressures. The same measurements were then taken on the aluminum cylinder with epoxy on its ends. Comparisons of the results showed the p-wave velocity through the epoxy dependent upon the confining and axial pressures applied. The correction factor was found to be best expressed in terms of the propagation time as reflected in the following equation:

$$\Delta T_p = (12.19 - 0.80 P_A - 0.64 \frac{P_C}{P_A}) L_E \quad A2.1$$

where

ΔT_p = correction factor to be subtracted from p-wave propagation times measured through the rock samples (usec).

P_A = axial pressure (kpsi)

P_C = confining pressure (kpsi)

L_E = total thickness of the epoxy coatings (inches)

The pressures and sample deformation data needed for the calibration equations in Table A2-1 and for the epoxy correction factor equation (A2.1) were measured with digital voltmeters. The recorded voltages were converted to useable units via the sensitivities given in Table A2-2.

TABLE A2-1

Equipment Calibrations as Functions of Pressure

| <u>System Designation</u> | <u>Type Device</u> | <u>Calibration Equation</u> ^{1,2} |
|--------------------------------|-------------------------------|--|
| Axial Pressure | Load Cell | $\Delta P_A (\text{kpsi}) = (7.5 \times 10^{-3}) P_C$ |
| Sample Deformation | Strain Gauges | $\Delta \epsilon \left(\frac{\text{in}}{\text{in}} \right) = (5.48 \times 10^{-6}) P_C$ |
| Pore Fluid Volume ³ | Tubing & Valving ³ | $\Delta V_w (\text{cc}) = (0.153) P_O$ |
| p-Wave Propagation | Transducer Cell Heads | $\Delta T_p (\mu\text{sec}) = (5 \times 10^{-3}) P_A$ |

Notes: 1.) All Pressures In kpsi

2.) All Calibration Functions Were Subtracted From The
Respective Measured Parameters

3.) The Pore Fluid Volume Change With Pressure Was A Result
Of Not Only Tubing And Valving Expansion But Also Brine
Compressibility^{31,36}

TABLE A2-2
Sensitivities for Pressure-Sensing Devices
And Rosette Strain Gauges

| <u>System Designation</u> | <u>Type of Device</u> | <u>Brand</u> | <u>Range</u> | <u>Sensitivity</u> |
|---------------------------|-----------------------|--------------------|----------------|---|
| Pore Pressure | Pressure Transducer | BLH Electronics | 0 - 20,000 psi | $1.25 \frac{\text{kpsi}}{\text{V}}$ |
| Confining Pressure | Pressure Transducer | BLH Electronics | 0 - 20,000 psi | $2.5 \frac{\text{kpsi}}{\text{V}}$ |
| Axial Pressure | Load Cell | BLH Electronics | 0 - 25,000 psi | $2.5 \frac{\text{kpsi}}{\text{V}}$ |
| Sample Deformation | Strain Gauges | Micro-Measurements | - | $5.48 \times 10^{-4} \frac{\text{in/in}}{\text{V}}$ |
| Differential Pressure | Variable Reluctance | Validyne | 0 - 50 psi* | $5.0 \frac{\text{psi}}{\text{V}}$ |

* with diaphragm used

NOMENCLATURE

| | |
|----------------------|--|
| A | = Area perpendicular to current flow |
| a | = Coefficient in the generalized Archie's equation |
| C | = Constant |
| C' | = Constant |
| C _B | = Rock bulk compressibility |
| C _R | = Rock matrix compressibility |
| E | = Young's Modulus |
| F | = Formation factor |
| i | = Current flow |
| $\frac{K_e}{K_{e'}}$ | = Geometric correction factor |
| k | = Permeability |
| L | = Axial length |
| L _E | = Thickness of epoxy |
| L ₀ | = Original Perspex cylinder length |
| m | = Cementation factor |
| m _i | = Coefficients of the cementation factor |
| n _i | = Coefficients of the formation factor |
| P | = Pressure |
| P _A | = Axial Pressure |
| P _C | = Confining Pressure |
| P _E | = Effective stress |
| P _O | = Pore Pressure |

| | |
|----------------|---|
| q | = Flow rate |
| R_B | = Resistivity of the saturating brine |
| R_f | = Correction factor for decreased flow rate |
| R_R | = Resistivity of the 100% brine saturated rock |
| r | = Internal radius of Perspex cylinder under pressure |
| r_0 | = Original Perspex cylinder internal radius |
| T_P | = p-wave propagation time |
| V | = Voltage |
| V_B | = Bulk volume |
| V_C | = Voltage drop across resistor measuring contact resistance |
| V_K | = Voltage drop of resistivity line circuitry |
| V_M | = Voltage drop across the digital voltmeter |
| V_O | = Initial bulk volume |
| V_P | = Pore volume |
| V_R | = Voltage drop across the rock sample |
| V_T | = Voltage signal from signal conditioner |
| V_W | = Water volume |
| v_f | = Measured p-wave velocity through the sample |
| v_m | = p-wave velocity through the matrix material |
| v_t | = p-wave velocity through the brine |
| Δ_{eff} | = Volumetric strain due to effective stress |
| ν | = Poisson's Ratio |
| ϵ | = Strain |
| ϵ_R | = Radial strain |
| ϵ_z | = Axial Strain |
| μ | = Viscosity |

- ϕ = Porosity
- ϕ_0 = Initial Porosity
- ϕ_1 = Porosity by water volume and strain measurement method
- ϕ_2 = Porosity by water volume measurement method
- ϕ_3 = Porosity by volumetric strain measurement method
- ϕ_4 = Porosity by resistivity measurement method
- ϕ_5 = Porosity by Wyllie Time Average method
- η = Coefficient in the effective stress equation

BIBLIOGRAPHY

1. Bebout, D. G., Loucks, R. G., and Gregory, A. R.: "Geological Aspects of Pleasant Bayou Geopressured Geothermal Test Well, Austin Bayou Prospect, Brazoria County, Texas," Proceedings, Fourth U. S. Gulf Coast Geopressured-Geothermal Energy Conference: Research and Development, Vol. 1, University of Texas at Austin, (October 1979), pp. 11-45.
2. Scorer, J. D. T. and Miller, F. G.: "A Review of Reservoir Rock Compressibility, and Its Relationship to Oil and Gas Recovery," Institute of Petroleum, IP 74-003.
3. Friedman, M.: "Porosity, Permeability, and Rock Mechanics - A Review," Proceedings, 17th U. S. Symposium on Rock Mechanics, Snowbird, Utah, (August 1976), pp. 2A1-1 to 2A1-17.
4. Terzaghi, K.: Principles of Soil Mechanics, IV - Settlement and Consolidation of Clay, Engg. News Record, Vol. 95, (1925), pp. 874-878.
5. Biot, M. A.: "General Theory of Three-Dimensional Consolidation," Journal of Applied Physics, Vol. 12, (February 1941), pp. 155-164.
6. Geertsma, J.: "The Effect of Fluid Pressure Decline on Volumetric Changes of Porous Rocks," Petroleum Transactions, AIME, Vol. 210, (1957), pp. 331-340.
7. Nur, A. and Byerlee, J. D.: "An Exact Effective Stress Law for Elastic Deformation of Rock with Fluids," Journal of Geophysical Research, Vol. 76, No. 26, (1971), pp. 6414-6419.

8. Hall, H. N.: "Compressibility of Reservoir Rocks," Petroleum Transactions, AIME, Vol. 198, (1953), pp. 309-311.
9. Fatt, I.: "The Effect of Overburden Pressure on Relative Permeability," Petroleum Transactions, AIME, Vol. 198, (1953), pp. 325-326.
10. Gangi, A. F.: "Hertz Theory Applied to the Porosity-Pressure, Permeability-Pressure and Failure Strength-Porosity Variations of Porous Rocks," Proceedings, 17th U. S. Symposium on Rock Mechanics: Site Characterization, (August 1976), pp. 2A5-1 to 2A5-8.
11. Yoelin, S. D.: "Water Injection in the Lower Jones Sands, Huntington Beach Offshore Field," Journal of Petroleum Technology, (February 1968), p. 127.
12. Gray, K. E., Jogi, P. N., Morita, N., and Thompson, T. W.: "The Deformation Behavior of Rocks From the Pleasant Bayou Wells," Proceedings, Fourth U. S. Gulf Coast Geopressured-Geothermal Energy Conference: Research and Development, Vol. 2, University of Texas at Austin, (October 1979), pp. 1031-1058.
13. Wyllie, M. R. J.: The Fundamentals of Well Log Interpretation, Academic Press Inc., New York, (1963), pp. 9-23.
14. Archie, G. E.: "The Electrical Resistivity Log as an Aid in Determining Some Reservoir Characteristics," Petroleum Transactions, AIME, Vol. 146, (1942), pp. 54-62.
15. Winsauer, W. O., Shearin, H. M., Jr., Marson, P. H., and Williams, M.: "Resistivity of Brine-Saturated Sands In Relation to Pore Geometry," Bulletin of the American Association of Petroleum Geologists, Vol. 36, No. 2, (February 1952), pp. 253-277.

16. Guyod, H.: "Fundamental Data for the Interpretation of Elastic Log," *The Oil Weekly*, (October 30, 1944), pp. 38-46.
17. Wyllie, R. J. and Rose, W. D.: "Some Theoretical Considerations Related to the Quantitative Evaluation of the Physical Characteristics of Reservoir Rock From Electrical Log Data," Petroleum Transactions, AIME, Vol. 189, (1950), pp. 105-118.
18. Owen, J. E.: "The Resistivity of a Fluid-Filled Porous Body," Petroleum Transactions, AIME, Vol. 195, (1952), pp. 169-174.
19. Wyble, D. O.: "Effect of Applied Pressure on the Conductivity, Porosity and Permeability of Sandstones," Petroleum Transactions, AIME, Vol. 213, (1958), pp. 430-432.
20. Fatt, I.: "Effect of Overburden and Reservoir Pressure on Electric Logging Formation Factor," Bulletin of the American Association of Petroleum Geologists, (1957), pp. 2456-2466.
21. Glanville, C. R.: "Laboratory Study Indicates Significant Effect of Pressure on Resistivity of Reservoir Rock," *Journal of Petroleum Technology*, (April 1959), pp. 20-26.
22. Redmond, J. C.: "Effect of Simulated Overburden Pressure on the Resistivity, Porosity, and Permeability of Selected Sandstones," Ph.D. Dissertation, The Pennsylvania State University, (1962).
23. Wyllie, M. R. J., and Spangler, M. B.: "Application of Electrical Resistivity Measurements to Problems of Fluid Flow in Porous Media," Bulletin of the American Association of Petroleum Geologists, (1952), 36, No. 2, pp. 359-403.
24. Boggus, R. F.: "Directional Permeabilities, Material Properties, and Resistivities of Sandstones," M. S. Thesis, University of Texas

at Austin, (1967).

25. Tixier, M. P.: "Evaluation of Permeability from Electric Log Resistivity Gradients," Oil and Gas Journal, (June 16, 1949).
26. Lebourg, M. P., Tanguy, D. R., Kisling, J. W., and Nutter, B. P.: "Improved Formation Evaluation with Log-Test-Log Technique," Journal of Petroleum Technology, (November 1966), pp. 1411-1418.
27. Tellinghuisen, C. M.: "Simultaneous Determination of Permeability and Resistivity," M. S. Thesis, The University of Texas at Austin, (1976).
28. Morita, N.: "Three Dimensional Permeability Measurements," Ph. D. Dissertation, The University of Texas at Austin, (1974).
29. Evans, W. M.: "A System for Combined Determination of Dynamic and Elastic Properties, Permeability, Porosity, and Resistivity of Rocks," Ph. D. Dissertation, The University of Texas at Austin, (1973).
30. Ucok, H., Ershanghi, I., and Olhoeft, G. R., "Electrical Resistivity of Geothermal Brines," Journal of Petroleum Technology, (April 1980), pp. 717-727.
31. Gibson, R. E.: "The Influence of Concentration on the Compressions of Aqueous Solutions of Certain Sulfates and a Note on the Representation of the Compressions of Aqueous Solutions as a Function of Pressure," Journal of the American Chemical Society, Vol. 56, No. 1, (January 1934), pp. 4-14.
32. Dunlap, H. F., Bilharty, H. L., Shuler, E., and Bailey, C. R.: "The Relation Between Electrical Resistivity and Brine Saturation in Reservoir Rocks," Petroleum Transactions, AIME, (October 1949),

pp. 259-264.

33. Rust, C. F.: "Electrical Resistivity Measurements on Reservoir Rock Samples by the Two-Electrode and Four-Electrode Methods," Petroleum Transactions, Vol. 195, (1952), pp. 217-224.
34. Quist, A. S. and Marshall, W. L.: "Electrical Conductances of Aqueous Sodium Chloride Solutions from 0 to 800° and at Pressure to 4,000 Bars," The Journal of Physical Chemistry, Vol. 72, No. 2, (February 1968), pp. 684-703.
35. Jessop, H. T. and Harris, F. C.: Photoelasticity Principles and Methods, Dover Publications, Inc., (1940), p. 182.
36. Dorsey, N. T.: Properties of Ordinary Water-Substance, Reinhold Publishing Corporation, New York, (1940), pp. 207-254.
37. Wyllie, M. R. J., Gregory, A. R., and Gardner, G. H. H.: "Elastic Wave Velocities in Heterogeneous and Porous Media," Geophysics, Vol. 21, No. 1, (January 1956).

